

Fall 10-31-2018

SYNTHESIS, CHARACTERIZATION AND APPLICATION OF STRUCTURALLY DIVERSE POLY(CHALCOGENYLENE VINYLENE)S

Zhen Zhang
University of New Mexico

Follow this and additional works at: https://digitalrepository.unm.edu/chem_etds

 Part of the [Physical Chemistry Commons](#)

Recommended Citation

Zhang, Zhen. "SYNTHESIS, CHARACTERIZATION AND APPLICATION OF STRUCTURALLY DIVERSE POLY(CHALCOGENYLENE VINYLENE)S." (2018). https://digitalrepository.unm.edu/chem_etds/148

This Dissertation is brought to you for free and open access by the Electronic Theses and Dissertations at UNM Digital Repository. It has been accepted for inclusion in Chemistry ETDs by an authorized administrator of UNM Digital Repository. For more information, please contact disc@unm.edu.

Zhen Zhang

Candidate

Chemistry and Chemical Biology

Department

This dissertation is approved, and it is acceptable in quality and form for publication:

Approved by the Dissertation Committee:

Prof. Yang Qin, Chairperson

Prof. Ramesh Giri

Prof. John K. Grey

Prof. Mehran Tehrani

**SYNTHESIS, CHARACTERIZATION AND APPLICATION OF
STRUCTURALLY DIVERSE POLY(CHALCOGENYLENE
VINYLENE)S**

by

ZHEN ZHANG

B. S. Chemistry, Lanzhou University, China, 2013

DISSERTATION

Submitted in Partial Fulfillment of the
Requirements for the Degree of

**Doctor of Philosophy
Chemistry**

The University of New Mexico
Albuquerque, New Mexico

December 2018

Dedication

-To my wife, who always gives me the most support on whatever I decide to do!

-To my parents for always putting my education in the first place!

ACKNOWLEDGEMENTS

First and foremost, I would like to thank my advisor Dr. Yang Qin for offering me the opportunity to work with him, for patiently leading me onto the right track of chemistry research about how to do, to think and to solve the problems. I would like to thank him for giving me the freedom, encouragement and confidence to explore and to succeed. I would like to thank him for all the kind help he gave me whenever I need a hand no matter whether in research or my life. Without his help and guidance, I can't imagine obtaining the great achievement during my PhD course! Thank you!

Secondly, I would like to thank Dr. John Grey and Dr. Ramesh Giri. Quantum chemistry is difficult for me, however, I have been keeping learning from Dr. Grey and his students, and I can definitely feel I am growing under their great help and our wonderful collaborations. Thanks to Dr. Giri for his constructive advice to my research proposal and his generous help to my research!

Thirdly, I would like to thank both my former and present labmates for their help on my research. I had a great time in the lab with Jianzhong, Wenhan, Keda, Brad et al., to whom I can always talk about all kinds of interesting, exciting or even funny things. I am missing and will miss the wonderful time a lot in Qin Lab!

Finally, I would like to thank my wife, my son, my parents and my brother, for all the great family time they have been giving me!

Synthesis, Characterization and Application of Structurally Diverse Poly(chalcogenylene vinylene)s

By

Zhen Zhang

Bachelor, Chemistry, Lanzhou University, China, 2013

PhD, Chemistry, University of New Mexico, USA, 2018

Abstract

Conjugated polymers have found widespread applications in flexible and printable electronic devices, among which poly(thienylene vinylene) (PTV) displays outstanding optoelectronic properties and promising applications. However, further studies of its *structure-property-function* relationship have been greatly impeded mainly due to the synthetic difficulty of generating new structures beyond its rudimentary form.

To further investigate this class of material, I have developed a facile methodology for the preparation of structurally diverse poly(chalcogenylene vinylene)s (PCVs) through a combination of acyclic diene metathesis (ADMET) polymerization and post-polymerization modification techniques. Specifically, a series of halogenated and cross-conjugated PCVs have been designed and synthesized, followed by complete characterizations. It was found the physical and optoelectronic properties of the obtained polymers can be fine-tuned through introducing halogen atoms and specific conjugated

side chains. Interestingly, the PTVs with strong electron withdrawing cyano groups were found to be emissive, which is rarely observed in this class of materials. The newly prepared polymers combining with PCBM (electron acceptor) were eventually fabricated into solar cell devices. Power conversion efficiency of ca. 1.6%, 2-fold higher than the parent PTV, was achieved, resulting from the optimized energy levels, crystallinity and broadened absorption via chemical modifications. Our methodologies provide a facile tool to effectively diversify PTV's structures and then systematically study their *structure-property-function* relationships, which enhanced our basic understanding on this type of materials and will potentially lead to new materials for advanced electronic applications.

The other part of the dissertation is about the preparation, photophysical studies and application of a conjugated Pt-containing small molecule. The incorporation of Pt atom into this molecule is supposed to increase the triplet exciton generation after radiation due to the heavy atom effect, offering us the opportunity to investigate the formation and transport of the triplet excitons and eventually capture them for solar cells. This acceptor is composed of our previously designed Pt-containing electron-rich unit in the middle and strong electron-deficient units on both sides. It was found that this acceptor-donor-acceptor Pt-containing compound possesses broad absorption from 300 to 1000 nm, good crystallinity and low LUMO energy level, which are prerequisite for a good acceptor material of organic solar cells. The device performance of the Pt-containing compound is currently under investigation.

TABLE OF CONTENTS

LIST OF FIGURES	ix
LIST OF SCHEMES.....	xv
LIST OF TABLES.....	xvi
LIST OF ABBREVIATIONS	xvii
Chapter 1 Introduction	
1.1 Overview of Organic Photovoltaics.....	1
1.2 Basics of Organic Solar Cells	2
1.3 Conjugated Polymers for Organic Solar Cells	5
1.4 Poly(thienylene vinylene)s	
1.4.1 Overview.....	8
1.4.2 Structural Design Rationale to tune the Properties and Performance.....	9
1.4.3 Synthetic Methodologies	12
Chapter 2 Synthesis, Characterization and Application of Structurally Diverse Poly(thienylene vinylene)s	
2.1 Introduction.....	14
2.2 Synthesis, Characterization and Discussion of Halogenated and Cross-conjugated PTVs	15
2.3 Synthesis, Characterization and Discussion of Alkyne-containing PTVs	33
2.4 Application of PTVs in Solar Cell Devices	46

2.4.1	Solar Cell Performance of Halogenated and Cross-conjugated PTVs	47
2.4.2	Solar Cell Performance of Alkyne-containing PTVs.....	48
2.5	Conclusion	49
2.6	Experimental.....	50
Chapter 3 Synthesis, Characterization and Application of Structurally Diverse Poly(selenylene vinylene)s		
3.1	Introduction.....	64
3.2	Synthesis, Characterization and Discussion of Poly(selenylene vinylene) and Poly(selenylene vinylene)- <i>co</i> -Poly(thienylene vinylene).....	66
3.3	Synthesis, Characterization and Discussion of Cross-conjugated Poly(selenylene vinylene)s.....	75
3.4	Solar Cell Performance of PSVs.....	84
3.5	Conclusion	86
3.6	Experimental.....	86
Chapter 4. Acceptor-Donor-Acceptor Type Pt-containing Conjugated Molecule for Photophysical Studies.		
4.1	Introduction.....	96
4.2	Synthesis Characterization and Discussion	99
4.3	Experimental.....	103
Conclusion		106
Reference		108

LIST OF FIGURES

Figure 1.1 Working mechanism for donor-acceptor heterojunction solar cells. (1) Photoexcitation of the donor to generate a Coulomb-correlated electron-hole pair, an exciton. (2) Exciton diffusion to the D-A interface. (3) Bound exciton dissociation at the D-A interface to form a geminate pair. (4) Free charge transportation and collection at electrodes.

Figure 1.2 (a) Schematic illustration of a polymer–fullerene BHJ solar cell and its active layer morphology; (b) Typical J-V curve for PSCs under simulated solar irradiation.

Figure 1.3 Chemical structures of PPV, Polythiophene and PBDTTD *D-A* copolymer.

Figure 1.4 (a) Conventional scheme of photoexcitation in P3TV. (b) For excitation energies above 2.1 eV, the new decay pathway of activated singlet fission.

Figure 1.5 Synthesis of PTV from polymeric precursor.

Figure 2.1 Gas chromatograms (GC, left column), measured isotope patterns of mass spectra of molecular ions (MS, black, right column) and predicted isotope patterns (green) of TV-F, TV-Cl, TV-Br and TV-I, respectively.

Figure 2.2 Kinetics studies of ADMET polymerization of TV-Br with (filled circle) and without (filled star) CuI as the additive.

Figure 2.3 ¹H NMR spectra of PTV-H, PTV-F, PTV-Cl, PTV-Br and PTV-I, from top to bottom; # denotes propenyl end-group signals and * denotes solvent impurities including THF and methanol.

Figure 2.4 ^1H NMR spectra of (top to bottom) PTV-Br, PTV-Th, PTV-ThCHO and PTV-ThCN in CDCl_3 .

Figure 2.5 Density functional theory (DFT) calculation results (B3LYP, 6-31G*) for oligomers containing three repeating units of corresponding functionalized PTVs. For the halogenated PTVs, the dihedral angles are averages between the three main-chain thiophene rings. For the cross-conjugated PTVs, the first dihedral angles are averages between the three main-chain thiophene rings and the second angles are averages between the three sets of side-chain and main-chain thiophene rings, respectively.

Figure 2.6. X-ray diffraction (XRD) profiles of thin films of PTVs. Corresponding d -spacings and domain sizes calculated from respective first-order scattering peaks are shown in insert.

Figure 2.7. (A) Raman spectra of chlorobenzene solutions of halogenated and cross-conjugated PTVs; (B) expanded region of the Raman spectra between 1100 and 1700 cm^{-1} .

Figure 2.8. UV-vis absorption spectra of halogenated PTV polymers (A) in chlorobenzene solutions (10^{-5} M) and (B) as thin films spun-cast on glass substrates.

Figure 2.9. (A) UV-vis absorption spectra of cross-conjugated PTV polymers in chlorobenzene solutions (10^{-5} M); (B) UV-vis absorption spectra of cross-conjugated PTVs as thin films spun-cast on glass substrates.

Figure 2.10 Emission spectra of PTV-ThCN in chlorobenzene solution (10^{-5} M); peaks marked with asterisks are due to higher order diffraction of the excitation light.

Figure 2.11. Cyclic voltammetry (CV) graphs of solutions (1 mM in THF) of halogenated and cross-conjugated PTV polymers. Voltages are referenced to ferrocene redox couple (-4.8 eV). The supporting electrolyte is 0.1 M Bu₄NPF₆ in acetonitrile. Scan rate: 100 mV/S.

Figure 2.12. ¹H NMR spectra of the cross-conjugated PTVs in CDCl₃.

Figure 2.13. Size exclusion chromatography (SEC) profiles of the cross-conjugated PTV polymers in CH₃Cl (1 mL/min, RI detector).

Figure 2.14. Infrared (IR) spectra of the cross-conjugated PTVs as powders in attenuated total reflection (ATR) mode.

Figure 2.15. Raman spectra of the cross-conjugated PTVs in chlorobenzene solutions. The bottom panel displays the magnified region between 1100 and 1700 cm⁻¹.

Figure 2.16. UV-vis absorption spectra of the cross-conjugated PTVs (A) in chlorobenzene solutions (10⁻⁵ M repeat units) and (B) as thin films drop cast from chlorobenzene solutions on glass substrates. Insert in (A): emission spectrum of PTV-A-ThCN in solution excited at 700 nm.

Figure 2.17. Cyclic voltammograms (CV) of thin films of the cross-conjugated PTVs deposited onto the glassy carbon working electrodes (supporting electrolytes: 0.1 M Bu₄NPF₆ in acetonitrile, scan rate: 100 mV/s).

Figure 2.18. Density functional theory (DFT, B3LYP, 6-31G*) calculation results of the cross-conjugated PTVs. The structures contain five main-chain thienyl groups terminated with propenyl groups on both ends. Long alkyl side-chains are replaced with methyl groups.

Figure 2.19. Absorption profile (left axis) and external quantum efficiency (EQE) trace (right axis) of the optimized device employing PTV-ThCN and PCBM (1/4 by wt.).

Figure 3.1. (A) Gas chromatography (GC) trace of 3DSV and (B) low resolution mass spectrum (MS) of the molecular ion of 3DSV.

Figure 3.2. ^1H NMR spectra overlay of 3DSV, 3DTV, cis-3DTV, P3DSV, P3DTV, and P3DSV-co-P3DTV.

Figure 3.3. (A) Raman spectra of chlorobenzene solutions of and (B) IR spectra of powders of P3DSV (black), P3DTV (red), P3DSV-co-P3DTV (blue) and P3DSV/P3DTV blends (50/50, wt./wt., green).

Figure 3.4. UV-vis absorption spectra of P3DSV (black), P3DTV (red), P3DSV-co-P3DTV (blue) and P3DSV/P3DTV blends (50/50, wt./wt., green): (A) in chlorobenzene solutions (ca. 10^{-5} M r.p. units) and (B) as thin films spun cast from chlorobenzene solutions onto glass substrates.

Figure 3.5. Cyclic voltammograms of P3DSV (black), P3DTV (red) and P3DSV-co-P3DTV (blue) in THF (0.01 M); Bu_4NPF_6 as supporting electrolyte (0.1 M) and referenced against ferrocene/ferrocenium redox couple (scan rate: 100 mV/s).

Figure 3.6. Powder X-ray diffraction (XRD) profiles of P3DSV (black), P3DTV (red) and P3DSV-co-P3DTV (blue).

Figure 3.7. Gas chromatograms (GC, left column), measured isotope patterns of mass spectra of molecular ions (MS, black, right column) and predicted isotope patterns (green)

of SV-Br.

Figure 3.8 ^1H NMR of PSV-Br (Compound 6).

Figure 3.9. ^1H NMR spectra of (top to bottom) PSV-Br, PSV-Th, PSV-ThCHO, and PSV-ThCN in CDCl_3 .

Figure 3.10. Size exclusion chromatograms (SECs) of PSV-Br, PSV-Th, PSV-ThCHO and PSV-ThCN (CHCl_3 w/ 0.5% NEt_3 , 1 mL/min, RI detector).

Figure 3.11. Raman spectra of chlorobenzene solutions of PDSV, PSV-Br, PSV-Th, PSV-ThCHO and PSV-ThCN.

Figure 3.12 UV-vis absorption spectra of PSVs: (A) in chlorobenzene solutions (ca. 10^{-5} M r.p. units) and (B) as thin films spun-cast from chlorobenzene solutions onto glass substrates.

Figure 3.13 Cyclic voltammograms (CV) of thin films of the cross-conjugated of PSV-Br, PSV-Th, PSV-ThCHO and PSV-ThCN deposited onto the glassy carbon working electrodes (supporting electrolytes: 0.1 M Bu_4NPF_6 in acetonitrile, scan rate: 100 mV/s).

Figure 4.1 (a) The ITIC molecule includes electron-pushing and electron-pulling units, where the electron-pushing units are shield by bulky non-conjugated side chains. (b) Top and side views of the optimal geometry of the ITIC molecule. (c) Bimolecular packing mode.

Figure 4.2. UV-vis absorption spectra of the Pt-containing acceptor in chlorobenzene solutions (ca. 10^{-5} M r.p. units) and as thin films spun cast from chlorobenzene solutions onto glass substrates.

Figure 4.3. Cyclic voltammograms of the Pt-containing acceptor; Bu_4NPF_6 as supporting electrolyte (0.1 M) and referenced against ferrocene/ferrocenium redox couple (scan rate: 100 mV/s).

Figure 4.4 X-ray diffraction (XRD) profiles of thin films of the Pt-containing acceptor.

LIST OF SCHEMES

Scheme 2.1 Synthesis of TV-X and PTV-X.

Scheme 2.2 Synthesis of Alkyne-spaced Cross-conjugated Polymers.

Scheme 3.1 Synthetic Route of Poly(selenylene vinylene) and Poly(selenylene vinylene)-*co*-Poly(thienylene vinylene).

Scheme 3.2 Synthetic Route of Brominated and Cross-conjugated PSVs.

Scheme 4.1 Synthetic Route of Pt-containing Non-fullerene OSCs acceptor.

LIST OF TABLES

Table 2.1 Physical and Electronic Properties of Halogenated and Cross-Conjugated PTV Polymers.

Table 2.2 Physical and Optical Properties of the PTV Polymers.

Table 2.3 Optimized OSC Device Performances Employing Halogenated and Cross-Conjugated PTV Polymers.

Table 2.4 Optimized OSC Device Performances Employing Alkyne-containing PTV Polymers.

Table 3.1 Electronic Properties of Polymers.

Table 3.2 Physical and Optical Properties of the PSV Polymers.

Table 3.3 Optimized OSC Device Performances Employing PSV Polymers.

List of Abbreviations

PSCs	Polymer solar cells
OPVs	Organic photovoltaics
CPs	Conjugated polymers
BHJ	Bulk Heterojunction
<i>D-A</i>	Donor-acceptor
P_{out}	Maximum Electrical Power
P_{in}	Total Incident Optical Power
FF	Fill Factor
V_{oc}	Open-Circuit Voltage
J_{sc}	Short-Circuit Current
LUMO	Lowest Unoccupied Molecular Orbital
HOMO	Highest Occupied Molecular Orbital
MDMOPPV	Poly[2-methoxy-5-(3,7-dimethyloctyloxy)]-1,4-phenylenevinylene)
MEH-PPV	Poly(2-methoxy-5(2'-ethylhexyloxy)-1,4-phenylenevinylene)
P3HT	Poly(3-hexylthiophene)
PPV	Poly(<i>p</i> -phenylene vinylene)
P3CTV	Carboxylate substituted PTV
OLED	Organic light-emitting diode
PCBM	Phenyl C61-butyric acid methylester

OFET	Organic field effect transistor
<i>rr</i> -P3AT	Regioregular poly(3-alkylthiophene)
PCVs	Poly(chalcogenylene vinylene)s
SF	Singlet fission
G2	Grubbs' second-generation catalyst
SEC	Size exclusion chromatography
M_n	Number-average molecular weight
\bar{D}	Polydispersity index
MWs	Molecular weights
CV	Cyclic voltammetry
DP	Degrees of polymerization
DFT	Density functional theory
XRD	X-ray diffraction
λ_{\max}	Wavelength of maximum absorbance
PDAs	Polydiacetylenes
ICT	Intramolecular charge transfer
IR	Infrared spectra
ATR	Attenuated total reflection mode
DSC	Differential scanning calorimetry
EQE	External Quantum Efficiencies
PSVs	Poly(selenylene vinylenes)s

TCB	1,2,4-trichlorobenzene
PSV-Br	Poly(3-bromo-4-dodecylselenylene vinylene)
PC ₇₁ BM	Phenyl-C ₇₁ -butyric acid methyl ester
NF	Non-fullerene
<i>A-D-A</i>	Acceptor-donor-acceptor
TMs	Transition metals
mPEG	Poly(ethylene glycol) methyl ether

Chapter 1

Introduction

1.1 Overview of Organic Photovoltaics

Renewable resource is attracting more and more interest in recent decades, which can help to alleviate the global demand for fossil fuels due to their decreasing availability and detrimental effects on the environment from the green house emission. World energy consumption is predicted to increase from about 17 TW in 2010 to 27 TW in 2040.⁵ Although advanced technologies can help improve the energy efficiency and find more resources, it's clear that alternative renewable energy resources have to be fully developed and used for future global needs. There are many different kinds of renewable resources, like wind power, hydropower, geothermal power, but solar power is probably the most promising one, which is inexhaustible and available all over the world.

Photovoltaic technology, which can convert solar energy into electrical energy, is a possible way to solve the energy crisis. Intensive research has been devoted to achieving high power conversion efficiency with low fabrication cost. Currently, the solar cell market is dominated by inorganic materials (like silicon, CdTe, CIGS) based devices because of their relatively high efficiency.⁶ However, efficiency is not the only metric to determine whether the technologies can be applied in a large scale or not. Perhaps, the most important factor is the cost. These inorganic devices have their limitations due to complex fabrication processes, toxic materials, and high installation costs.⁷ Moreover, most of the inorganic materials-based cells are rigid and heavy, which greatly limit their wide-scale production

and application.⁸ To overcome these disadvantages, organic photovoltaics (OPVs) have seen increasing interests, which offer various promising properties, including light weight, solution processability, transparency and flexibility.⁹ OPVs are divided into two categories based on whether they are made with small or large (polymers) molecules, which are different in terms of synthesis, purification, fabrication. Polymer solar cells (PSCs) are attractive because of better film-forming ability of polymer and thus more easily controlled morphologies, low material consumption resulting from high absorption coefficient, the utilization of solution process and low manufacturing energy requirements.¹⁰

1.2 Basics of Organic Solar Cells

The process from photon absorption to electricity generation in the active layer of OSCs is well understood nowadays as illustrated in figure 1.1. Electron-hole pairs, the so-called

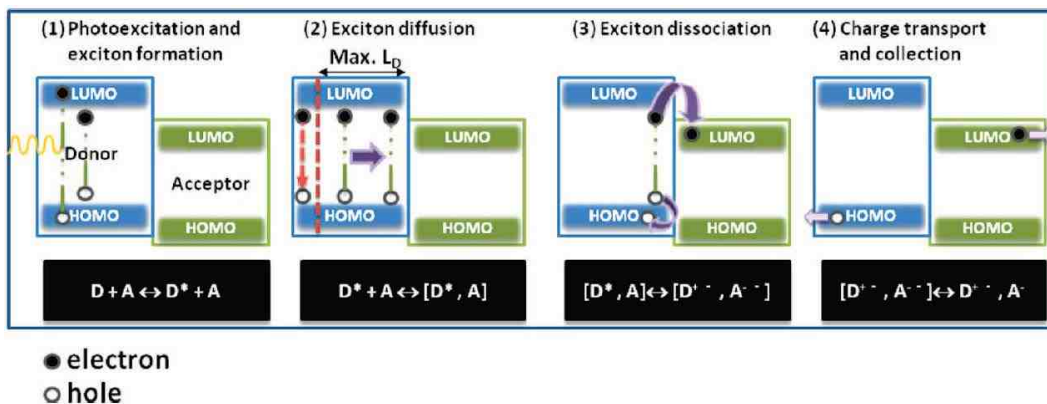


Figure 1.1 Working mechanism for donor-acceptor heterojunction solar cells. (1) Photoexcitation of the donor to generate a Coulomb-correlated electron-hole pair, an exciton. (2) Exciton diffusion to the D-A interface. (3) Bound exciton dissociation at the D-A interface to form a geminate pair. (4) Free charge transportation and collection at electrodes. Adapted the copyright of Ref.³ Copyright (2009), American Chemical Society.

excitons, are generated in the active layer upon sunlight radiation. Due to the low dielectric

constant of organic semiconductors, excitons are strongly bound by coulomb attraction and not separated into free charges under room temperature, which is always observed in single-layer OSCs, leading to very low device performance. Thus, it is highly necessary to add the second component (acceptor) with lower lowest unoccupied molecular orbital (LUMO) energy or higher electron affinity. The energy difference between LUMOs of donor and acceptor, generally accepted as about 0.3 eV,¹¹ provides the driving force to split the excited electron-hole pairs at the interfaces of the donor and acceptor materials. Since the dissociation only happens at the interfaces, it's very important for the excited electron-hole pairs to diffuse to the interfaces before recombination, and previous measurement on several prototype conjugated polymers (CPs)-based OSCs indicates the diffuse length of excitons is in the range of 10 nm.¹² After dissociation, the electrons and holes are transported out from the active layer and collected by the respective electrodes, resulting in the generation of electricity.

The earliest examples of OSCs is composed of one layer of active material sandwiched between two metal electrodes with different work functions. In this type of architecture, PCE of ca. 1% can barely achieved mainly because of their poor FF.¹³ With continuous efforts from the researchers in this field, more efficient active layer structures are designed, which are composed of two types of materials with different electron affinity, the so-called donor and acceptor. Due to the excellent optical properties and fast charge carrier transport,¹⁴ conjugated small molecules and polymers are always applied as donor materials, and fullerene derivatives as well as recently designed donor-acceptor (*D-A*) type

small molecules^{2, 15-17} as acceptor materials.

Although researches on photovoltaic effects in organic cells have already been explored to large extent in the 1950s,¹³ it's not until the first two-layered OSC was fabricated with copper phthalocyanine (donor) and perylene tetracarboxylic derivative (acceptor) by Tang in 1985 and relatively high PCE of about 1% was achieved,¹⁸ then this field really grabbed tremendous attention both in academia and industry due to its promising potentials to replace traditional fossil fuels and solve energy crisis as well as a series of environmental problems, including global warming and air pollution. Later on, in 1995, Heeger *et al.* did a landmark work to prepare the active layer by mixing the donor and acceptor materials and fabricated the bulk-heterojunction (BHJ) OSCs.¹⁹ This novel design, which allows the donor and acceptor to intermix at the nanometer scale, is critical to achieve high PCE, attributed to the nanometer range diffusion length of excitons and incredibly increased donor-acceptor interfaces compared to the bilayer structures.

Nowadays the most efficient design of PSCs contains an active organic layer sandwiched between two electrodes and frequently an interlayer between the active layer and the electrodes (Figure 1.2a). The active layer is composed of electron donors (CPs) and electron acceptors (fullerene derivatives), which is arranged in BHJ type architecture in order to maximize the exciton dissociation efficiencies.^{1, 20, 21} With the normal architectures, the holes are transported to the anode, which typically consists of a substrate coated with transparent conducting electrodes and modified by hole selective/electron blocking layer between the electrode and active layer. The most commonly used anode is tin-doped indium

oxide due to its high work function and large optical transparency. And the electrons are transported to the cathode, which is comprised of a low work function metal with electron selective layer between the electrode and active layer. The most frequently observed material for cathode is aluminum because of its low work function and high reflectivity. The most important parameter for PSC is the PCE, which is the ratio of the maximum

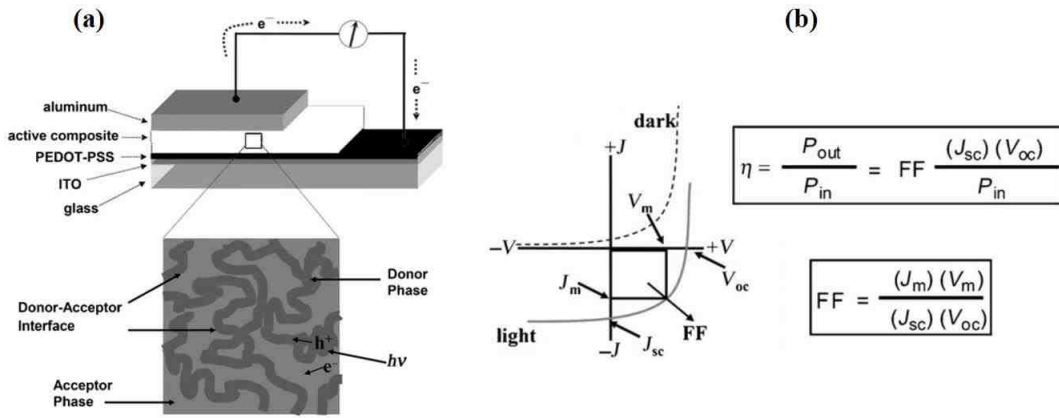


Figure 1.2 (a) Schematic illustration of a polymer–fullerene BHJ solar cell and its active layer morphology; (b) Typical J-V curve for PSCs under simulated solar irradiation. Adapted the copyright of Ref.¹ Copyright (2008) Wiley-VCH Verlag GmbH & Co. KGaA, Weinheim.

electrical power, P_{out} , generated by the device to the total incident optical power, P_{in} , and it's defined as the equation: $PCE = P_{out}/P_{in} = (V_{oc} * J_{sc} * FF)/P_{in}$, where FF is defined by the equation $FF = (V_m * J_m)/(V_{oc} * J_{sc})$. V_{oc} refers to open-circuit voltage, which is proportional to the built-in voltage between the LUMO of the acceptor and the highest occupied molecular orbital (HOMO) of the donor.³ J_{sc} is the short-circuit current, and its value is related to the amount of absorbed photons, the efficiency of exciton dissociation, separation of geminate excitons and the charge mobilities in the active layer.²⁰

1.3 Conjugated Polymers for Organic Solar Cells

Research on PSCs generally focuses on solution processable organic semiconducting polymers.²⁰ Important representatives of hole conducting donor-type semiconducting polymers are: (i) poly(*p*-phenylene vinylene) (PPV)-based CPs such as poly[2-methoxy-5-(3,7-dimethyloctyloxy)]-1,4-phenylenevinylene) (MDMOPPV); (ii) derivatives of

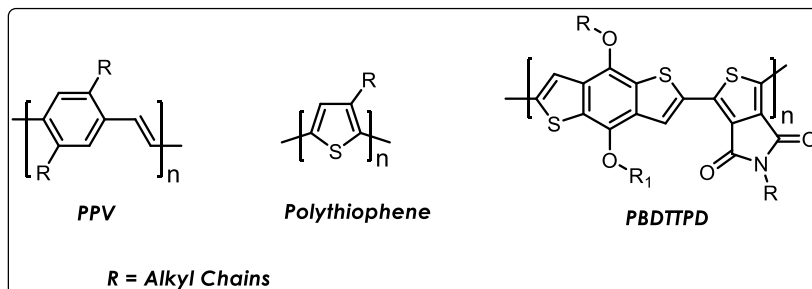


Figure 1.3 Chemical structures of PPV, Polythiophene and PBDTTPD *D-A* copolymer.

poly(thiophene) such as poly(3-hexylthiophene) (P3HT); (iii) the recently applied *D-A* low bandgap copolymers. The examples of each type of the above polymers are shown in figure 1.3.

PPV and its derivatives are among the earliest well-studied CPs for electronic devices and have attracted long-term attention due to their relatively good conducting and photoluminescence properties. The first CPs-based organic light-emitting diode (OLED) was fabricated by employing PPV as the active layer, which emits green-yellow light.²² The rapid development and continuously intensive research studies of PPVs on OLED also benefit their applications on photovoltaic devices. Wienk *et al.* demonstrated that after condition optimization, PCE of 3.0% can be reached with the blend of MDMO-PPV and Methano[70]fullerene as the active layer in BHJ solar cell device,²³ which is the highest

efficiency to date that has been achieved for PPVs-based single BHJ OSCs. Further PCE improvement was achieved from polythiophene-based OSCs, resulting from the reduced bandgap and increased charge carrier mobility. Through intensive device condition optimization and molecular engineering over years, best PCE of ca. 5% was achieved by applying a layer of solution-based titanium oxide on top of the *rr*-P3HT: fullerene active layer.²⁴ However, subsequent efforts of further improving the efficiencies during the past several years, including incorporation of *rr*-P3HT nanofibers and inorganic quantum dots to improve charge mobility and absorption,^{25, 26} haven't seen much success intrinsically due to the poor match between the absorption of P3HT and solar emission spectrum. The problem of poor absorption of solar emission is greatly alleviated with the emerging of *D-A* (*push-pull*) copolymers. *D-A* copolymers are composed of alternating electron-rich (donor) and electron-deficient (acceptor) moieties in their backbones. The push-pull effect leads to low bandgap, good mainchain planarity and high charge mobility, which significantly enhanced the device performance.^{27, 28} And with this type of material, PCE of ca. 10% can be reached.²⁹⁻³¹ Even though, there is still a long way to go before CPs-based OSCs can be widely applied, considering the high PCE of ca. 20% along with the long-term stability of commercially available Si-based solar cells⁶ and the commonly complicated synthesis procedure to approach these *D-A* copolymers. Following the above evolution logic of polymer materials for OSCs, in order to push the device performance to a higher level, a deeper molecular *structure-property-function* understanding and subsequent better design of polymer structure are essentially required.

1.4 Poly(thienylene vinylene)s

1.4.1 Overview

PPV and polythiophene-based polymers as well as the *D-A* copolymers have been intensively studied for electronic applications, and further performance improvement, especially for OSCs, has seen great limits due to their inherent molecular properties. On the other hand, poly(thienylene vinylene)s, a hybrid polymer of PPV and polythiophene, has been far less studied despite of its excellent physical and optoelectronic properties. Theoretically, PTVs are another type of polythiophene-based CPs with one vinylene unit inserted into every two adjacent thiophene units. In the presence of vinylene units, the polymer backbone becomes more planar due to the decreased steric hindrance between the thiophene rings, so more effective conjugation, lower bandgap and better charge mobility are usually observed from PTVs compared with polythiophenes.³² However, applications of PTVs in solar cell devices have not seen much achievement in their efficiency. Even after various optimization of device conditions, PCEs of these PTV-based OSCs are generally low (0.2%–0.9%), despite that the absorption of PTVs has a better match with solar emission.³³ In order to understand why PTV-based PSCs display such low PCEs, Heeger and coworkers have investigated an oligo(butoxyl-thienylene vinylene) (OOTV):PCBM composite through ultrafast spectroscopy.³⁴ They observed a very low quantum efficiency of photoinduced electron transfer in OOTV:PCBM (less than 5%) and a very short nonradiative decay time (0.6 ps). Such a fast nonradiative decay rate makes OOTV itself non-luminescent. And the relative small ionization potential, resulting from

the electron rich backbone, can lead to reduced ambient stability. Thus, in order for PTVs to be more applicable for OSCs and other electronics, structural modifications and subsequent optimization in physical/optoelectronic properties are necessary.

1.4.2 Structural Design Rationale to Tune the Properties and Performance

Ultrafast spectroscopy measure demonstrated the ultrafast nonradiative decay process of photoinduced excited states in PTVs-based solar cell devices, which significantly limit their performance. Further mechanism studies of this ultrafast nonradiative process through femtosecond transient absorption and photoluminescence measurements proposed the

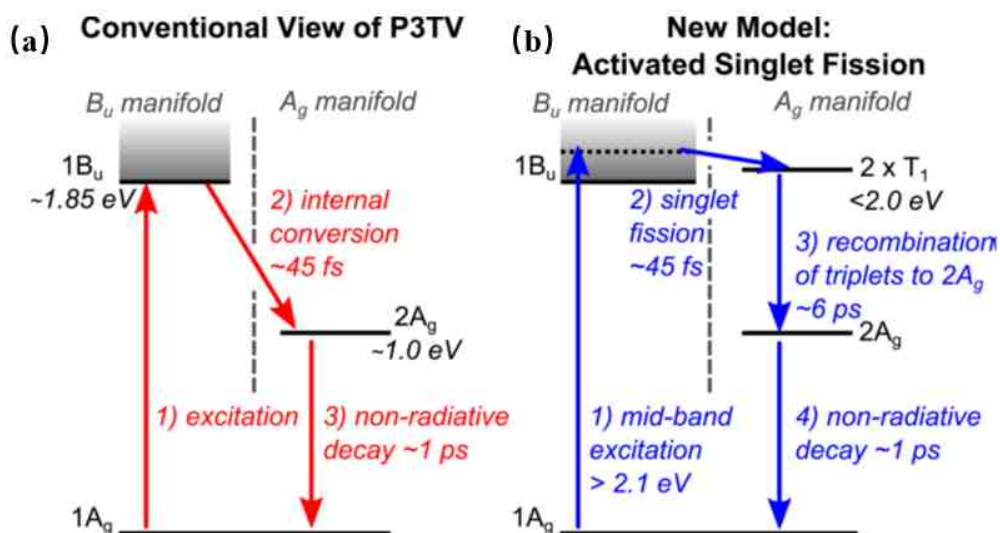


Figure 1.4 (a) Conventional scheme of photoexcitation in P3TV. (b) For excitation energies above 2.1 eV, the new decay pathway of activated singlet fission. Adapted the copyright of Ref.⁴ Copyright (2013), American Chemical Society.

existence of the $2A_g$ dark state, which lies between the $1B_u$ excited state and $1A_g$ ground state.^{4, 35-37} Olejnik et al. demonstrated that ultrafast decay of the photogenerated $1B_u$ excitons into the dark $2A_g$ exciton happened in femtosecond timescale, followed by the nonradiative decay to $1A_g$ ground state within timescale of ca. 1 picosecond as shown in

figure 1.4a. This ultrafast nonradiative process limits the photoluminescence quantum efficiency to ca. 2×10^{-4} , making PTV generally nonluminescent.³⁷ Later on, an amended energy level diagram of PTV was proposed involving the extra singlet fission process (ca. 45 fs) as shown in figure 1.4b.⁴ In general, it's well accepted that the $2A_g$ dark state is mainly responsible for the ultrafast excited state decay process, eventually leading to poor electronic performance. In order to solve this problem of PTV, it is highly necessary to change its electronic structure or even flip the excited state orderings making the $2A_g$ state higher than $1 B_u$ state and consequently increasing the excited state lifetime through chemical modifications. Through quantum chemistry calculations coupled with the correlation function formalism for excited state decay and optical spectra, Jiang *et al.* demonstrated that PTV derivatives with electron-deficient groups, like -COOH, -CHO and -NO₂, could possess strong luminescence and much longer excited state lifetime due to the inverted excited state orderings induced by the electron-withdrawing effects, which would theoretically improve their light-emitting and photovoltaic performance.³⁸ Huo *et al.* prepared carboxylate substituted PTV, P3CTV, in 2009 through Stille coupling reaction.³⁹ The resulted P3CTV displayed unexpected emission and greatly enhanced PCE of 2.01%, presumably ascribed to the increased exciton lifetime. Overall, PTV is a promising class of material, but before a decent performance can be obtained, better understanding of its *structure-property-function* relationship is in high demand, which can be achieved by preparing structurally diverse PTV derivatives, followed by a systematically investigation on their properties and applications.

The existing PTVs all have similar structures featuring alternating thiophene and double bond moieties having alkyl, or less commonly, alkoxy substituents on the thiophene rings. Structural variations in these PTVs are simply alterations of alkyl chain lengths and topologies (linear *vs* branched), resulting in similar electronic properties among the existing examples. In order to perturb the electronic structures of PTVs and finely tune their optoelectronic properties, we came up with three strategies as following:

- i. Halogenation of the polymer backbone. Halogenation has been repeatedly proved to be an effective way to tune the properties of various polymer systems. The electron-withdrawing effect (coupled with electron-donating effect for fluorine atoms) of halogen atoms and sometimes the formed hydrogen bonds from fluorine atoms generally result in decreased HOMO and LUMO energy levels, smaller bandgaps and increased crystallinity (for F-containing polymers), which can usually improve the thermal stability, charge mobility and device performance of the halogenated polymers. Fei *et al.* showed that the charge mobility of P3AT can be enhanced by 4 times through fluorination of the backbone.⁴⁰ Zheng *et al.* achieved greatly improved PCE from 1.19% to 4.60% after chlorination of the Isoindigo-based donor material for solar cell device.⁴¹
- ii. Installation of conjugated side chains on the thiophene unit. The incorporation of conjugated side chains can increase the absorption of the resulted PTVs,⁴² which will theoretically improve the solar cell performance. Besides, the polymeric packing structure can be slightly tuned through introducing appropriate conjugated groups

and the electronic interaction between polymer mainchain and sidechain could sometimes generate interesting properties.

- iii. Replacement of the sulfur atom in thiophene unit with selenium atom. The larger sizes, enhanced polarizability, and stronger spin-orbit coupling effects of selenium atoms are expected to result in significantly different physical/electronic properties over their sulfur counterparts.⁴³⁻⁴⁵ Selenium-containing analogues of thiophene-based CPs have been frequently found to possess reduced bandgap,⁴⁶ higher charge carrier mobility⁴⁷ and improved solar cell performance.⁴⁸⁻⁵⁰

1.4.3 Synthetic Methodologies

Over the years, there have been mainly three-type synthetic methodologies developed for the preparation of PTV. The first one is the elimination from polymeric precursors as shown in figure 1.5.⁵¹⁻⁵³ For this method, a two-stage route was used to first produce a high molecular weight, soluble, non-conjugated precursor polymer (2) that could be easily cast into films from solutions, followed by thermal conversion into the final conjugated polymer. However, this methodology generally suffers from incompletely thermal conversion from the precursor to the final polymer, leading to defects in the polymer backbone and

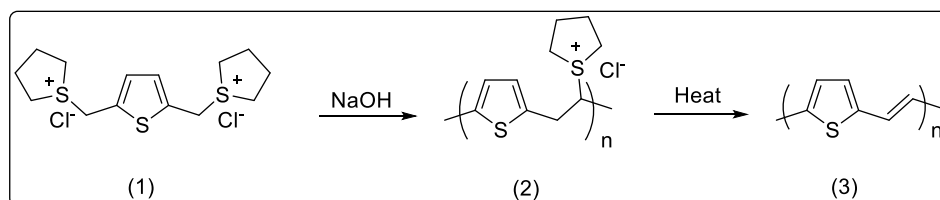


Figure 1.5 Synthesis of PTV from polymeric precursor.

decreased performance in the application of electronic devices. The second one involves

McMurry coupling and Wittig-type reactions of aldehyde-containing monomers.⁵¹⁻⁵³ The third-type methodology for the preparation of PTV, which is widely applied nowadays, involves transition-metal-catalyzed techniques, including Stille coupling reaction,⁴⁷ Heck coupling reaction⁵⁴ and acyclic diene metathesis (ADMET).⁵⁵ As discussed in the previous section, we were trying to introduce halogen atoms on the PTV monomers and then find a suitable methodology to polymerize them. Unfortunately, the commonly-used Stille coupling reaction and Heck coupling reactions, reactions for halide compounds, are not compatible with the halogenated monomers. In addition, these two coupling reactions have been known to induce homo coupling defects into the polymer backbones,⁵⁴ which could significantly decrease the device performance of the prepared polymers. Thus, we finally chose ADMET technique to polymerize our pre-designed PTV monomers. ADMET is a type of olefin metathesis reaction catalyzed commonly by Ru-based catalysts nowadays. This reaction is unlikely to introduce defects into the resulted polymers. Most importantly, it's well compatible with halogen groups, which allows us to polymerize our halogenated PTV monomers. Thus, we have inclusively applied ADMET technique to prepare our structurally diverse PTVs and PSVs.

Chapter 2 Synthesis, Characterization and Application of Structurally

Diverse Poly (thienylene vinylene)s

(Reproduced with permission from *Macromolecules* **2016**, 49, 3318–3327.

Copyright © 2016 American Chemical Society

And manuscript under preparation)

2.1 Introduction

Low bandgap PTV derivatives are a unique class of materials possessing high charge mobilities and environmental and thermal stability. The recently discovered activated singlet fission (SF) processes in PTVs⁴ have been considered a viable way to boost solar cell theoretical efficiencies beyond the Shockley–Queisser limit.^{56, 57} Applications of these soluble PTVs in organic electronic devices have been scarce, among which several examples of applying PTVs in OSCs have been described but only low to moderate device efficiencies, typically less than 1%, have been obtained.^{33, 58} Despite morphology controllability issues,⁵⁹ extremely short exciton lifetimes in PTVs caused by ultrafast nonradiative decay have been ascribed as the main causes for low OSC performance.³⁷ Thus, in order for PTVs to be more applicable for OSCs and other optoelectronic applications in general, systematic structural modifications, especially those that perturb the main-chain electronic structures, optimization in physical/electronic properties and, most importantly, better understanding on structure-property relationships are necessary. However, all of these aspects have been explored to a very limited extent mainly due to the limitations in PTV structural variations by conventional synthetic procedures.

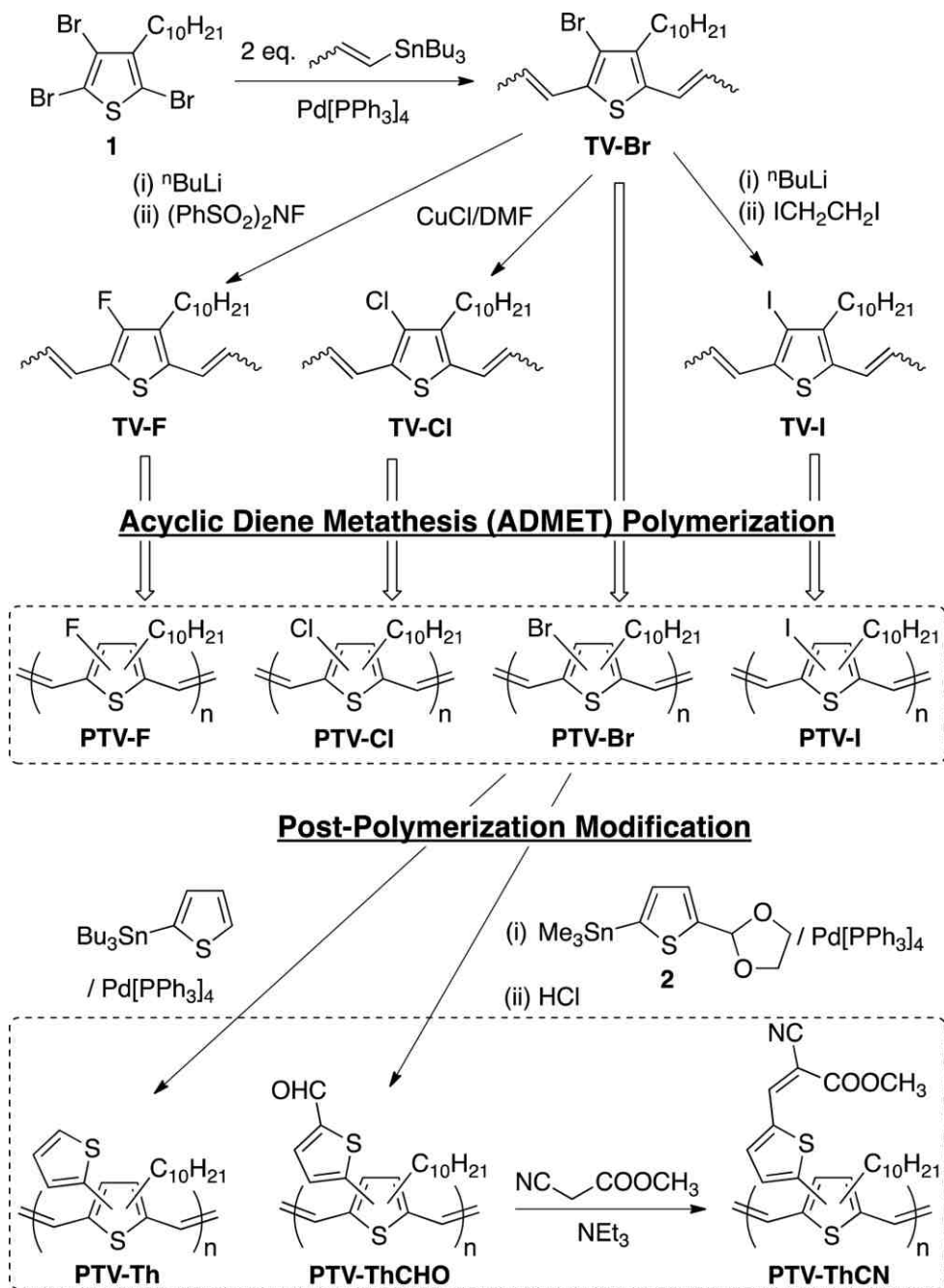
We report here versatile synthetic methodologies combining ADMET and post-

polymerization modification techniques toward structurally diverse PTVs with systematically varied substituents on the thiophene rings. We have prepared a series of novel halogenated and cross-conjugated PTVs, studied in detail their physical and electronic properties, and applied them in OSC devices. Our strategies have shown not only versatility in fine-tuning PTV physical and electronic properties but also promises in applying these polymers in organic electronic devices, which sets a general platform for tailor-designed structural modifications and a better understanding of the structure-property relationships.

2.2 Synthesis, Characterization and Discussion of Halogenated and Cross-conjugated PTVs

Synthesis of halogenated monomers (TV-X) and corresponding PTV polymers (PTV-X), as well as the cross-conjugated PTVs, is summarized in Scheme 2.1. Synthetic and characterization details are included in the experimental section. Monomer 1, 2,3,5-tribromo-4-decylthiophene, was prepared via bromination of 3-decylthiophene and used as the common starting reagent. Palladium catalyzed Stille coupling reaction of 1 with 2 equiv. of tri-*n*-butyl(1-propenyl)tin led to monomer TV-Br bearing two propenyl groups at the 2,5-positions of thiophene ring. Selectivity of this reaction was confirmed as follows. TV-Br reacted with a slight excess of *n*-BuLi in THF at -78 °C, leading to Li-Br exchange, and quenched with water. The product was then carefully analyzed to be quantitatively 3-decyl-2,5-dipropenylthiophene that showed identical NMR and mass spectra with the same compound and similar nuclear magnetic resonance (NMR) signals in the aromatic regions

with other 3-alkyl-2,5-dipropenylthiophenes, all of which were synthesized previously



Scheme 2.1 Synthesis of TV-X and PTV-X.

through independent methods.⁶⁰⁻⁶²

TV-Br was then converted into other halogenated monomers, TV-F, TV-Cl, and TV-I, in

high yields via methods shown in Scheme 2.1. In order to confirm quantitative conversions of these transformations, we employed GC-MS measurements on these monomers, and the spectra are shown in Figure 2.1. All four monomers displayed three peaks in the GC

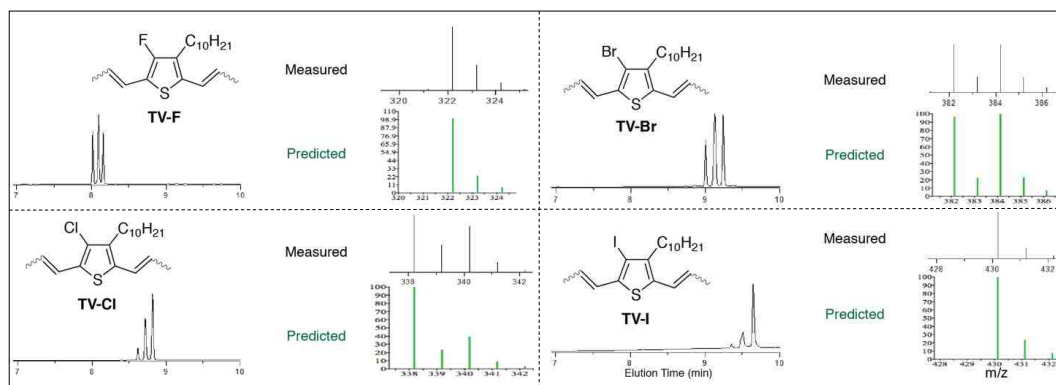


Figure 2.1 Gas chromatograms (GC, left column), measured isotope patterns of mass spectra of molecular ions (MS, black, right column) and predicted isotope patterns (green) of TV-F, TV-Cl, TV-Br and TV-I, respectively.

chromatograms, and all three peaks for each monomer gave exactly the same molecular weight and isotope patterns that match those predicted for the target structures, respectively. The absence of GC peaks corresponding to TV-Br in respective spectra of TV-F, TV-Cl, and TV-I confirms the quantitative conversions during these monomer syntheses. Because of the asymmetric structures of TV-X and presence of *trans/cis* configurations of the double bonds, four stereoisomers are expected to exist for each monomer, which are reflected by the complexity of their ^1H NMR spectra. Detailed assignments of these NMR signals have been discussed previously.^{55, 62} Briefly, all monomers show similar spectra, in which two sets of multiplets within 5.5-6.2 and 1.7-2.2 ppm ranges are characteristic. The peaks centered at ca. 5.7 and 2.0 ppm are respectively from vinyl and methyl groups of the propenyl double bonds having *cis* configuration, while peaks centered at ca. 6.1 and 1.8

ppm are from double bonds of trans configuration. Noticeably, the *cis/trans* ratio is higher in TV-Br and smaller in the other three monomers. This is presumably caused by thermally induced *cis* to *trans* conversions during the reactions since trans double bonds are more thermodynamically stable, which also likely explains the observations of only three instead of four GC peaks, because the all-*cis* isomers are more easily converted to the other *trans*-containing isomers when passing through heated GC columns. Attempts to separate these stereoisomers through column chromatography and distillation have all failed due to the nearly identical polarity and boiling points among the isomers. Although it has been previously shown that *cis* double bonds react faster under ADMET conditions, the resulting PTVs from monomers having different *cis/trans* ratios contain exclusively trans double bonds along the main chains and display identical physical and electronic properties.^{55, 62} We next attempted the synthesis of PTV-X, for which conventional methods are not applicable. For example, Stille coupling reactions are not compatible with the desired halogen substituents on PTV-X, especially in the cases of PTV-Br and PTV-I. McMurry and Wittig type reactions require polar solvents such as THF that are poor solvents for PTVs, and this solubility limitation generally leads to polymers of low molecular weights. On the other hand, ADMET is a variation of alkene metathesis that works on carbon-carbon double bonds and is compatible with halogen substituents.⁶³⁻⁶⁵ We thus performed ADMET polymerization of TV-Br using conditions for PTV synthesis previously optimized by others and us.^{55, 60-62, 66-68} Specifically, the reactions were conducted in 1,2,4-trichlorobenzene at 90 °C under dynamic vacuum (ca. 100 mTorr), and up to five aliquots

of 1 mol % Grubbs' second-generation catalyst (G2) were added every 24 h. The polymerization progress can be conveniently monitored by the color changes of the reaction mixtures gradually going from nearly colorless to yellow, red, purple, and eventually pure blue, indicating formation of polymers of relatively high molecular weights. In the case of TV-Br, however, the color of the reaction mixtures changed very slowly to

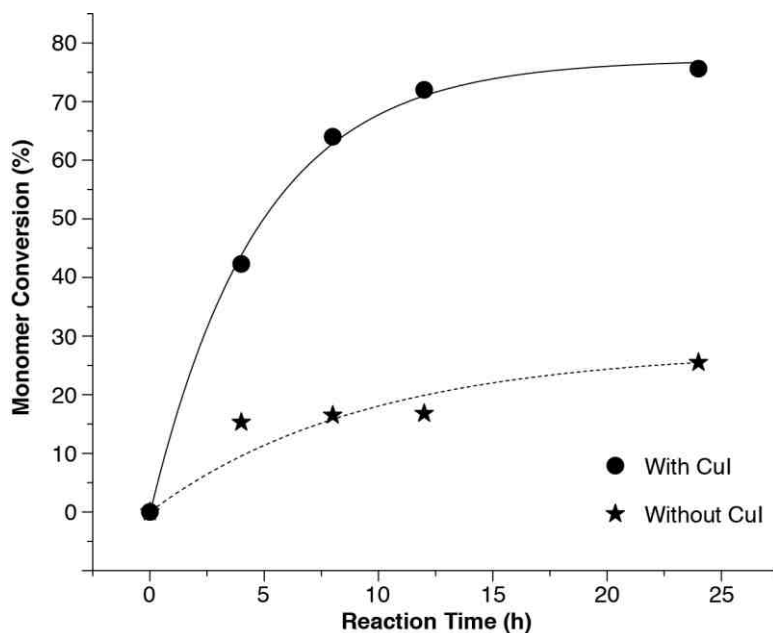


Figure 2.2 Kinetics studies of ADMET polymerization of TV-Br with (filled circle) and without (filled star) CuI as the additive.

red even after 5 days, and only oligomers were obtained as suggested by NMR and size exclusion chromatography (SEC) analyses. We thus performed kinetics studies of the polymerization as shown in Figure 2.2, which showed only ca. 20% double bond conversion within the first 24 h of reaction. We suspected that the electron-withdrawing effect and bigger sizes of the Br atoms compared with the H atoms effectively reduce the double bond reactivity and slow down the ADMET polymerization rates. Wagener *et al.*

have previously shown that addition of Lewis acids as an additive can increase metathesis rates of olefins using Grubbs second generation catalyst.⁶⁹ We thus used ca. 10 mol % of CuI as an additive in the polymerization of TV-Br under identical conditions, and a drastic increase in ADMET rate was observed. As shown in Figure 2.2, the double bond conversion reached ca. 80% within the first 24 h, and after five aliquots of G2 catalyst, PTV-Br was isolated via precipitation as a black solid with a number-average molecular weight (M_n) of ca. 14.0 *kDa* and polydispersity index (\mathcal{D}) of 2.0 as estimated from SEC (Table 1). The exact mechanism of how the Cu(I) additives increase ADMET rate is currently under more detailed investigation. Consequently, we performed ADMET polymerizations of TV-F, TV-Cl, and TV-I in the presence of Cu(I) additives, and molecular weights of the resulting polymers are summarized in Table 2.1. All polymers possess reasonably high molecular weight, except for PTV-I despite repeated attempts. We suspect that the largest sizes of I atoms severely impede metathesis reaction rates of the double bonds. From the ¹H NMR of PTV-I (Figure 2.3), signals corresponding to unreacted propenyl groups are clearly seen, integration of which gives an average number of repeating units of ca. 15, matching the results obtained from SEC analysis. On the other hand, no signals from propenyl end-groups can be observed for PTV-F, PTV-Cl, and PTV-Br, confirming high molecular weight of these polymers. The ¹H NMR spectra of these PTV-X polymers are compiled in Figure 2.3, and the spectrum of unfunctionalized PTV-H ($M_n = 12.0$ *kDa*, $\mathcal{D} = 1.8$) is also included for comparison. The halogenated PTVs display significantly broader signals than those of

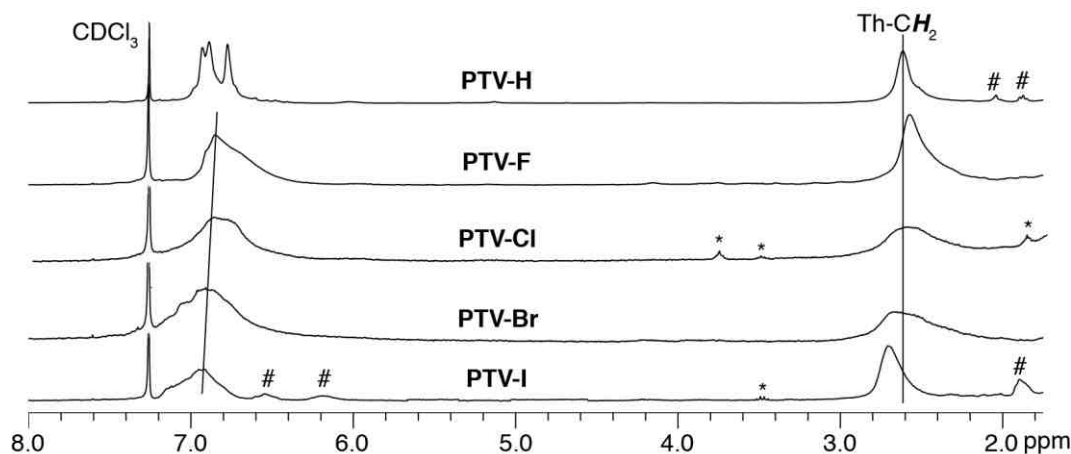


Figure 2.3 ^1H NMR spectra of PTV-H, PTV-F, PTV-Cl, PTV-Br and PTV-I, from top to bottom; # denotes propenyl end-group signals and * denotes solvent impurities including THF and methanol.

PTV-H. The signals corresponding to the double bonds and Th-CH₂ protons show gradual downfield shift with heavier halogen substitutions (F to I), while the Th-CH₂ signal of PTV-F is more upfield shifted than that of PTV-H. This trend can be explained by the resonance effects from the halogen substituents. Since the F-C bonds are the shortest, resonance of the lone pair electrons on F with the aromatic rings is expected to be the strongest, leading to increased electron density and enhanced shielding effects for the Th-CH₂ protons. With increasing sizes of halogens and consequently larger halogen-carbon bond lengths, the resonance effects decrease accordingly, resulting in deshielding and gradually downfield shifted NMR signals.

One effective method of tuning CPs electronic properties is to attach conjugated side-chains that are cross-conjugated with the main-chain.⁷⁰ Our halogenated PTVs can thus be conveniently utilized for installing conjugated side-chains through cross-coupling reactions. On the basis of considerations for high reactivity and reasonable molecular

Table 2.1 Physical and Electronic Properties of Halogenated and Cross-Conjugated PTV Polymers.

	PTV- H	PTV- F	PTV- Cl	PTV- Br	PTV- I	PTV- Th	PTV- ThCHO	PTV- ThCN
M_n (kDa) ^a	12.0	17.8	12.2	14.0	4.8	13.9	13.8	14.9
D ^b	1.8	2.0	1.7	2.2	1.6	1.9	1.9	1.8
DP ^c	48	67	43	43	13	42	38	34
E_g^{opt} (eV) ^d	1.84;	1.74;	1.71;	1.71;	1.79;	1.79;	1.76;	1.54;
	1.68	1.67	1.68	1.66	1.66	1.73	1.71	1.52
E_{HOMO} (eV) ^e	-	-	-	-	-	-	-	-
	4.76; - 4.95	5.03; - 5.18	5.06; - 5.28	5.05; - 5.26	5.09; - 5.20	4.98; - 5.15	5.09; - 5.19	4.89; - 5.01
E_{LUMO} (eV) ^f	-	-	-	-	-	-	-	-
	2.94; - 2.80	3.12; - 2.97	3.20; - 3.00	3.22; - 3.05	3.33; - 3.06	3.01; - 3.01	3.20; - 3.09	3.32; - 3.51
E_g^{CV} (eV) ^g	1.82;	1.91;	1.86;	1.83;	1.76;	1.97;	1.89;	1.57;
	2.15	2.21	2.28	2.21	2.14	2.14	2.10	1.50

^a Number average molecular weight as estimated from size exclusion chromatography (SEC). ^b Polydispersity index. ^c Average degree of polymerization estimated from M_n values. ^d Optical bandgap estimated from the absorption onset; solution data first and thin film data second. ^e Highest occupied molecular orbital (HOMO) energy estimated from oxidation onset by cyclic voltammetry (CV); solution data first and thin film data second. ^f Lowest unoccupied molecular orbital (LUMO) energy estimated from reduction onset by CV; solution data first and thin film data second. ^g Electronic bandgap estimated from CV; solution data first and thin film data second.

weight, we chose PTV-Br as the platform for post-polymerization modification. As shown in Scheme 2.1, we employed Stille coupling reactions to install 2-thienyl and 5-formyl-2-thienyl substituents leading to PTV-Th and PTV-ThCHO, respectively. The aldehyde groups in PTV-ThCHO were further converted into cyanoester vinyl groups through Knoevenagel condensation reactions resulting in PTV-ThCN (Scheme 2.1). From SEC analyses, these post-polymerizations modified polymers show degrees of polymerization (DP) close to that of the starting material, PTV-Br. The slightly decreased DP of PTV-

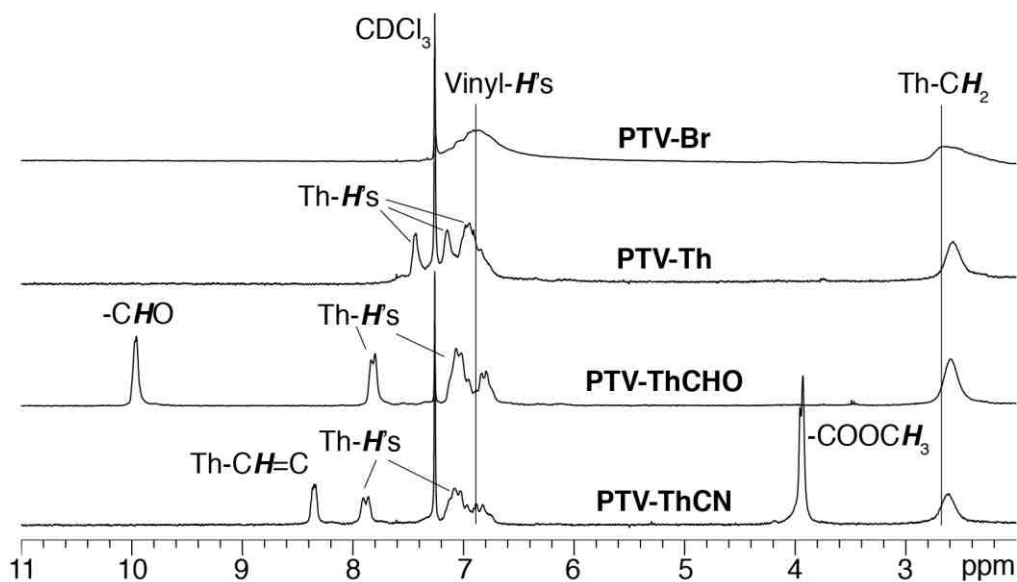


Figure 2.4 ^1H NMR spectra of (top to bottom) PTV-Br, PTV-Th, PTV-ThCHO and PTV-ThCN in CDCl_3 .

ThCN is likely caused by interactions of the $-\text{CN}$ functional groups with SEC column materials. Thus, these post-polymerization reactions did not induce noticeable polymer cross-linking or degradation. ^1H NMR spectra of these PTVs are overlaid in Figure 2.4. Interestingly, signals of the cross-conjugated PTVs become sharper and more resolved than those of the precursor PTV-Br. Signal broadening in polymers can often be ascribed to aggregation, which would suggest that the post-polymerization modified PTVs are less aggregated than PTV-Br in NMR solutions, likely caused by the large and rigid thienyl substituents that are twisted with respect to the mainchains (*vide infra*). The Th- CH_2 signals from the cross-conjugated PTVs are all upfield shifted compared with that of PTV-Br, while become slightly downfield shifted with electron-withdrawing substituents. This trend can again be explained by the resonance effects from the cross-conjugated thiophene substituents, which are more pronounced than that from simple halogens and weakened by

electron-withdrawing substituents. Careful analyses and integrations of these NMR signals suggest quantitative transformations of the post-polymerization modification reactions with undetectable remaining bromine substituents or debrominated moieties.

In order to better understand the measured polymer properties, we first performed density functional theory (DFT) calculations (B3LYP, 6-31G*)^{38, 71, 72} on oligomers containing three repeat units of corresponding PTV polymers. For simplicity, methyl groups are used as the alkyl side-chains during the calculations, and selective results are shown in Figure 2.5. From the optimized structures, PTV-F has the most planar geometry with an average dihedral angle among main-chain thiophene rings of only 1.3°. Such a planarization effect has been observed in many fluorinated compounds and polymers, likely induced by π - π_F , F-H, F-F, and F- π interactions.⁷³ With increasing sizes of the halogen substituents, the main-chains of PTV-X become more and more twisted while PTV-I has the largest average dihedral angle of 71.9°. This likely explains the difficulty to obtain high molecular weight PTV-I caused by the severe steric hindrance from the large I atoms. Compared with PTV-H, the halogenated PTV-X polymers possess deeper HOMO and LUMO energy levels, caused by the more electron-negative halogen substituents. Both the HOMO and LUMO orbitals are delocalized along the polymer main-chains with the halogen lone pair electrons participating mostly in the HOMO orbitals. The calculated bandgaps of PTV-X increase with increasing sizes of the halogen atoms, originated mostly by the gradual lowering of HOMO energy levels. This trend of increasing bandgaps can be explained by the increasingly twisted mainchains caused by steric effects of the halogen

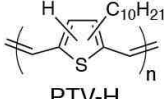



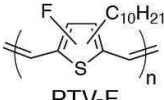



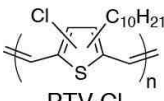



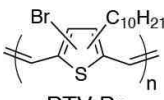



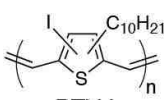



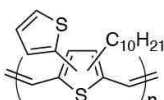



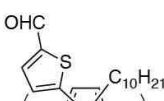



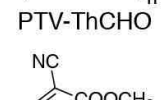



	Side-Views Dihedral Angles	HOMO	LUMO	Bandgap
 PTV-H	 7.3°	 -4.52 eV	 -1.97 eV	-2.55 eV
 PTV-F	 1.3°	 -4.67 eV	 -2.13 eV	-2.54 eV
 PTV-Cl	 10.8°	 -4.92 eV	 -2.18 eV	-2.74 eV
 PTV-Br	 45.5°	 -4.93 eV	 -2.17 eV	-2.76 eV
 PTV-I	 71.9°	 -5.05 eV	 -2.11 eV	-2.94 eV
 PTV-Th	 $16^\circ ; 60^\circ$	 -4.60 eV	 -2.05 eV	-2.55 eV
 PTV-ThCHO	 $23^\circ ; 60^\circ$	 -5.05 eV	 -2.46 eV	-2.59 eV
 PTV-ThCN	 $24^\circ ; 58^\circ$	 -5.12 eV	 -2.74 eV	-2.38 eV

Figure 2.5. Density functional theory (DFT) calculation results (B3LYP, 6-31G*) for oligomers containing three repeating units of corresponding functionalized PTVs. For the halogenated PTVs, the dihedral angles are averages between the three main-chain thiophene rings. For the cross-conjugated PTVs, the first dihedral angles are averages between the three main-chain thiophene rings and the second angles are averages between the three sets of side-chain and main-chain thiophene rings, respectively.

atoms. In the case of cross-conjugated PTVs, the main-chain dihedral angles are similar

and relatively small at ca. 16° – 24° , while there are significant twists between the side-chain and main-chain thiophene units (ca. 60° dihedral angles in all three cases). PTV-Th shows similar electronic properties with those of PTV-H while the HOMO and LUMO of PTV-ThCHO are relatively lowered due to the electron-withdrawing aldehyde substituents, leading to an overall slight increase of the bandgap. On the other hand, PTV-ThCN possesses the deepest HOMO and LUMO levels and the smallest bandgap, likely caused by the strong electron-withdrawing cyanoester groups. Interestingly, the HOMO level of PTV-ThCN is located along the polymer main-chain while the LUMO is mainly on the side-chains. Such spatial separation of frontier energy levels indicates charge transfer characters in electronic transitions that can potentially affect absorption and emission properties of the polymer. We then studied the polymer thin films by X-ray diffraction (XRD) measurements to probe the solid-state structures of these polymers, and the results are shown in Figure 2.6. While PTV-H, PTV-F, PTV-Cl, and PTV-Br display diffraction signals corresponding to lamellar stacking distances and thus certain crystallinity, PTV-I and the cross-conjugated polymers are completely amorphous. PTV-H and PTV-F show three orders of scattering peaks and PTV-Cl has two, while PTV-Br only gives the first-order signal, suggesting decreasing crystalline order with increasing sizes of the halogen substituents. Furthermore, the lamellar stacking distances, corresponding to the alkyl–alkyl packing motifs between polymer chains, increase gradually from 1.57 nm for PTV-H to 1.68 nm for PTV-Br. These observations are consistent with theoretical calculations in that the planarity of polymers, and thus crystallinity, should decrease with increasing sizes of

the halogen and cross-conjugated substituents, accompanied by more expanded crystal lattices. Meanwhile, the domain sizes of PTV-H, PTV-F, PTV-Cl, and PTV-Br are all similar at ca. 10 nm, as calculated from the first-order diffraction peak by the Scherrer equation,⁷⁴ which are considerably smaller than other highly crystalline conjugated polymers such as *rr*-P3HT.⁷⁵

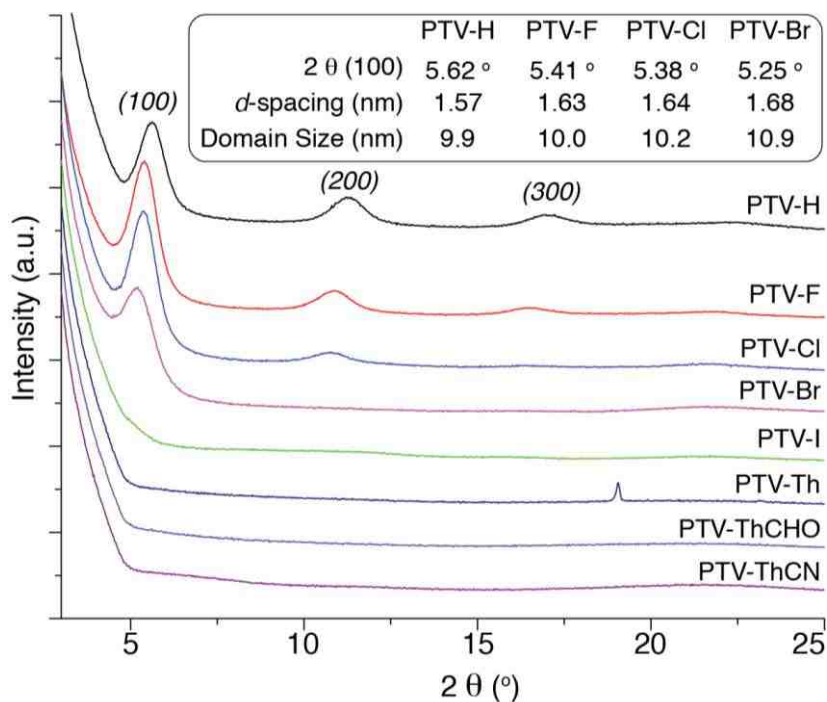


Figure 2.6. X-ray diffraction (XRD) profiles of thin films of PTVs. Corresponding *d*-spacings and domain sizes calculated from respective first-order scattering peaks are shown in insert.

We next employed Raman spectroscopy to probe the electronic and structural identities of the newly prepared PTV polymers, and the results are summarized in Figure 2.7. All polymers show very similar Raman scattering profiles, and the three major peaks between 1200 and 1600 cm^{-1} have been previously assigned to vinyl C–H bend, ring C=C stretch, and vinyl C=C stretch (from low to high Raman shifts).⁵⁹ These peaks experience a slight

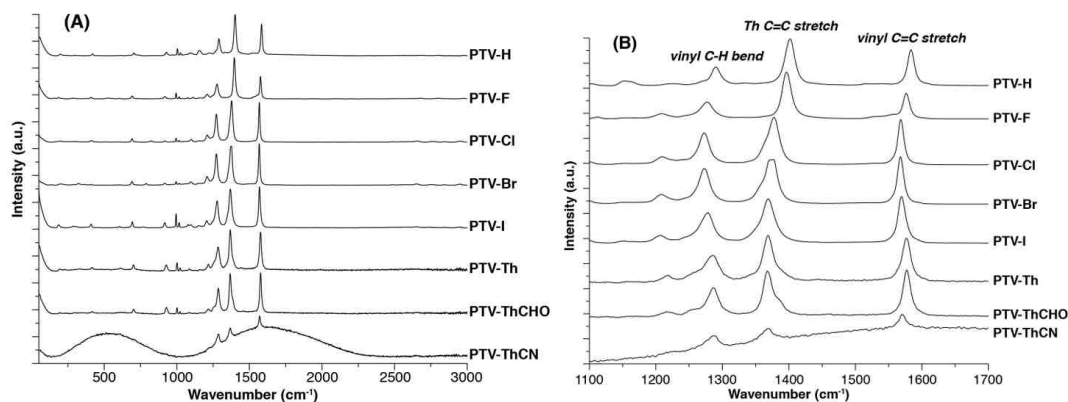


Figure 2.7. (A) Raman spectra of chlorobenzene solutions of halogenated and cross-conjugated PTVs; (B) expanded region of the Raman spectra between 1100 and 1700 cm^{-1} .

red-shift in halogen-substituted and cross-conjugated PTVs relative to those in PTV-H, while such shifts are smaller in cross-conjugated PTVs. These decreases in vibrational frequencies indicate weakening of the strengths of the bonds involved, presumably caused by the electron-withdrawing and conjugation effects from the halogen and cross-conjugated side-chains. Interestingly, two broad peaks centered at ca. 520 and 1620 cm^{-1} are observed for PTV-ThCN, which are absent for the other polymers. We suspect that these broad signals can potentially originate from weak fluorescence of PTV-ThCN since the DFT calculations indicated different electronic structures of this polymer due to strong electron-withdrawing cyanoester groups. We thus performed UV-vis absorption and fluorescence emission spectroscopy measurements on these PTV polymers both in dilute solutions and as thin films, and the spectra are shown in Figures 2.8, 2.9, and 2.10. We also performed cyclic voltammetry on these polymers to assess the frontier energy levels, and the results are summarized in Table 2.1 and Figure 2.11.

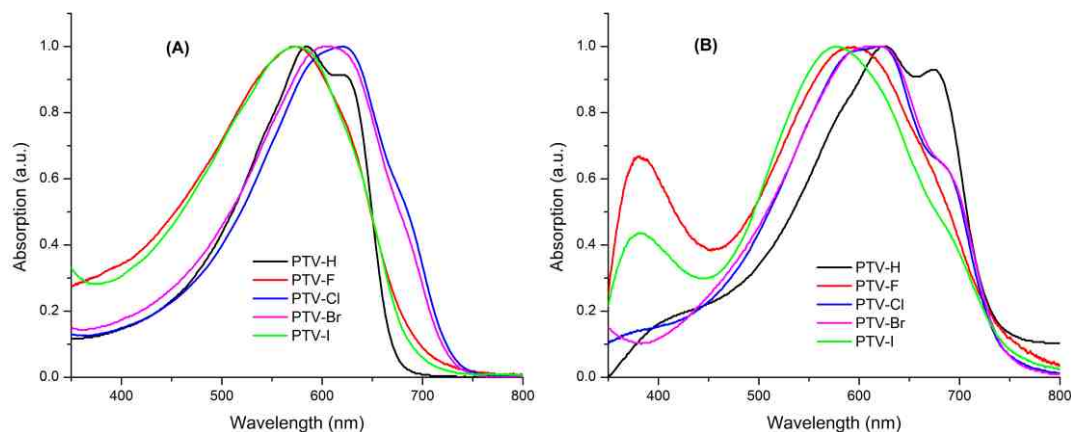


Figure 2.8. UV-vis absorption spectra of halogenated PTV polymers (A) in chlorobenzene solutions (10^{-5} M) and (B) as thin films spun-cast on glass substrates.

The halogenated PTVs show very similar absorption profiles with those of PTV-H, except for PTV-I. The λ_{max} of PTV-I is more blue-shifted, and its absorption profiles are less structured than those of PTV-H and other PTV-X's both in solutions and as thin films. Such deviation is caused by the low molecular weight of PTV-I and the presence of oligomeric species having chain lengths shorter than the persistence length. We thus exclude PTV-I in the following discussions. The other PTV-X's and PTV-H display three nearly identical absorption peaks at ca. 585, 625, and 675 nm that do not change noticeably from solutions to films. In solutions, PTV-H displays only two peaks at 585 and 625 nm, while in thin films, the 675 nm peak becomes significantly enhanced and the 585 nm peak becomes relatively suppressed. Such behaviors are reminiscent of red chain polydiacetylenes (PDAs)^{76, 77} and have been ascribed to aggregation of polymers and more pronounced J-type aggregates.⁷⁸⁻⁸⁰ For PTV-X's in solutions, the shoulders at 675 nm are clearly observed, which indicates higher degree of aggregation of these halogenated PTVs. This is consistent with our ^1H NMR analyses in which PTV-F, PTV-Cl, and PTV-Br all

display much broader signals than those of PTV-H. Such aggregation tendency is possibly induced by halogen-halogen and halogen-hydrogen interactions. On the other hand, in thin films of these polymers, PTV-H displays the highest relative intensity of the 675 nm peak, followed by PTV-F, while PTV-Cl and PTV-Br have very similar profiles having slightly enhanced intensity of this 675 nm shoulder peak. These observations are consistent with our calculations and XRD measurements, which suggest PTV-H and PTV-F to possess the highest crystallinity and coplanarity in the solid state, thus favoring more enhanced J-type aggregates. From the absorption onsets, the optical bandgaps of thin films of PTV-H and PTV-X's are nearly identical while CV measurements show that the HOMO and LUMO energy levels of PTV-X's are respectively lowered by similar amounts from those of PTV-H. Although the electronic contributions from different halogen substituents, including electron-withdrawing and resonance effects, are expected to be different, increased disruptions of main-chain coplanarity with bigger halogen atoms seemingly offset the electronic effects, leading to very similar optical properties between the PTV-X's and PTV-H.

Interestingly, the cross-conjugated PTVs display distinctly different optical properties as shown in Figure 2.9. Unlike PTV-H and PTV-X's that show similar absorption profiles, absorption spectra of the cross-conjugated PTVs contain intense high-energy electronic transitions at ca. 312, 306, and 370 nm in solutions and at 327, 307, and 376 nm in thin films, for PTV-Th, PTV-ThCHO, and PTV-ThCN, respectively. These peaks are attributed to the conjugated side-chains, and the slight redshifts from solutions to thin films are

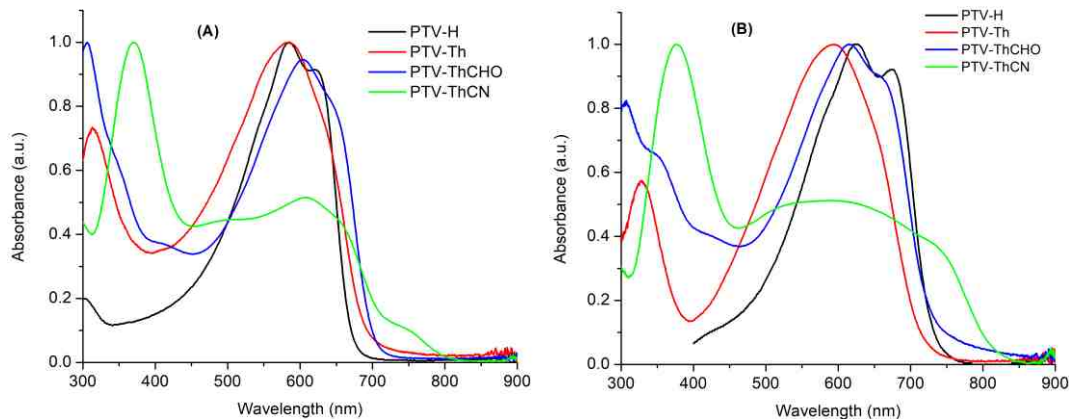


Figure 2.9. (A) UV-vis absorption spectra of cross-conjugated PTV polymers in chlorobenzene solutions (10^{-5} M); (B) UV-vis absorption spectra of cross-conjugated PTVs as thin films spun-cast on glass substrates.

presumably caused by planarization due to aggregation. The absorption profiles between 400 and 700 nm, corresponding to the PTV mainchains, are little structured for the cross-conjugated PTVs while the λ_{max} 's for PTV-Th, PTV-ThCHO, and PTV-ThCN are respectively located at 585, 605, and 610 nm in solutions and at 593, 615, and 590 nm in thin films. The very similar absorption profiles in both solutions and thin films confirm the amorphous nature of these cross-conjugated PTVs, consistent with the XRD observations. Intriguingly, a low-energy shoulder peak between 700 and 800 nm is observed for PTV-ThCN, which leads to a low bandgap of ca. 1.5-1.6 eV and is absent for any other PTVs in this study. As indicated from theoretical calculations, we assign this electronic transition to main-chain to side-chain intramolecular charge transfer (ICT) transition. ICT transitions have been the basic concept in constructing low bandgap conjugated polymers by using alternating electron-rich and electron-poor building blocks, which seems also effective in lowering the bandgaps in cross-conjugated systems like the PTV-ThCN studied here. Since

the Raman spectra indicated possible fluorescence of PTV-ThCN, we also performed

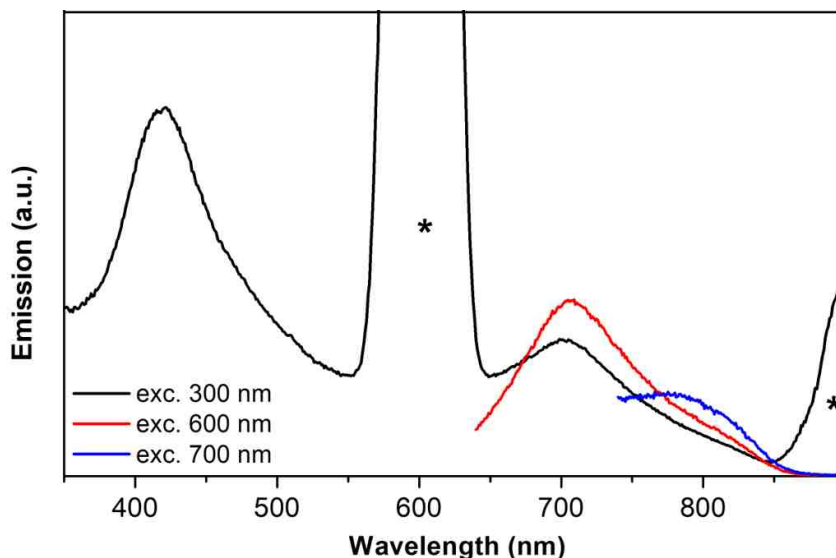


Figure 2.10 Emission spectra of PTV-ThCN in chlorobenzene solution (10^{-5} M); peaks marked with asterisks are due to higher order diffraction of the excitation light.

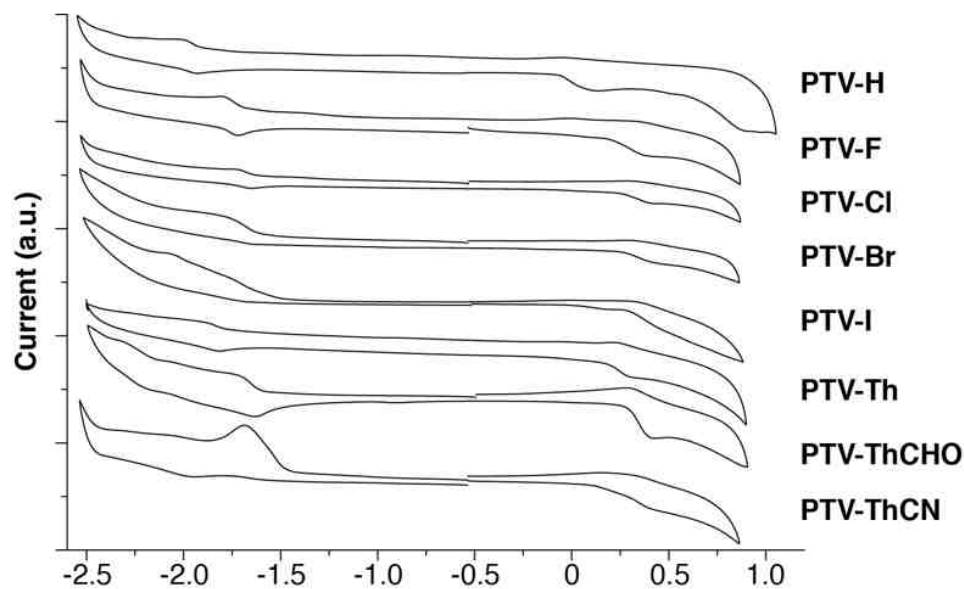


Figure 2.11. Cyclic voltammetry (CV) graphs of solutions (1 mM in THF) of halogenated and cross-conjugated PTV polymers. Voltages are referenced to ferrocene redox couple (-4.8 eV). The supporting electrolyte is 0.1 M Bu_4NPF_6 in acetonitrile. Scan rate: 100 mV/S.

emission measurements on this polymer in solution. Indeed, three emission peaks centered

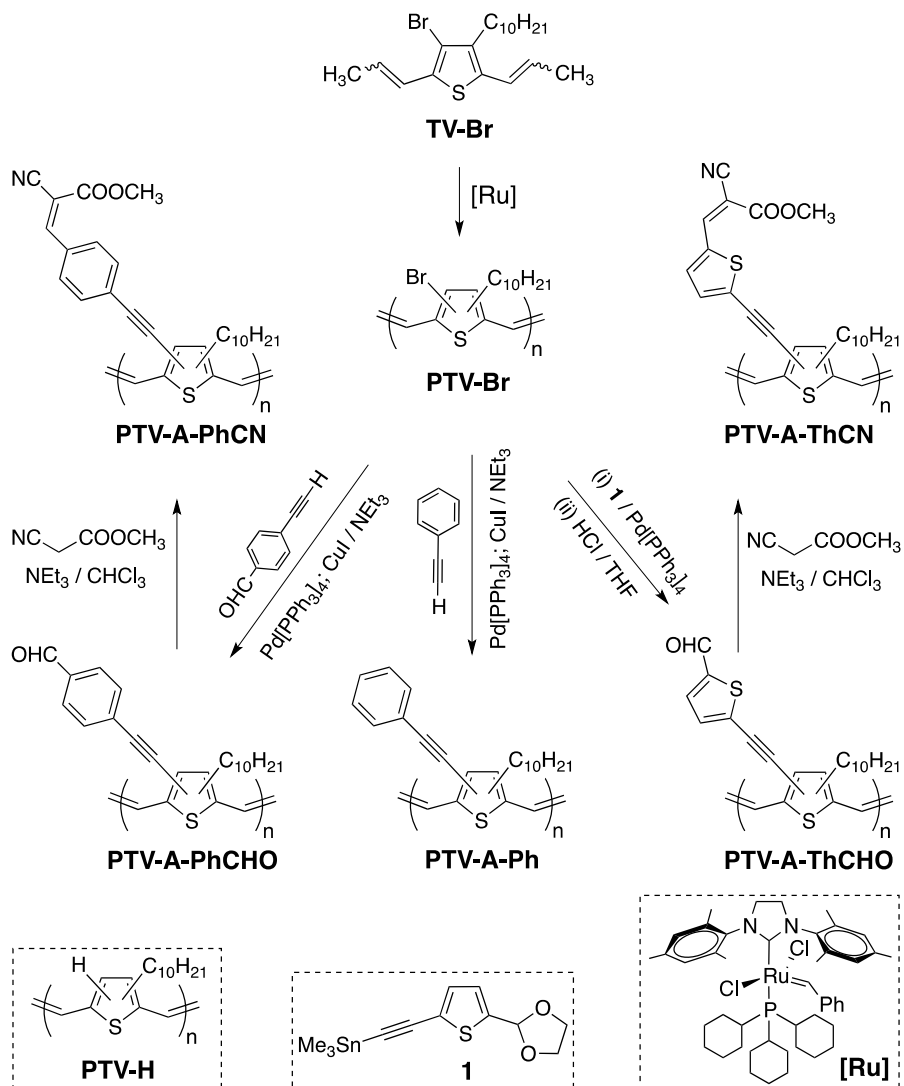
at ca. 420, 700, and 780 nm are observed as shown in Figure 2.10. We tentatively assign the 420 nm peak to emission from the side-chain only and the other two low-energy emissions from the main-chain to side-chain ICT transitions. From CV measurements (Figure 2.11), HOMO and LUMO levels of the cross-conjugated PTVs are both lowered when compared with those of PTV-H, while PTV-ThCN possesses the deepest LUMO level and PTV-ThCHO has the lowest HOMO level. Noticeably, the HOMO level of PTV-ThCN is elevated when compared to those of the other two cross-conjugated PTVs despite the strongly electron-withdrawing side-chains. We do not understand this abnormality that may merit more sophisticated theoretical calculations in the future.

2.3 Synthesis, Characterization and Discussion of Alkyne-containing PTVs

As discussed in section 2.2, we have developed a facile method based on ADMET^{55, 81-84} and post-polymerization modification techniques for the access of a series of cross-conjugated PTVs having differently substituted 2-thienyl groups directly attached to every main-chain thiophene repeat unit.⁸⁵ It was found that side-chains bearing strongly electron withdrawing substituents led to polymers possessing reduced bandgaps and rarely observed fluorescence, mainly resulted from main-chain to side-chain intramolecular charge transfer excitations. On the other hand, caused by steric repulsion, the main-chain and side-chain thiophene rings in these cross-conjugated PTVs are twisted out of plane, leading to diminished crystallinity and potentially reduced main-chain/side-chain electronic communication. Herein, we report the synthesis of a new series of cross-conjugated PTVs having phenyl and thienyl-based side-chains connected to the main-chain thiophene rings

through triple bonds that are expected to eliminate steric repulsion and induce more planar structures. Physical and electronic properties of these polymers are studied in detail, and their application in OSCs was evaluated.

Detailed synthetic procedures are summarized in Scheme 2.2 and physical and electronic



Scheme 2.2 Synthesis of Alkyne-spaced Cross-conjugated Polymers.

properties of the PTVs are compiled in Table 2.2. Our method is based on ADMET polymerization of a single monomer, TV-Br, and subsequent modification on the same

brominated PTV polymer, PTV-Br. Such post-polymerization modification method allows systematic installment of cross-conjugated functional groups that may not be compatible with the polymerization method. For example, the triple bonds present in all cross-conjugated PTVs, if pre-installed on the monomer structures, can potentially interfere with the ruthenium metathesis catalysts applied. The synthesis of TV-Br and PTV-Br, as well as the unfunctionalized PTV-H, was reported previously.⁸⁵ One thing worth pointing out is that it was crucial to add ca. 10 mol% CuBr as a Lewis acid additive in order to speed up the ADEMT polymerization rate and to afford polymers with reasonably high molecular weights. Sonagashira coupling reactions were exclusively applied to install the alkyne-spaced cross-conjugated side-chains. Five such polymers will be discussed in detail, namely PTV-A-Ph, PTV-A-PhCHO, PTV-A-PhCN, PTV-A-ThCHO, and PTV-A-ThCN (see Scheme 2.2 for structures), having alkyne spaced side-chains with phenyl or thienyl moieties bearing aldehyde or strongly electron withdrawing cyanoester substituents.

The post-polymerization modification reactions on PTV-Br were closely monitored by ¹H NMR spectroscopy and the corresponding spectra are overlaid in Figure 2.12. Upon replacement of the bromine atoms in PTV-Br with the various alkyne spaced side-chains, the broad signals at ca. 6.9 ppm, corresponding to the double bond protons, systematically shift toward lower field and overlap with proton signals from the aromatic side groups. The signals at ca. 2.6 ppm from the -CH₂ protons attached to thiophene rings in PTV-Br also experience slight down-field shifts upon the PPM reactions, the extents of which were larger in polymers containing phenyl substituents than those having thiophene side-chains.

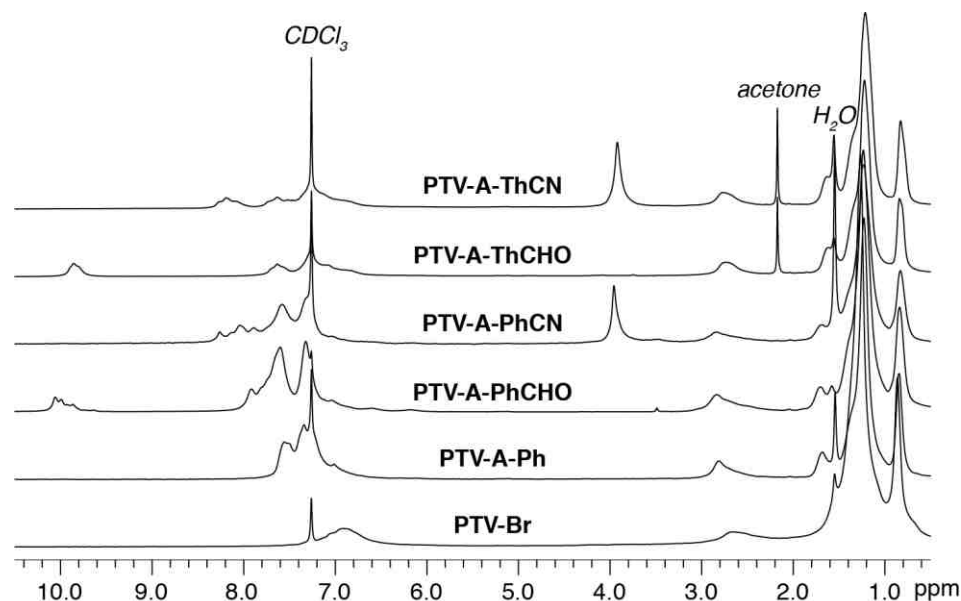


Figure 2.12. ^1H NMR spectra of the cross-conjugated PTVs in CDCl_3 .

Table 2.2. Physical and Optical Properties of the PTV Polymers.

PTV-	H	Br	A-Ph	A-PhCHO	A-PhCN	A-ThCHO	A-ThCN
M_n (kDa) ^a	12.0	14.0	13.1	13.5	13.6	13.8	14.2
\bar{D} ^b	1.8	2.3	1.9	1.8	1.8	1.7	1.6
λ_{sol} (nm) ^c	585	607	345, 619	363, 636	369, 644	382, 652	413, 671
λ_{film} (nm) ^d	628	617	343, 645	362, 652	378, 663	388, 681	424, 703
E_g^{opt} (eV) ^e	1.84 (1.71)	1.71 (1.68)	1.70 (1.59)	1.63 (1.55)	1.59 (1.52)	1.58 (1.50)	1.53 (1.48)
HOMO (eV) ^f	-4.76	-5.05	-5.10	-5.02	-5.08	-4.90	-5.15
LUMO (eV) ^g	-2.94	-3.22	-3.21	-3.30	-3.58	-3.40	-3.63
E_g^{CV} (eV) ^h	1.82	1.83	1.89	1.72	1.50	1.50	1.52

^a Number average molecular weight estimated from size exclusion chromatography (SEC) against polystyrene standards. ^b Dispersity index. ^c Absorption maxima in chlorobenzene solution (ca. 10^{-5} M repeat unit). ^d Absorption maxima of polymer thin films on glass substrates. ^e Electronic bandgap estimated from optical absorption onsets, thin film data in parentheses. ^f Highest occupied molecular orbital energy estimated from cyclic voltammetry. ^g Lowest unoccupied molecular orbital energy estimated from cyclic voltammetry. ^h Electronic bandgap estimated from cyclic voltammetry.

Such down-field shift trends in proton signals are likely caused by anisotropic effects from

the triple bond and aromatic side groups. More distinct changes are observed from the appearance of -CHO signals at ca. 10 ppm and ca. 9.8 ppm for PTV-A-PhCHO and PTV-A-ThCHO, and the cyanoester methyl signals at ca. 3.9 ppm and ca. 3.8 ppm for PTV-A-PhCN and PTV-A-ThCN, respectively. Integrations of these signals indicate ca. one side-chain per main-chain thiophene unit, suggesting nearly quantitative, if not absolutely 100%, functionalization and the effectiveness of our post-polymerization modification method. It is worth noting that the signals from -CHO groups appear to be multiplets, presumably caused by the different arrangements of neighboring groups due to *regio*-random nature of the PTVs, which is expected from ADMET polymerization and consistent with our previous results.⁸⁵ SEC profiles of all PTVs are shown in Figure 2.13. All PTVs display

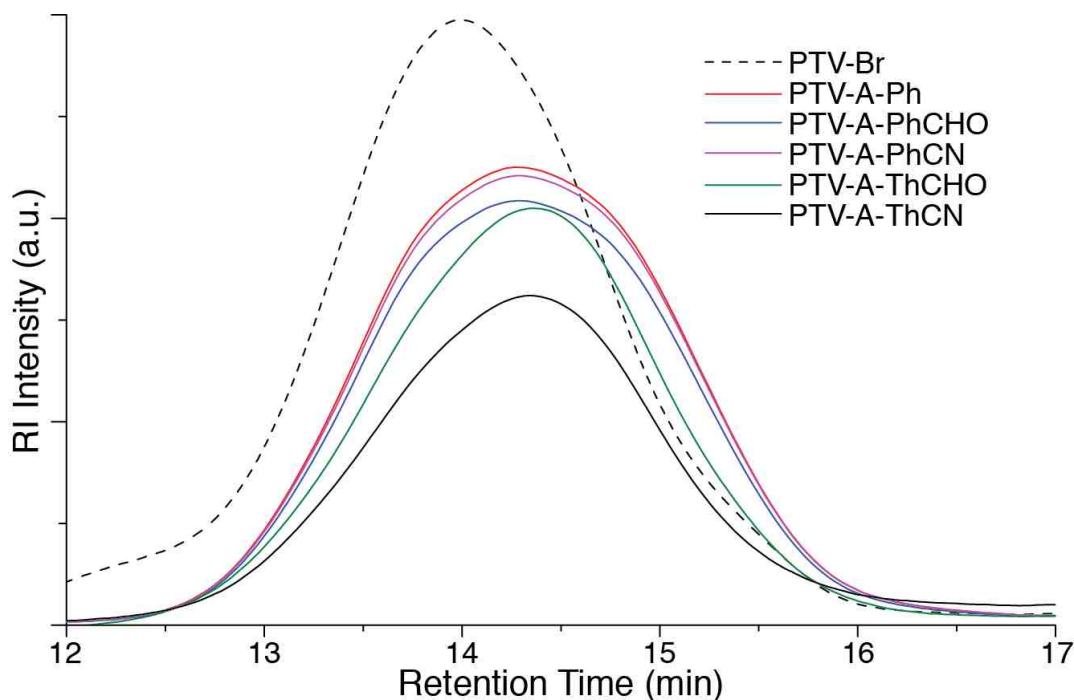


Figure 2.13. Size exclusion chromatography (SEC) profiles of the cross-conjugated PTV polymers in CH_3Cl (1 mL/min, RI detector).

mono-modal profiles while those of the cross-conjugated PTVs become slightly broadened and all shift toward higher evolution times, leading to apparent lower molecular weights. We suspect such observations are caused by column-polymer interactions, likely from the triple bonds and polar side-chains, since we could not observe any signs of polymer degradation or cross-linking during the post-polymerization modification reactions by NMR spectroscopy and other analyses discussed below.

We further characterized these new PTVs by infrared (IR) and Raman spectroscopy, and the results are shown in Figure 2.14 and 2.15, respectively. From the IR spectra, the

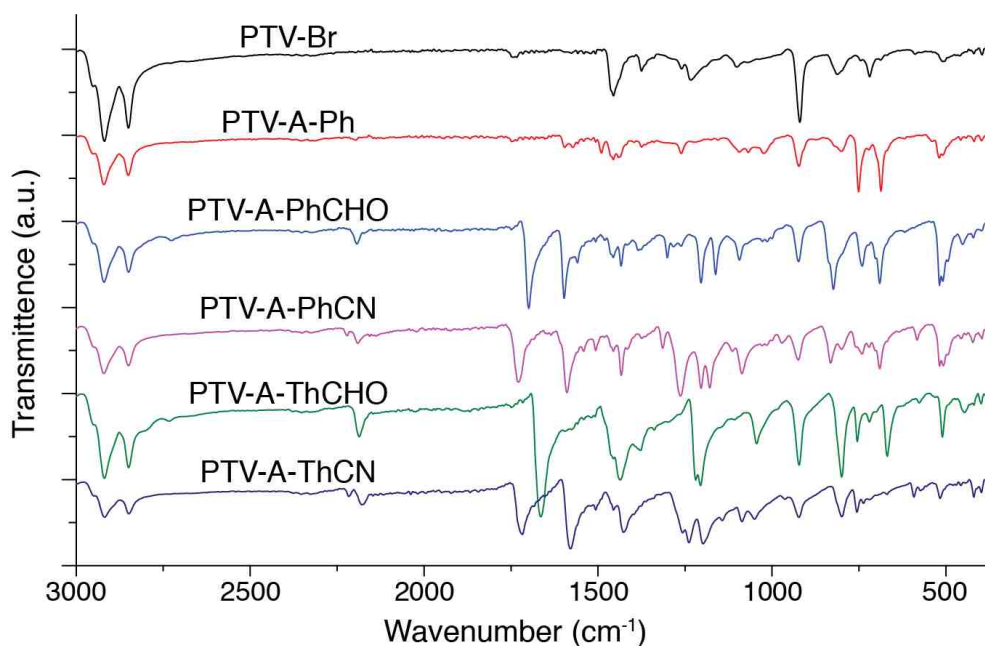


Figure 2.14. Infrared (IR) spectra of the cross-conjugated PTVs as powders in attenuated total reflection (ATR) mode.

signals from carbon-carbon triple bond stretching mode at ca. $2170\text{-}2200\text{ cm}^{-1}$ are clearly observed for the cross-conjugated PTVs, except for PTV-A-Ph where only a very weak signal can be identified. The vibration frequencies generally red-shift slightly from phenyl

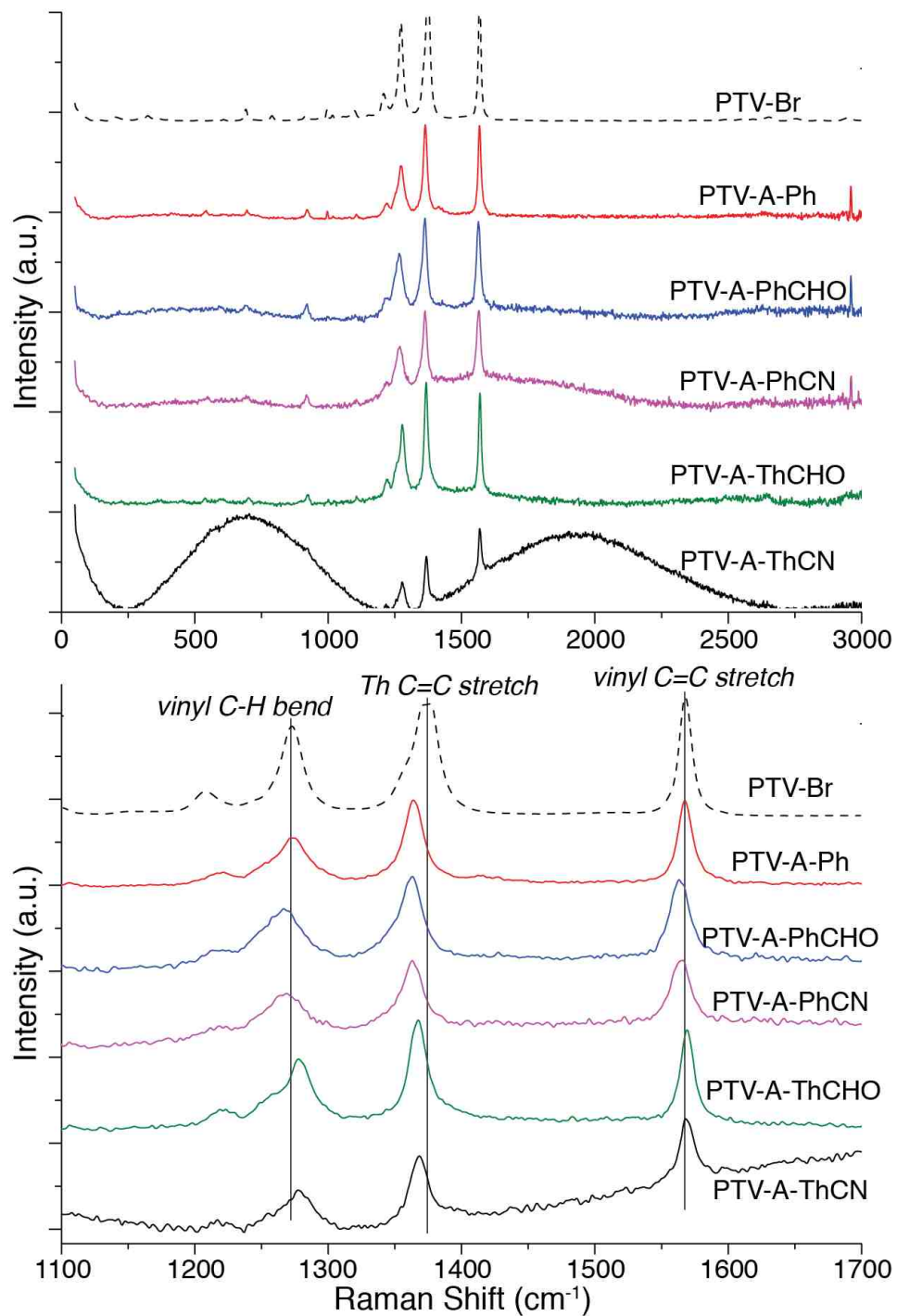


Figure 2.15. Raman spectra of the cross-conjugated PTVs in chlorobenzene solutions. The bottom panel displays the magnified region between 1100 and 1700 cm^{-1} .

side-groups to thienyl side-groups, and from aldehyde to cyanoester substituents. Such

trend is understandable in that the bond strengths of triple bonds are slightly reduced through electronic delocalization in systems containing less aromatic thienyl moieties and cyanoester substituents that are strongly electron withdrawing and are longer in conjugation length. Small signals at ca. 2230 and 2219 cm^{-1} are respectively observed for PTV-A-PhCN and PTV-A-ThCN, corresponding to the cyano group stretching mode. The red-shifted signal in the later also suggests enhanced electronic delocalization in the thiophene containing side-chains, which can potentially pose stronger effects in perturbing the PTV main-chain electronic properties (*vide infra*). On the other hand, the Raman spectra of the cross-conjugated PTVs are very similar to each other. Compared with that of PTV-Br, the stretching frequencies of the thiophene carbon-carbon double bonds in cross-conjugated PTVs slightly red-shift, likely caused by electronic delocalization to the conjugated side-chains. Interestingly, there are two broad signals centered around 700 cm^{-1} and 1900 cm^{-1} in the Raman spectrum of PTV-A-ThCN, which are absent in those of the other PTVs. We suspect that these broad signals are weak background emission from this polymer, likely resulted from the main-chain to side-chain charge transfer excitation. We have thus performed absorption and emission experiments on the PTV polymers in both dilute solutions and as thin films, and the results are summarized in Figure 2.16.

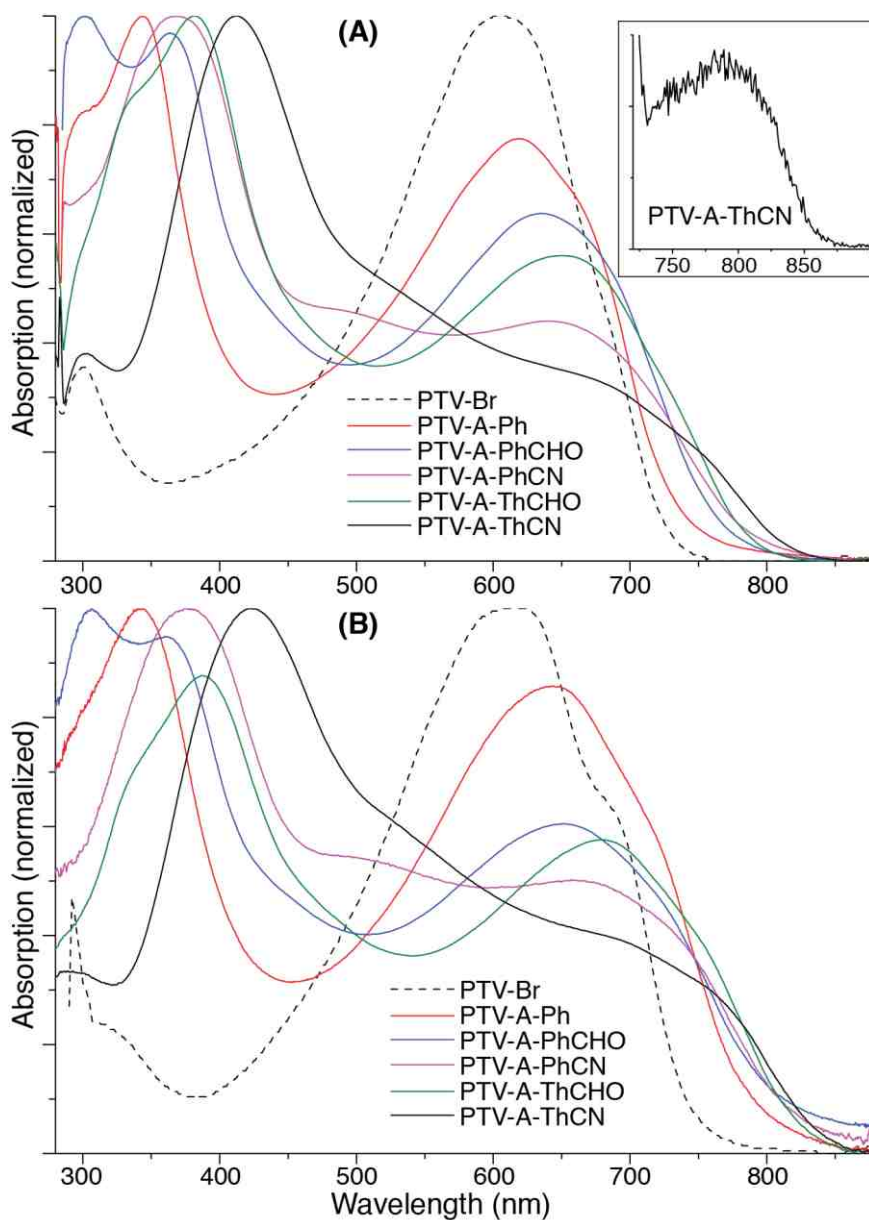


Figure 2.16. UV-vis absorption spectra of the cross-conjugated PTVs (A) in chlorobenzene solutions (10^{-5} M repeat units) and (B) as thin films drop cast from chlorobenzene solutions on glass substrates. Insert in (A): emission spectrum of PTV-A-ThCN in solution excited at 700 nm.

In the absorption spectra of cross-conjugated PTVs in solutions (Figure 2.16A), two major bands can be observed. The high energy bands ranging from ca. 350 nm to ca. 450 nm, which is absent in the spectrum of PTV-Br, can be ascribed to originate from the

conjugated side-chains. This band continually red-shifts when the aromatic side-chain substituents change from phenyl to thienyl groups and from aldehyde to cyanoester functionalities. This trend is consistent with our observations in IR and Raman measurements such that the electronic delocalization is most pronounced in the side-chains of PTV-A-ThCN. The main absorption bands between 500 nm and 800 nm are from the PTV main-chains with λ_{\max} values systematically increases from 607 nm for PTV-Br, to 619 nm for PTV-A-Ph, and eventually to ca. 670 nm for PTV-A-ThCN. Optical bandgaps estimated from the absorption onsets follow the same trend giving PTV-A-ThCN the lowest solution bandgap of ca. 1.53 eV. It is clear that the cross-conjugation not only broadens the PTV absorption ranges by adding the high energy absorption features intrinsic to the side-chains themselves but also perturbs the main-chain electronic properties through electronic conjugation with the side-chains. This effect seems the strongest if the side-chains possess longer conjugation, enhanced electronic delocalization, and electron withdrawing substituents. Close examination of the absorption spectrum of PTV-A-ThCN reveals a long wavelength shoulder at ca. 750 nm, which we attribute to main-chain to side-chain charge transfer excitation. This charge transfer peak is almost identical to that of our previously reported PTV-ThCN polymer having identical cross-conjugated cyanoester thienyl side-chains but without the alkyne spacers. Large dihedral angles were found between the side-chain and main-chain thienyl rings in PTV-ThCN, which has been thought to reduce main-chain to side-chain electronic communication. Insertion of alkyne spacers can potentially eliminate such steric repulsion and leads to more planar structures,

as demonstrated by density functional theory (DFT) calculations below. On the other hand, the electron deficient alkyne spacers seem to decrease electronic communications between the main-chain and side-chain cyanoester groups, resulting in similar overall charge transfer absorption peaks in PTV-A-ThCN and PTV-ThCN. Interestingly, when excited at 700 nm, PTV-A-ThCN gives weak fluorescence centered around 800 nm, which is also similar to that of PTV-ThCN. When cast into thin films, absorption spectra of all the cross-conjugated PTVs remain similar in shape and experience small red-shift in λ_{max} by 16-29 nm. Highly crystalline PTV-H has been shown to experience large bathochromic shift from solutions to the solid state and shows more structured absorption spectra in films. The lack of significant spectral red-shift and the similarity between solution and film absorption profiles suggest lack of crystallinity in the cross-conjugated PTVs. Indeed, we have performed differential scanning calorimetry (DSC) and XRD measurements on powders of the cross-conjugated PTVs, and respectively did not find any thermal transitions or scattering peaks, both of which suggest amorphous nature of the cross-conjugated PTVs.

HOMO and LUMO energies of the newly synthesized cross-conjugated PTVs were estimated by CV measurement on thin films as shown in Figure 2.17 and Table 2.2. All polymers displayed pseudo-reversible oxidation and non-reversible reduction events. From the oxidation onsets, the HOMO energy levels of the cross-conjugated PTVs are all significantly lower than that of PTV-H, while the HOMO levels of PTVs containing phenyl and cyanoester groups in the side-chains are respectively lower than those containing thienyl and aldehyde groups in the side-chains. Similar trend is observed in the LUMO

energy levels of the cross-conjugated PTVs, and PTV-A-ThCN has the deepest LUMO

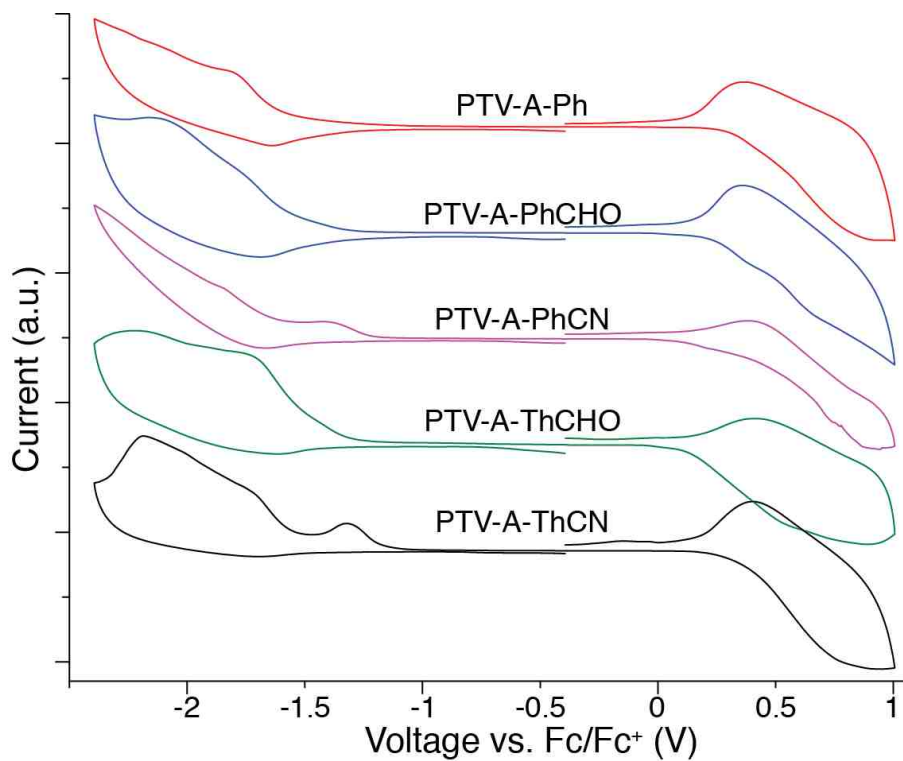


Figure 2.17. Cyclic voltammograms (CV) of thin films of the cross-conjugated PTVs deposited onto the glassy carbon working electrodes (supporting electrolytes: 0.1 M Bu_4NPF_6 in acetonitrile, scan rate: 100 mV/s).

level of ca. -3.63 eV.

In order to aid understanding on the structure-property relationships of these cross-conjugated PTVs, we have performed DFT calculations (B3LYP, 6-31G*) on representative oligomers containing five main-chain thienyl rings terminated with propenyl groups on both ends and long alkyl side-chains replaced with methyl groups, and the results are shown in Figure 2.18. It is clearly observed that the cross-conjugated PTVs have almost completely planar structures, which is in contrast to those previously reported PTVs bearing identical aromatic side-chains but without the alkyne spacers, where large main-

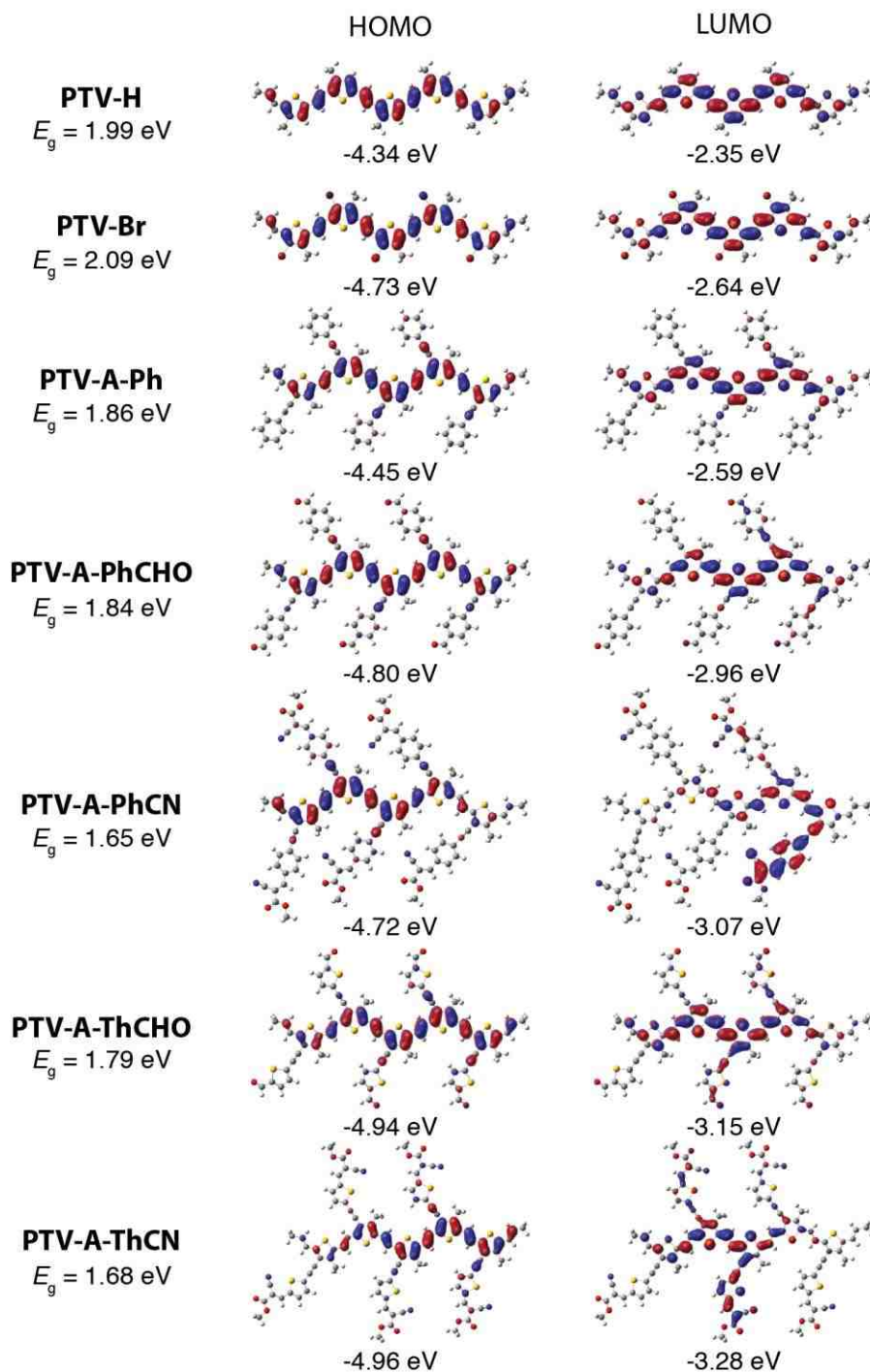


Figure 2.18. Density functional theory (DFT, B3LYP, 6-31G*) calculation results of the cross-conjugated PTVs. The structures contain five main-chain thienyl groups terminated with propenyl groups on both ends. Long alkyl side-chains are replaced with methyl groups.

chain to side-chain dihedral angles of ca. 60° were found. However, the alkyne-spaced

cross-conjugated PTVs are still amorphous in the solid state despite the calculated planarity. We speculate that such lack of solid state order may stem from the *regio*-randomness of the polymers and thus our ongoing efforts are focused on preparing *regio*-regular PTVs possessing cross-conjugated side-chains with and without alkyne spacers. From the calculations, the HOMO and LUMO orbitals are exclusively localized along the main-chains for the PTV structures considered, except for those of PTV-A-PhCN and PTV-A-ThCN, where the LUMO orbitals are delocalized into the side-chains. Such main-chain to side-chain charge transfer HOMO-LUMO transitions are in agreement with the optical measurements.

2.4 Application in solar cell devices

OSCs are considered as promising low-cost and renewable alternative energy sources, and PSCs have attracted the most attention due to their amenability to large throughput roll-to-roll and inkjet printing techniques.^{86, 87} The attractiveness of low bandgap CPs for OSCs thus arises from the ability to absorb a larger portion of the red and near-IR photons in the solar spectrum, one of the prerequisites for high performance devices. Despite the low bandgaps, PTVs applied in OSCs to date have all shown poor efficiencies typically less than 1%. With the structural variations described above, we applied the newly synthesized PTVs in OSCs in order to further study the *structure-property-function* relationships in these materials. Conventional single junction device geometries of ITO/glass/MoO₃ (10nm)/organic layer (100 nm)/Al (100 nm) were applied. Devices using each polymer have been optimized separately by changing the polymer/PCBM ratios, thermal

annealing time and temperature, and solvent annealing conditions.

2.4.1 Solar Cell Performance of Halogenated and Cross-conjugated PTVs

Table 2.3. Optimized OSC Device Performances Employing Halogenated and Cross-Conjugated PTV Polymers.^a

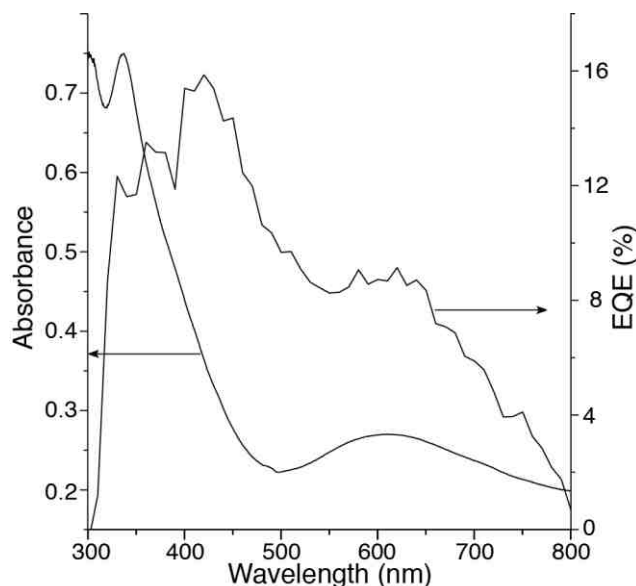


Figure 2.19. Absorption profile (left axis) and external quantum efficiency (EQE) trace (right axis) of the optimized device employing PTV-ThCN and PCBM (1/4 by wt.).

^a Average numbers and standard deviations from at least five devices under optimized conditions are given. Highest parameter numbers are given in parentheses. ^b Weight ratio. ^c Short circuit current. ^d Open circuit voltage. ^e Fill factor. ^f Power conversion efficiency.

Solar cell performance of halogenated and cross-conjugated PTVs are summarized in Table 2.3. Devices employing PTV-H give average power conversion efficiencies of ca. 0.5% that is similar to those obtained from previous attempts.^{88, 89} Except for PTV-F, all other functionalized PTVs displayed improved performance with PTV-ThCHO and PTV-ThCN having the best average *PCEs* of ca. 1.4%, a nearly 3-fold increase from that of PTV-H. The improvement comes from increases in all three device parameters including J_{sc} , V_{oc}

and *FF*. Since PTV-ThCN showed unique optical properties, we also studied its devices in more detail by measuring the external quantum efficiencies (EQE) as shown in Figure 2.19. The EQE trace follows the device absorption profile except in the blue region, where the absorption of excess PCBM dominates. The spectral response between 700 nm and 800 nm confirms photocurrent generation from the main-chain to side-chain ICT transitions.

2.4.2 Solar Cell Performance of Alkyne-containing PTVs

Table 2.4. Optimized OSC Device Performances Employing Alkyne-containing PTV Polymers.^a

PTV	Br	A-Ph	A-PhCHO	A-PhCN	A-ThCHO	A-ThCN
<i>Ratio</i> ^b	1:2	1:3	1:3	1:3	1:2	1:3
<i>J_{sc}</i> ^c	2.85 ± 0.46 (3.40)	1.65 ± 0.26 (1.96)	1.57 ± 0.30 (2.05)	1.71 ± 0.31 (2.03)	2.33 ± 0.51 (3.20)	2.61 ± 0.32 (3.09)
<i>V_{oc}</i> ^d	0.69 ± 0.01 (0.70)	0.62 ± 0.01 (0.64)	0.63 ± 0.00 (0.63)	0.64 ± 0.01 (0.64)	0.72 ± 0.01 (0.74)	0.75 ± 0.00 (0.76)
<i>FF</i> ^e	51 ± 2 (55)	49 ± 4 (52)	40 ± 4 (46)	41 ± 2 (44)	48 ± 2 (51)	55 ± 1 (56)
<i>PCE</i> ^f	1.00 ± 0.14 (1.17)	0.50 ± 0.11 (0.63)	0.39 ± 0.07 (0.47)	0.44 ± 0.09 (0.56)	0.81 ± 0.22 (1.17)	1.08 ± 0.13 (1.28)

^a Average numbers and standard deviations from at least five devices under optimized conditions are given. Highest parameter numbers are given in parentheses. ^b Weight ratio of PTVs and PCBM. ^c Short circuit current, unit in mA/cm^2 . ^d Open circuit voltage. ^e Fill factor. ^f Power conversion efficiency.

OSC devices employing Alkyne-containing PTVs were also fabricated and tested and the results are summarized in table 2.4. The *PCE* of OSC devices employing PTV-H is limited to ca. 0.5%, consistent with previously reported values. As expected, the *V_{oc}* values of devices applying alkyne-containing PTVs all increase due to the lower lying HOMO levels that has been shown to be a determining factor in device voltages.⁹⁰ Most of the

alkyne-containing PTVs show improved FF s but the PTVs containing phenyl side-chains all display smaller short circuit currents (J_{SC}), and the overall PCE s are comparable or even slightly worse than that of PTV-H. The best performance was found in devices employing PTV-A-ThCN, giving the highest V_{OC} of 0.75 V and the largest FF of 55%.

Although the overall device performances from these functionalized PTVs are still relatively low, our methodologies for the structural diversification of PTVs are effective in changing polymer physical and electronic properties and can potentially lead to more promising materials for OSCs as well as other electronic devices. We are currently studying the excited state dynamics and charge generation processes in more detail in order to obtain better understanding on the structure-property relationship in these functionalized PTVs.

2.5 Conclusion

In summary, we have developed facile methodologies based on ADMET and post-polymerization modification reactions for the preparation of a series of novel PTV polymers bearing halogens and cross-conjugated substituents at every thiophene ring along the polymer backbone. The halogen functionalized PTV-X's display similar optical properties and decreased crystallinity with increasing sizes of the halogen atoms. The brominated polymer, PTV-Br, was conveniently applied toward cross-conjugated PTVs having differently substituted thienyl side-chains. PTV-ThCN, PTV-A-PhCN and PTV-A-ThCN, having strong electron withdrawing cyanoester substituents, display low bandgaps of ca. 1.5 eV caused by main-chain to side-chain ICT transitions that have never been observed in conventional PTVs. The newly prepared PTVs showed improved OSC

performance with increasing in all three device parameters. Our synthetic methodology is highly versatile and can be applied to further synthesis of PTVs having tailor-designed structures in order to gain deeper understanding in electronic processes of this class of materials and to open up new opportunities in organic electronic devices.

2.6 Experimental

Materials and General Methods. All reagents and solvents were used as received from Sigma-Aldrich or Alfa Aesar unless otherwise noted. 3-decylthiophene (3DT) was synthesized according to a literature procedure.⁶² THF was distilled from Na/benzophenone prior to use. 300.13 MHz ¹H and 75.48 MHz ¹³C NMR spectra were recorded on a Bruker Avance III Solution 300 spectrometer. All solution ¹H and ¹³C NMR spectra were referenced internally to solvent signals. Size exclusion chromatography (SEC) analyses were performed in chloroform with 0.5% (v/v) triethylamine (1 mL/min) using a Waters Breeze system equipped with a 2707 autosampler, a 1515 isocratic HPLC pump and a 2414 refractive index detector. Two styragel columns (Polymer Laboratories; 5 μm Mix-C), which were kept in a column heater at 35 °C, were used for separation. The columns were calibrated with polystyrene standards (Varian). Infrared (IR) spectra were recorded on a Bruker Alpha-P instrument, using powder samples in ATR mode. Ultraviolet-visible (UV-vis) absorption spectra were recorded on a Shimadzu UV-2401 PC spectrometer over a wavelength range of 240–900 nm. Fluorescence emission and excitation spectra were obtained using a Varian Cary Eclipse Fluorometer. Raman spectra were obtained on a DXR SmartRaman spectrometer over a frequency range of 50.5–3350

cm⁻¹. Cyclic voltammetry was performed at 25 °C on a CH Instrument CHI604xD electrochemical analyzer using a glassy carbon working electrode, a platinum wire counter electrode, and a Ag/AgCl reference electrode calibrated using ferrocene redox couple (4.8 eV below vacuum). GC-MS measurements were performed on an Agilent 7820A system. X-ray diffraction data was collected using a Rigaku SmartLab diffractometer in Bragg-Brentano mode employing Cu K-alpha radiation and a D/tex 1-dimensional detector. A nickel filter was used to remove the Cu K-beta radiation component. Data was collected over the two-theta range 3 to 40 degrees using a 0.02-degree step size at a scan rate of 6.2 degree/minute. The domain sizes of the polymers were calculated through Scherrer equation from the first-order diffraction peak using the software JADE.⁷⁴

Solar Cell Fabrication and Testing. A conventional structure of ITO/MoO₃ (10 nm)/active layer (100 nm)/Al (100 nm) was adopted for the solar cells studies. Devices were fabricated according to the following procedures. Polymers and PCBM (American Dye Source, Inc.) at predetermined weight ratios were dissolved in chlorobenzene (CB) and stirred at 80 °C for 10 h in a nitrogen glovebox (Innovative Technology, model PL-He-2GB, O₂ < 0.1 ppm, H₂O < 0.1 ppm). ITO-coated glass substrates (China Shenzhen Southern Glass Display. Ltd, 8 Ω/□) were cleaned by ultrasonication sequentially in detergent, DI water, acetone and isopropyl alcohol, each for 15 min. These ITO-coated glass substrates were further treated by UV-ozone (PSD Series, Novascan) for 45 min before transferred into a nitrogen glovebox (Innovative Technology, model PL-He-4GB-1800, O₂ < 0.1 ppm, H₂O < 0.1 ppm) for MoO₃ deposition. MoO₃ (10 nm) was deposited

using an Angstrom Engineering Åmod deposition system at a base vacuum level $<7 \times 10^{-8}$ Torr. The blend solution was first filtered through a 0.45 μm PTFE filter and spin-coated on top of the MoO_3 layer at preset speeds for 30 s. Typical thickness of organic layers was ca. 100 nm. Al (100 nm) was finally thermally evaporated through patterned shadow masks as cathodes. Current–voltage (I–V) characteristics were measured by a Keithley 2400 source-measuring unit under simulated AM1.5G irradiation (100 mW cm^{-2}) generated by a Xe arc-lamp based Newport 67005150-W solar simulator equipped with an AM1.5G filter. The light intensity was calibrated by using a Newport thermopile detector (model 818P-010-12) equipped with a Newport 1916-C Optical Power Meter.

2,3,5-Tribromo-4-decylthiophene. To a stirring solution of 3-decylthiophene (5.57 g, 24.8 mmol) in AcOH (10 mL), was added Br_2 (10.2 mL, 0.196 mol) slowly. The reaction mixture was covered with Aluminum foil and kept at room temperature for 24 h. The reaction mixture was poured into Na_2SO_3 solution (50 mL) and extracted with diethyl ether ($2 \times 50 \text{ mL}$); the combined organic phase was then dried over anhydrous Na_2SO_4 . After solvent removal under reduced pressure, the residue was further purified by column chromatography over silica gel to give the title compound as a clear liquid (4.35 g, 38% yield). $^1\text{H NMR}$ (300MHz, CDCl_3): δ (ppm) = 0.86~0.90 (t, 3H), 1.27 (m, 14H), 1.51 (m, 2H), 2.61~2.66 (t, 2H).

3-Bromo-4-decyl-2, 5-dipropenylthiophene (TV-Br). 2,3,5-Tribromo-4-decylthiophene (3.86 g, 8.38 mmol) and tri-n-butyl(1-propenyl) tin (5.57 g, 16.8 mmol) were charged into a pressure vessel. $\text{Pd}(\text{PPh}_3)_4$ (484 mg, 0.419 mmol) and DMF (5 mL)

were added into the vessel in an argon filled glovebox. The mixture was stirred at 110 °C for 24 h. The reaction mixture was poured into water and extracted with diethyl ether (2×50 mL); the combined organic phase was then dried over anhydrous Na₂SO₄. After solvent removal under reduced pressure, the residue was further purified by column chromatography over silica gel to give the title compound as a light-yellow liquid (2.33 g, 72.6%). ¹H NMR (300MHz, CDCl₃): δ (ppm) = 0.86~0.90 (t, 3H), 1.26 (m, 14H), 1.47 (m, 2H), 1.86~2.02 (d, 6H), 2.57~2.64 (t, 2H), 5.65~6.20 (m, 2H), 6.44~6.68 (d, 2H).

3-Decyl-4-fluoro-2, 5-dipropenylthiophene (TV-F). To a stirring solution of TV-Br (0.560 g, 1.46 mmol) in THF (5.5 mL) was added n-butyllithium (0.88 mL, 2.19 mmol) slowly at -78 °C. After 20 minutes, a solution of N-fluorobenzenesulfonimide (921 mg, 2.92 mmol) in THF (5 mL) was added to the reaction mixture. The reaction mixture was stirred for 2 h at -78 °C and then kept at room temperature for 24 h. The reaction mixture was quenched with water and then extracted with diethyl ether (2×50 mL); the combined organic phase was dried over anhydrous Na₂SO₄. After solvent removal under reduced pressure, the residue was further purified by column chromatography over silica gel to give the title compound as a light-yellow liquid (275 mg, 58.4%). ¹H NMR (300MHz, CDCl₃): δ (ppm) = 0.88 (t, 3H), 1.25 (m, 14H), 1.50 (m, 2H), 1.85~2.01 (d, 6H), 2.43~2.54 (t, 2H), 5.60~6.09 (m, 2H), 6.40~6.55 (d, 2H). ¹⁹F NMR (282.4MHz, CDCl₃): δ (ppm) = -132.71, -130.59, -130.53, -128.49.

3-Chloro-4-decyl-2, 5-dipropenylthiophene (TV-Cl). TV-Br (1.00 g, 2.60 mmol), CuCl (7.37 g, 74.4 mmol) and DMF (5 mL) were charged into a pressure vessel in an argon

filled glovebox. The mixture was stirred at 110 °C for 72 h. The reaction mixture was poured into water (50 mL) and extracted with diethyl ether (2×50 mL); the combined organic phase was then dried over anhydrous Na₂SO₄. After solvent removal under reduced pressure, the residue was further purified by column chromatography over silica gel to give the title compound as a clear liquid (400 mg, 45% yield). ¹H NMR (300MHz, CDCl₃): δ (ppm) = 0.86~0.90 (t, 3H), 1.26 (m, 14H), 1.48 (m, 2H), 1.85~2.01 (d, 6H), 2.51~2.63 (t, 2H), 5.68~6.16 (m, 2H), 6.43~6.69 (d, 2H).

3-Decyl-4-iodo-2, 5-dipropenylthiophene (TV-I). To a stirring solution of TV-Br (300 mg, 0.78 mmol) in THF (5 mL) was added n-butyllithium (0.38 mL, 0.94 mmol) slowly at -78 °C. After 15 minutes, ICH₂CH₂I (308 mg, 1.1 mmol) was added. The reaction mixture was kept at -78 °C for 45 minutes and then was quenched with Na₂S₂O₃ solution. The mixture was extracted with diethyl ether (2×20 mL); the combined organic phase was dried over anhydrous Na₂SO₄, and the solvent was removed under reduced pressure to give the title compound as yellow liquid (300 mg, 89.1%). ¹H NMR (300MHz, CDCl₃): δ (ppm) = 0.86~0.90 (t, 3H), 1.26 (m, 14H), 1.43 (m, 2H), = 1.84~2.02 (d, 6H), 2.56~2.69 (t, 2H), 5.66~6.21 (m, 2H), 6.46~6.54 (d, 2H).

PTV-F. In a two-neck round bottom flask equipped with a condenser and rubber septum were added TV-F (200 mg, 0.62 mmol) and CuI (11.8 mg, 0.062 mmol). Grubbs 2nd generation catalyst (5.26 mg, 0.0062 mmol) in 0.8 mL 1, 2, 4-trichlorobenzene was then added and the reaction mixture was kept under dynamic vacuum while the condenser was cooled to 5 °C using a circulating chiller. The reaction mixture was gradually heated to

90 °C over 4 h and refluxed for 24 h. The reaction mixture was cooled down to room temperature and 5.26 mg Grubbs 2nd generation catalyst in 0.8 mL 1, 2, 4-trichlorobenzene was added and the reaction mixture was refluxed at 90 °C under dynamic vacuum for another 24 h. Such process was repeated for a total of 5 times and the mixture was poured into methanol (100 mL) to precipitate the polymer, which was purified by Soxhlet extraction with methanol, acetone, hexanes and chloroform to give the title compound as a black solid (70 mg, 42.4% yield). ¹H NMR (300MHz, CDCl₃): δ (ppm) = 0.87 (t, 3H), 1.27 (m, 14H), 1.56 (m, 2H), 2.57 (t, 2H), 6.85 (m, 2H). ¹³C NMR (75.48 MHz, CDCl₃): δ (ppm) = 14.11, 22.70, 25.12, 29.37, 29.65, 29.95, 31.92, 115.39, 118.80, 130.33, 133.01, 152.50, 156.08. ¹⁹F NMR (282.4MHz, CDCl₃): δ (ppm) = -126.79. SEC (CHCl₃, 1 mL/min): *M_n* = 17.8 KDa, *M_w* = 35.8 kDa, *D* = 2.0.

PTV-Cl. In a two-neck round bottom flask equipped with a condenser and rubber septum were added TV-Cl (200.0 mg, 0.59 mmol) and CuCl (5.9 mg, 0.059 mmol). Grubbs 2nd generation catalyst (5.0 mg, 0.0059 mmol) in 1 mL 1, 2, 4-trichlorobenzene was then added and the reaction mixture was kept under dynamic vacuum while the condenser was cooled to 5 °C using a circulating chiller. The reaction mixture was gradually heated to 90 °C over 4 h and refluxed for 24 h. The reaction mixture was cooled down to room temperature and 5.0 mg Grubbs 2nd generation catalyst in 1 mL 1, 2, 4-trichlorobenzene was added and the reaction mixture was refluxed at 90 °C under dynamic vacuum for another 24 h. Such process was repeated for a total of 5 times and the mixture was poured into methanol (200 mL) to precipitate the polymer, which was purified by Soxhlet

extraction with methanol, acetone, hexanes and chloroform to give the title compound as a black solid (120 mg, 71.9% yield). ^1H NMR (300MHz, CDCl_3): δ (ppm) = 0.86 (t, 3H), 1.27 (m, 14H), 1.54 (m, 2H), 2.59 (t, 2H), 6.87 (m, 2H). ^{13}C NMR (75.48 MHz, CDCl_3): δ (ppm) = 14.12, 22.72, 29.42, 29.70, 31.94, 118.77, 119.40, 126.37, 133.42, 139.16. SEC (CHCl_3 , 1 mL/min): M_n = 12.2 KDa, M_w = 20.1 kDa, D = 1.7.

PTV-Br. In a two-neck round bottom flask equipped with a condenser and rubber septum were added TV-Br (900 mg, 2.347 mmol) and CuI (35.7 mg, 0.187 mmol). Grubbs 2nd generation catalyst (20.0 mg, 0.0235 mmol) in 2.5 mL 1, 2, 4-trichlorobenzene was then added and the reaction mixture was kept under dynamic vacuum while the condenser was cooled to 5 °C using a circulating chiller. The reaction mixture was gradually heated to 90 °C over 4 h and refluxed for 24 h. The reaction mixture was cooled down to room temperature and 20.0 mg Grubbs 2nd generation catalyst in 2.5 mL 1, 2, 4-trichlorobenzene was added and the reaction mixture was refluxed at 90 °C under dynamic vacuum for another 24 h. Such process was repeated for a total of 5 times and the mixture was poured into methanol (200 mL) to precipitate the polymer, which was purified by Soxhlet extraction with methanol, acetone, hexanes and chloroform to give the title compound as a black solid (637 mg, 83% yield). ^1H NMR (300MHz, CDCl_3): δ (ppm) = 0.86 (t, 3H), 1.26 (m, 14H), 1.55 (m, 2H), 2.68 (t, 2H), 6.91 (m, 2H). ^{13}C NMR (75.48 MHz, CDCl_3): δ (ppm) = 14.13, 22.72, 29.43, 29.69, 31.94, 116.03, 120.02, 134.62, 141.29. SEC (CHCl_3 , 1 mL/min): M_n = 14.0 KDa, M_w = 30.9 kDa, D = 2.2.

PTV-I. In a two-neck round bottom flask equipped with a condenser and rubber septum were added TV-I (300 mg, 0.7 mmol) and CuI (13.3 mg, 0.07 mmol). Grubbs 2nd generation catalyst (5.9 mg, 0.007 mmol) in 1 mL 1, 2, 4-trichlorobenzene was then added and the reaction mixture was kept under dynamic vacuum while the condenser was cooled to 5 °C using a circulating chiller. The reaction mixture was gradually heated to 90 °C over 4 h and refluxed for 24 h. The reaction mixture was cooled down to room temperature and 5.9 mg Grubbs 2nd generation catalyst in 1 mL 1, 2, 4-trichlorobenzene was added and the reaction mixture was refluxed at 90 °C under dynamic vacuum for another 24 h. Such process was repeated for a total of 5 times and the mixture was poured into methanol (100 mL) to precipitate the polymer, which was purified by Soxhlet extraction with methanol, acetone, hexanes and chloroform to give the title compound as a dark black solid (47 mg, 18% yield). ¹H NMR (300MHz, CDCl₃): δ (ppm) = 0.86 (t, 3H), 1.27 (m, 14H), 1.54 (m, 2H), 2.71 (t, 2H), 6.92 (m, 2H). ¹³C NMR (75.48 MHz, CDCl₃): δ (ppm) = 14.13, 22.72, 29.44, 29.69, 31.95. SEC (CHCl₃, 1 mL/min): $M_n = 4.8$ KDa, $M_w = 7.5$ kDa, $D = 1.6$.

PTV-Th. PTV-Br (20 mg, 0.061 mmol) and tri-n-butyl(2-thienyl) tin (27.4 mg, 0.073 mmol) were charged into a pressure vessel. Pd(PPh₃)₄ (7.1 mg, 0.0061 mmol), DMF (0.5 mL) and Toluene (0.5 mL) were added into the vessel in an argon filled glovebox. The mixture was stirred at 110 °C for 24 h. PTV-Th was isolated by precipitation into methanol and drying under high vacuum as a black solid (8 mg, 39.6%). ¹H NMR (300MHz, CDCl₃): δ (ppm) = 0.86 (t, 3H), 1.22 (m, 16H), 2.57 (t, 2H), 6.98 (d, 2H), 7.15~7.43 (m, 3H). SEC (CHCl₃, 1 mL/min): $M_n = 13.9$ KDa, $M_w = 25.7$ kDa, $D = 1.9$.

2-(5-Bromothiophen-2-yl)-1, 3-dioxolane. 5-Bromo-2-thiophenecarboxaldehyde (5.00 g, 43.8 mmol), ethylene glycol (17.3 mL, 109.6 mmol) and a catalytic amount of *p*-toluenesulfonic acid (25 mg, 0.13 mmol) were dissolved in 35 mL toluene in a 100 mL round bottom flask equipped with a Dean–Stark apparatus. The reaction mixture was refluxed at 140 °C for 20 h. The reaction mixture was extracted by ethyl ether and followed by washing with saturated Na₂CO₃, DI H₂O and saturated brine solution. The combined organic phase was dried with anhydrous Na₂SO₄. After solvent removal under reduced pressure, the residue was further purified by distillation to give the title compound as a yellow liquid (5.0 g, 81.3% yield). ¹H NMR (300MHz, CDCl₃): δ (ppm) = 3.97~4.13 (t, 4H), 6.02 (s, 1H), 6.90~6.95 (d, 2H).

(5-(1, 3-Dioxolan-2-yl) thiophen-2-yl)trimethylstannane. To a stirring solution of 2-(5-bromothiophen-2-yl)-1, 3-dioxolane (2 g, 8.507 mmol) in dry THF (5 mL) at –78 °C, was added 5.1 mL ⁿBuLi (2.5 M in THF, 12.8 mmol) solution dropwise through a degassed syringe. After 15 minutes, Me₃SnCl solution (2.2 M in THF, 5 mL, 11.01 mmol) was added. The reaction mixture was warmed up and kept under room temperature for 4 hours. The resulting reaction mixture was extracted with diethyl ether (2×40 mL), followed by washing with saturated brine solution. The combined organic phase was dried over anhydrous Na₂SO₄. After solvent removal under reduced pressure, the crude compound was further dried under high vacuum and used for next step without further purification (2.57 g, 94.6%). ¹H NMR (300MHz, CDCl₃): δ (ppm) = 0.35 (s, 9H), δ (ppm) = 3.99~4.17 (t, 4H), = 6.15 (s, 1H), 7.07~7.27 (d, 2H).

PTV-ThCHO. PTV-Br (50 mg, 0.15 mmol) and compound 2 (68 mg, 0.214 mmol) were charged into a pressure vessel. Pd(PPh₃)₄ (35 mg, 0.031 mmol), DMF (0.5 mL) and Toluene (0.5 mL) were added into the vessel in an argon filled glovebox. The mixture was stirred at 110 °C for 24 h. The reaction mixture was dried under high vacuum to get rid of the solvent and the residue was used in next step without further purification. ¹H NMR (300MHz, CDCl₃): δ (ppm) = 0.85 (t, 3H), 1.22 (m, 14H), 1.40 (m, 2H), 2.60 (t, 2H), 4.05~4.17 (t, 4H), 6.15~6.19 (s, 1H), = 6.85~7.20 (m, 4H). The residual polymer from the previous step, THF (5 mL), H₂O (5 mL), and HCl (0.5 mL) were added into a one-neck flask. The reaction mixture was stirred at room temperature for 24 h. PTV-ThCHO was isolated by precipitation into methanol and drying under high vacuum as a black solid (42 mg, 77.2% yield). ¹H NMR (300MHz, CDCl₃): δ (ppm) = 0.85 (t, 3H), 1.21 (m, 14H), 1.37 (m, 2H), 2.59 (t, 2H), 6.80~7.84 (m, 4H), 9.96 (s, 1H). SEC (CHCl₃, 1 mL/min): $M_n = 13.8$ KDa, $M_w = 25.5$ kDa, $D = 1.9$.

PTV-ThCN. PTV-ThCHO (22 mg, 0.061 mmol) and methyl cyanoacetate (17 mg, 0.17 mmol) were charged into a pressure vessel. Triethylamine (25 mg, 0.25 mmol) and CHCl₃ (1 mL) were added into the vessel in an argon filled glovebox. The mixture was stirred at room temperature for 24 h. After solvent removal under reduced pressure, the solid was dissolved in chloroform (0.5 mL) and then dropped into methanol (30 mL) to precipitate the polymer as a black solid after drying under high vacuum (17 mg, 63 %). ¹H NMR (300MHz, CDCl₃): δ (ppm) = 0.84 (t, 3H), 1.20 ~ 1.25 (m, 16H), 2.62 (t, 2H), 3.93 (s, 3H),

6.83~7.08 (m, 3H), 7.86 (d, 1H), 8.34 (s, 1H). SEC (CHCl₃, 1 mL/min): $M_n = 14.9$ kDa, $M_w = 27.3$ kDa, $D = 1.8$.

PTV-A-Ph. PTV-Br (100 mg, 0.31 mmol), phenylacetylene (125 mg, 1.22 mmol), CuI (13.3 mg, 0.07 mmol), Pd(PPh₃)₄ (70.7 mg, 0.06 mmol), TEA (0.31 g, 3.1 mmol), THF (3.5 mL) and toluene (3.5 mL) were charged into a 50 mL pressure vessel in an argon-filled glovebox. The mixture was stirred at 110 °C for 24 h. PTV-A-Ph was isolated by precipitation into acetone and dried under high vacuum as a black solid (67 mg, 63%). ¹H NMR (300 MHz, CDCl₃): δ (ppm) = 0.85 (3H), 1.23 (14H), 1.68 (2H), 2.82 (2H), 7.02~7.56 (7H). ¹³C NMR (125.75 MHz, CDCl₃): δ (ppm) = 14.12, 22.69, 27.98, 29.40, 29.68, 30.38, 31.92, 83.90, 96.68, 120.85, 123.33, 128.40, 131.46, 134.92, 143.37. SEC (CHCl₃, 1 mL/min): $M_n = 13.1$ kDa, $M_w = 24.3$ kDa, $D = 1.85$.

PTV-A-PhCHO. PTV-Br (200 mg, 0.61 mmol), 4-ethynylbenzaldehyde (317.6 mg, 2.44 mmol), CuI (23.2 mg, 0.12 mmol), Pd(PPh₃)₄ (141 mg, 0.12 mmol), TEA (617.3 mg, 6.1 mmol), THF (5 mL) and toluene (5 mL) were charged into a 50 mL pressure vessel in an argon-filled glovebox. The mixture was stirred at 110 °C for 24 h. PTV-A-PhCHO was isolated by precipitation into acetone and dried under high vacuum as a black solid (75 mg, 65%). ¹H NMR (300 MHz, CDCl₃): δ (ppm) = 0.83 (3H), 1.23 (14H), 1.71 (2H), 2.84 (2H), 7.33~7.92 (6H), 9.87~10.06 (1H). ¹³C NMR (125.75 MHz, CDCl₃): δ (ppm) = 14.10, 22.66, 27.98, 29.37, 29.66, 30.41, 31.89, 87.88, 96.10, 120.98, 122.55, 127.96, 129.67, 131.82, 134.77, 191.05. SEC (CHCl₃, 1 mL/min): $M_n = 13.5$ kDa, $M_w = 24.3$ kDa, $D = 1.80$.

PTV-A-PhCN. PTV-A-PhCHO (100 mg, 0.27 mmol) and methyl cyanoacetate (52.6 mg, 0.53 mmol) were charged into a 50 mL pressure vessel. Triethylamine (107.5 mg, 1.06 mmol) and CHCl₃ (5 mL) were added into the vessel in an argon-filled glovebox. The mixture was stirred at room temperature for 24 h. After solvent removal under reduced pressure, the solid was dissolved in chloroform (0.5 mL) and then added dropwise into acetone (100 mL) to precipitate the polymer as a black solid after drying under high vacuum (85 mg, 70%). ¹H NMR (300 MHz, CDCl₃): δ (ppm) = 0.83 (3H), 1.25 (14H), 1.69 (2H), 2.85 (2H), 3.96 (3H), 7.31~8.26 (7H). ¹³C NMR (125.75 MHz, CDCl₃): δ (ppm) = 14.10, 22.66, 27.95, 29.37, 29.67, 30.40, 31.88, 53.48, 88.62, 96.34, 102.53, 115.40, 120.92, 122.70, 127.96, 131.17, 134.75, 143.84, 153.71, 162.86. SEC (CHCl₃, 1 mL/min): $M_n = 13.6$ kDa, $M_w = 24.2$ kDa, $D = 1.78$.

2-(5-Ethynylthiophen-2-yl)-1,3-dioxolane. 2-(5-Bromothiophen-2-yl)-1,3-dioxolane (4.06 g, 17.27 mmol), trimethylsilylacetylene (3.40 g, 34.6 mmol), CuI (658 mg, 3.45 mmol), Pd(PPh₃)₄ (998 mg, 0.86 mmol), TEA (8.74 g, 86.39 mmol), THF (10 mL) were charged into a 100 mL pressure vessel in an argon-filled glovebox. The mixture was stirred at room temperature for 20 h, followed by solvent removal under reduced pressure. To the stirring solution of the residue in methanol (37 mL) was added KOH (5.82 g, 0.104 mol). After stirring at room temperature for 6 h, the reaction mixture was poured into water and extracted with diethyl ether (2 × 50 mL); the combined organic phase was then dried over anhydrous Na₂SO₄. After solvent removal under reduced pressure, the residue was further purified by column chromatography over silica gel to give the title compound as a brown

liquid (2.01 g, 65% yield). $^1\text{H NMR}$ (300 MHz, CDCl_3): δ (ppm) = 3.34 (s, 1H), 3.98 ~ 4.13 (m, 4H), 6.06 (s, 1H), 7.01 (d, 1H), 7.15 (d, 1H).

(2-(5-(1,3-dioxolan-2-yl)thiophen-2-yl)ethynyl)trimethylstannane. To a stirring solution of compound 1 (1 g, 5.55 mmol) in THF (10 mL) was added n-butyllithium (3.1 mL, 11.10 mmol) slowly at $-78\text{ }^\circ\text{C}$. After 20 min, a solution of trimethyltin chloride (1.77 g, 13.88 mmol) in THF (5 mL) was added to the reaction mixture. The reaction mixture was stirred at $-78\text{ }^\circ\text{C}$ for 30 min and then kept at room temperature for 24 h. The reaction mixture was quenched with water and then extracted with diethyl ether ($2 \times 50\text{ mL}$); the combined organic phase was dried over anhydrous Na_2SO_4 . After solvent removal under reduced pressure, the residue was further purified by distillation to give the title compound as a light-yellow liquid (1.12 g, 60% yield). $^1\text{H NMR}$ (300 MHz, CDCl_3): δ (ppm) = 0.35 (s, 9H), 3.99 ~ 4.11 (m, 4H), 6.05 (s, 1H), 6.97 (d, 1H), 7.06 (d, 1H).

PTV-A-ThCHO. PTV-Br (100 mg, 0.31 mmol) and compound 2 (168 mg, 0.49 mmol) were charged into a 50 mL pressure vessel. $\text{Pd}(\text{PPh}_3)_4$ (71 mg, 0.061 mmol), DMF (2.5 mL), and toluene (2.5 mL) were added into the vessel in an argon-filled glovebox. The mixture was stirred at $110\text{ }^\circ\text{C}$ for 24 h. The reaction mixture was dried under high vacuum to remove volatile materials and the residue was used in next step without further purification. The residual polymer from the previous step, THF (2.5 mL), H_2O (2.5 mL), and 12 M HCl (0.5 mL) were added into a 50 mL round-bottom flask. The reaction mixture was stirred at room temperature for 24 h. PTV-A-ThCHO was isolated by precipitation into methanol and dried under high vacuum as a black solid (49 mg, 42% yield). $^1\text{H NMR}$

(300 MHz, CDCl₃): δ (ppm) = 0.84 (3H), 1.22 (14H), 1.62 (2H), 2.74 (2H), 6.68-7.63 (4H), 9.86 (1H). ¹³C NMR (125.75 MHz, CDCl₃): δ (ppm) = 14.10, 22.68, 27.93, 29.40, 29.70, 30.42, 31.90, 89.27, 92.68, 120.70, 121.78, 132.35, 136.00, 144.05, 182.03. SEC (CHCl₃, 1 mL/min): M_n = 13.8 kDa, M_w = 23.1 kDa, D = 1.67.

PTV-A-ThCN. PTV-A-ThCHO (50 mg, 0.13 mmol) and methyl cyanoacetate (26 mg, 0.26 mmol) were charged into a 50 mL pressure vessel. Triethylamine (53 mg, 0.52 mmol) and CHCl₃ (2 mL) were added into the vessel in an argon-filled glovebox. The mixture was stirred at room temperature for 24 h. After solvent removal under reduced pressure, the solid was dissolved in chloroform (0.5 mL) and then added dropwise into methanol (30 mL) to precipitate the polymer as a black solid after drying under high vacuum (35 mg, 58%). ¹H NMR (300 MHz, CDCl₃): δ (ppm) = 0.83 (3H), 1.22 (14H), 1.63 (2H), 2.76 (2H), 3.92 (3H), 6.84–7.63 (4H), 8.18 (1H). ¹³C NMR (125.75 MHz, CDCl₃): δ (ppm) = 14.10, 22.68, 27.94, 29.41, 29.70, 30.46, 31.91, 89.59, 94.28, 98.88, 115.69, 120.51, 121.60, 132.62, 136.56, 137.64, 145.38, 162.93. SEC (CHCl₃, 1 mL/min): M_n = 14.2 kDa, M_w = 22.9 kDa, D = 1.62.

Chapter 3 Synthesis, Characterization and Application of Structurally

Diverse Poly (selenylene vinylene)s

(Reproduced with permission from *ACS Macro Lett.* **2015**, 4, 679–683

Copyright © 2015 American Chemical Society

And manuscript under preparation)

3.1 Introduction

As discussed and illustrated in chapter 2, PTV is an interesting class of conjugated materials possessing outstanding optoelectronic properties and has been attracting a great deal of attention in a broad area. Halogenated and cross-conjugated PTVs, prepared through combination of ADMET technique and post-polymerization modification, already displayed improved solar cell performance. However, the overall PCE is still very limited compared to those from state-of-art devices. In order for PTVs to be more applicable in advanced electronic devices, continuous efforts should be made on further structure modification and property as well as performance investigation to reach a higher level of understanding on this type of material.

One of such structural modifications mentioned in chapter 1 is to replace the sulfur atoms in PTVs with selenium, the next heavier element in group 16, generating PSVs, which are expected to possess significantly different physical/optoelectronic properties over their sulfur counterparts.⁹¹⁻⁹³ For instance, poly(3-alkylselenophene)s (P3ASs) have been shown to possess smaller bandgaps and lower ionization potentials than that of the well-studied poly(3-alkylthiophene)s (P3ATs).^{94, 95} Heeney *et al.* and Zade *et al.* recently reported the

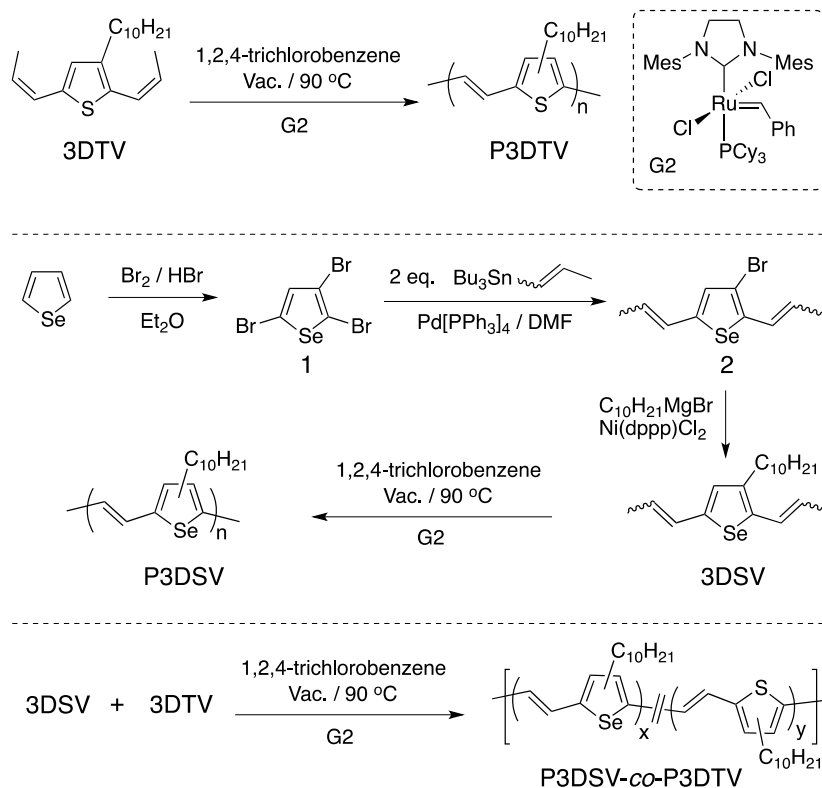
preparation of alkyl and cycloalkyl substituted PSV derivatives, respectively, through palladium catalyzed Stille coupling reactions.^{96, 97} During their synthesis, an AA+BB type condensation reaction was applied, which requires strict stoichiometry in order to achieve high molecular weights. ADMET, on the other hand, uses a single type of monomers, is compatible with a variety of functional groups and provides versatile end-group controllability.^{81, 98, 99} Preparation of PSV derivatives through ADMET has not been demonstrated.

Furthermore, by partially substituting the sulfur atoms in PTVs with selenium, copolymers of PTV and PSV are obtained, which provides additional pathways to further fine-tune the polymer properties. Such strategy has been applied in the synthesis of copolymers of P3AS and P3AT, which displayed tunable physical and electronic properties.¹⁰⁰ To the best of our knowledge, there have been no examples of such copolymers involving both PTV and PSV structures.

On the other hand, we have developed a versatile methodology to prepare structurally diverse PTVs by combining ADMET technique and post-polymerization modification and achieved great success as discussed in chapter 2.¹⁰¹ To further evaluate the universality of this synthetic methodology towards other PCVs as well as study the *structure-property-application* relationships of PSVs, we have prepared a series of cross-conjugated PSVs with systematically varied substituents on the selenophene rings, studied in detail their physical and electronic properties, and investigated their performance in OSCs devices.

3.2 Synthesis, Characterization and Discussion of Poly(selenylene vinylene) and Poly(selenylene vinylene)-*co*-Poly(thienylene vinylene)

The synthetic methods are summarized in Scheme 3.1 and detailed procedures are



Scheme 3.1 Synthetic Route of Poly(selenylene vinylene) and Poly(selenylene vinylene)-*co*-Poly(thienylene vinylene)

described in the experimental section. Preparation of P3DTV ($M_n = 21.3$ KDa, $PDI = 2.1$, SEC) has been reported previously.⁶² For the synthesis of the Se containing monomer, 3DSV, we started with selenophene. Tribromination using Br₂/HBr led smoothly to monomer 1 that has been fully characterized by ¹H and ¹³C NMR spectroscopy as well as GC-MS analysis. Cross-coupling reaction of 1 with exactly two equivalents of tri-*n*-butyl(1-propenyl)tin (mixture of *trans* and *cis* isomers) led to monomer 2. The substitution

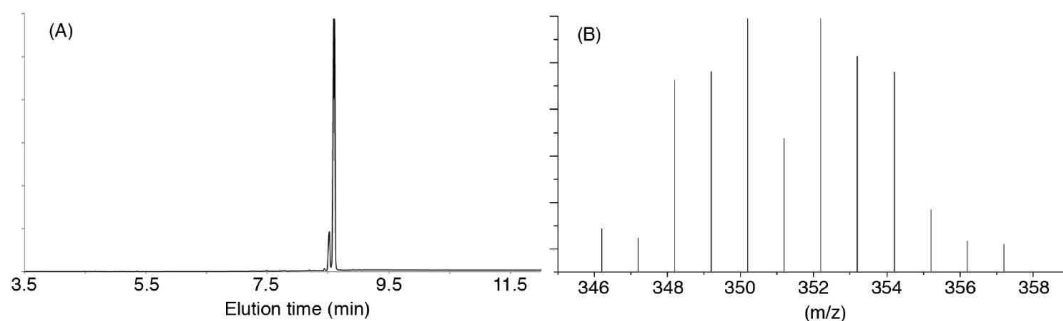


Figure 3.1. (A) Gas chromatography (GC) trace of 3DSV and (B) low resolution mass spectrum (MS) of the molecular ion of 3DSV.

took place only at the 2 and 5 positions of monomer 1 due to the enhanced reactivity, which was further proved after the next reaction step-alkylation at the 3 position through Grignard cross-coupling reaction leading to monomer 3DSV. GC-MS analysis of 3DSV proves the presence of several stereoisomers and possible regioisomers having exactly the same molecular weight for the expected structures (Figure 3.1). The ^1H NMR spectrum of 3DSV is very similar to those of related 2,5-dipropenylthiophene analogs^{55, 62} prepared from 3-alkylthiophene derivatives as shown in Figure 3.2. Signals from the CH_2 group attached to the selenophene ring appear at ca. 2.5 ppm that is typical of alkyl chains substituted at the 3-position, while chemical shifts from 2-substituted alkyl chains have been well-documented to appear at ca. 2.8-2.9 ppm.¹⁰² The absence of any signals in the 2.8-2.9 ppm region confirms the substitution pattern in 3DSV and selectivity of the cross-coupling reaction leading to monomer 2. Due to the unsymmetrical nature of 3DSV, there are four stereoisomers originated from combinations of *trans* and *cis* configurations of the 2- and 5-propenyl groups, respectively. From NMR integration, these isomers exist in roughly

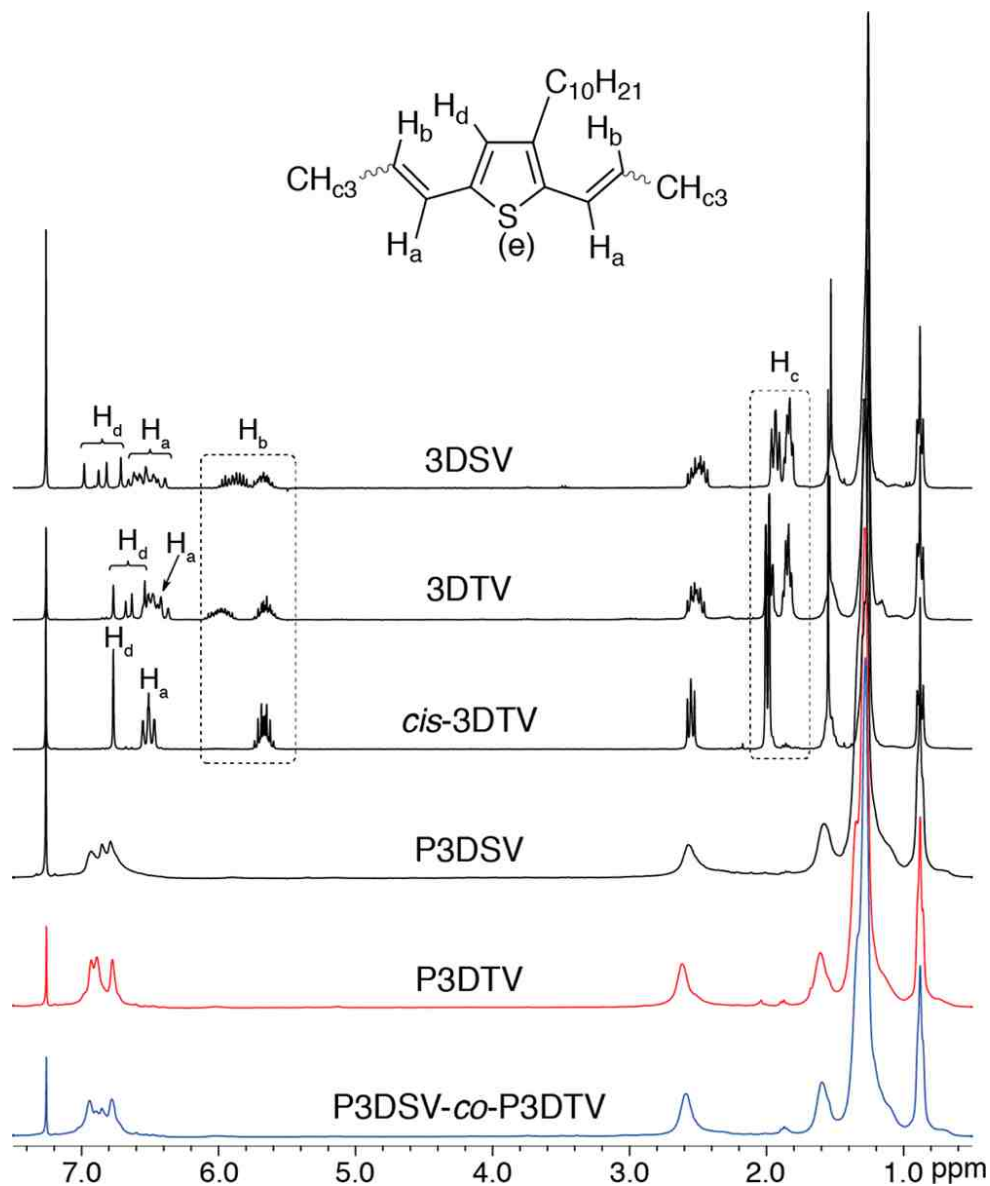


Figure 3.2. ¹H NMR spectra overlay of 3DSV, 3DTV, *cis*-3DTV, P3DSV, P3DTV, and P3DSV-*co*-P3DTV.

equal amount, which is not surprising since we started with a *trans/cis* mixture of tri-*n*-butyl(1-propenyl)tin and the Stille coupling reaction applied has no stereo-selectivity. It is worth noting that the thiophene monomer, 3DTV, is a single stereoisomer having exclusively *cis* double bonds and has displayed faster ADMET polymerization rates over

corresponding stereoisomer mixtures. However, during the synthesis of 3DTV, excess of Grignard reagents was applied, which is less amenable for the synthesis of 3DSV. We are currently optimizing the reaction conditions and seeking alternative routes for the preparation of 3DSV containing exclusively *cis* double bonds.

ADMET polymerization of 3DSV was conducted in 1,2,4-trichlorobenzene (TCB) under dynamic vacuum at 90 °C using Grubbs 2nd generation catalyst (G2, Scheme 1). Under such conditions, TCB was continuously refluxing, which could efficiently remove the 2-butene byproducts and drive the polymerization to high monomer conversions. The reaction mixture gradually turned from slightly yellow to red, then purple and eventually blue, indicating evolution of the conjugation lengths in P3DSV. The polymer was isolated by precipitation into methanol and purified by Soxhlet extraction as a black solid ($M_n = 14.3$ KDa, $PDI = 1.8$, SEC). The molecular weight is relatively smaller than that of P3DTV, presumably due to the presence of *trans* double bonds that have sluggish polymerization rates. The NMR spectra of P3DSV are very similar to those of P3DTV, in which signals are broad and no splitting patterns can be observed in the ¹H spectrum. These observations are consistent with previous reports on PTVs obtained through ADMET and indicate *regio*-random nature of the P3DSV structure, different from the *regio*-regular polymers synthesized from Horner-Emmons and Stille coupling reactions.^{103, 104} In order to prepare the copolymer and to avoid large difference in polymerization rates, we prepared another 3DTV monomer having similar *trans/cis* ratios as those in 3DSV through Stille coupling reaction of 2,5-dibromo-3-decylthiophene with tri-*n*-butyl(1-propenyl)tin.⁶² The

copolymer was synthesized similarly starting with a mixture of these two monomers in equal molar ratio (3DSV/3DTV ~ 10/9 by wt.) leading to a black solid ($M_n = 8.1$ KDa, $PDI = 1.8$, SEC). NMR spectra of the resulting P3DSV-*co*-P3DTV show broad overlapping signals with contributions from 3DSV and 3DTV units, confirming incorporation of both monomers (Figure 3.2).

The newly prepared polymers were first characterized by Raman and IR spectroscopy (Figure 3.3). For better comparison, data for P3DTV and an equal weight blend of P3DSV and P3DTV are also included. All polymers and blends show very similar Raman scattering profiles (Figure 3.3A). The three major peaks between 1200 and 1600 cm^{-1} have been previously assigned to vinyl C-H bend, ring C=C stretch and vinyl C=C stretch (from low to high Raman shifts).⁵⁹ Noticeably, the three peaks for P3DSV at 1277, 1394 and 1568 cm^{-1} are red-shifted from the values for P3DTV at 1289, 1402 and 1582 cm^{-1} , indicating more enhanced conjugation and thus reduced bandgap in P3DSV (*vide infra*). Expectedly, P3DSV-*co*-P3DTV shows peaks at 1284, 1400 and 1576 cm^{-1} , between those of corresponding homopolymers, respectively. On the other hand, the blend displays Raman profiles as an overlap of those of the homopolymers, which is most clearly seen as the vinyl C=C stretch appears as two peaks at 1572 and 1582 cm^{-1} . In the IR spectra (Figure 3.3B), several modes, at 792, 1011, 1086 and 1258 cm^{-1} that most likely originate from C-H deformations of the selenophene ring,^{105, 106} are strongly enhanced in P3DSV while depressed in P3DTV. Similarly, the blend shows a spectrum as superposition from those of the homopolymers. P3DSV-*co*-P3DTV, however, displays a spectrum more resembling

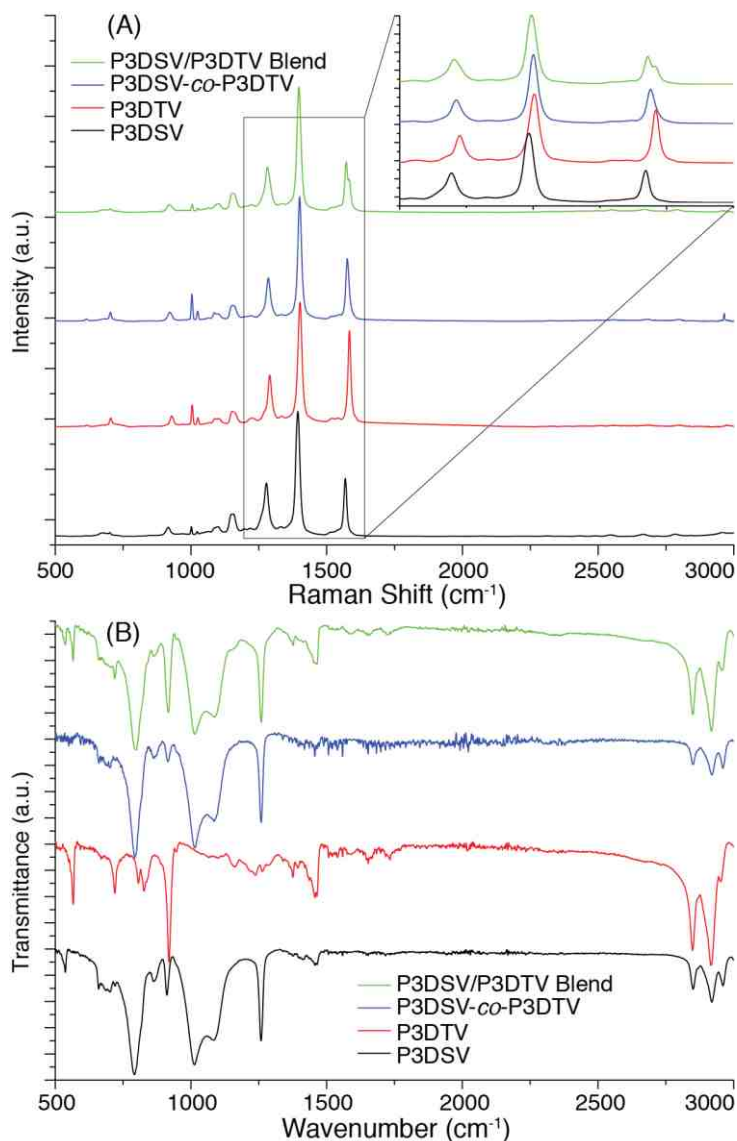


Figure 3.3. (A) Raman spectra of chlorobenzene solutions of and (B) IR spectra of powders of P3DSV (black), P3DTV (red), P3DSV-co-P3DTV (blue) and P3DSV/P3DTV blends (50/50, wt./wt., green).

that of P3DSV with depression of peaks at ca. 550 and 1460 cm^{-1} that are both present for the homopolymers.

The impact on polymer electronic properties through Se substitution is first studied by UV-vis absorption spectroscopy. In dilute solutions (Figure 3.4), both P3DTV and P3DSV display very similar structured absorption profiles, indicating collapsed conformation.

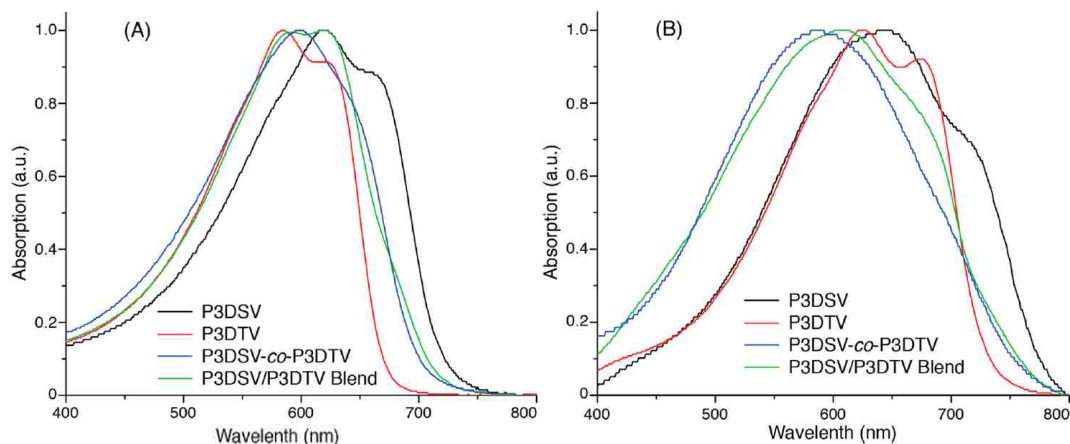


Figure 3.4. UV-vis absorption spectra of P3DSV (black), P3DTV (red), P3DSV-*co*-P3DTV (blue) and P3DSV/P3DTV blends (50/50, wt./wt., green): (A) in chlorobenzene solutions (ca. 10^{-5} M r.p. units) and (B) as thin films spin cast from chlorobenzene solutions onto glass substrates.

Compared with P3DTV that has λ_{\max} of 584 nm and absorption onset at 670 nm, λ_{\max} and onset of P3DSV are red-shifted to 617 nm and 721 nm, respectively, confirming the bandgap reducing effect of Se incorporation (ca. 1.85 eV for P3DTV and 1.72 eV for P3DSV). On the other hand, P3DSV-*co*-P3DTV has an only slightly structured absorption profile with λ_{\max} of 597 nm and onset at 700 nm, corresponding to a bandgap of ca. 1.77 eV. Both numbers are in between those of the P3DTV and P3DSV homopolymers, suggesting an averaging effect on electronic properties through copolymerization. Such effect is further confirmed by the absorption profile of the simple blend solution of the two homopolymers, which display two identical λ_{\max} s with those of P3DSV and P3DTV. CV measurement was also performed on solutions of the polymers to estimate the energy levels as shown in Figure 3.5 and summarized in Table 3.1. Quasi- to non-reversible redox behaviors are observed for all three polymers tested, from the onsets of which the HOMO and LUMO energy levels are calculated. Interestingly, P3DSV-*co*-P3DTV has a HOMO

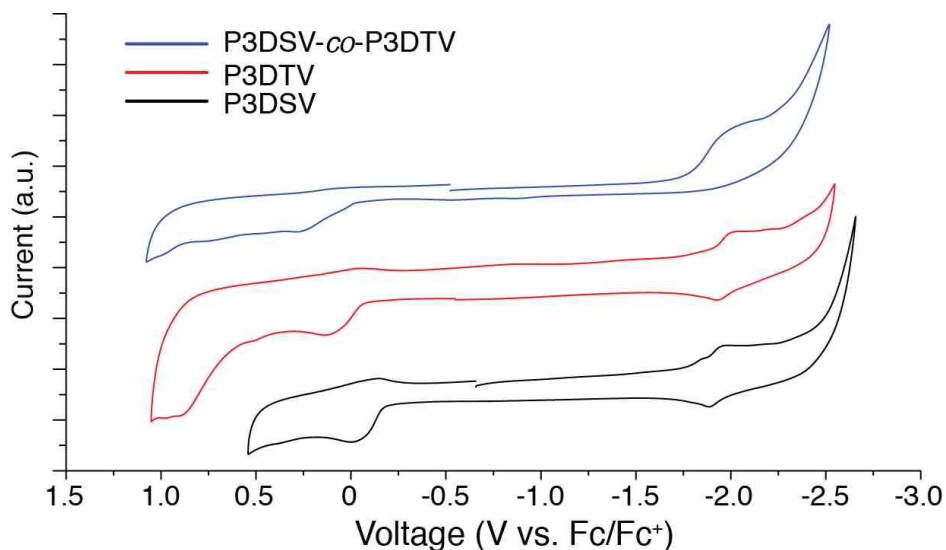


Figure 3.5. Cyclic voltammograms of P3DSV (black), P3DTV (red) and P3DSV-*co*-P3DTV (blue) in THF (0.01 M); Bu₄NPF₆ as supporting electrolyte (0.1 M) and referenced against ferrocene/ferrocenium redox couple (scan rate: 100 mV/s).

Table 3.1. Electronic Properties of Polymers.^a

	HOMO ^b	LUMO ^c	BG _{CV} ^d	BG _{Opt} ^e
P3DSV	-4.62	-3.05	1.57	1.72
P3DTV	-4.73	-2.92	1.81	1.85
P3DSV- <i>co</i> - P3DTV	-4.75	-3.03	1.72	1.77

^a All units in electron volt (eV); ^b highest occupied molecular orbital; ^c lowest unoccupied molecular orbital; ^d bandgap by cyclic voltammetry; ^e optical bandgap in solution.

level similar to that of P3DTV and a LUMO level close to that of P3DSV. Bandgap of the copolymer is in between those of the homopolymers, consistent with optical observations.

However, very different trends are observed for the thin films of these polymers as shown in Figure 3.4B. The absorption profiles of P3DTV and P3DSV are very similar to those reported earlier,^{62, 104} giving bandgaps of ca. 1.70 eV and 1.60 eV, respectively. The vibronic structures of P3DSV are less pronounced than those of P3DTV, indicating less efficient packing of P3DSV chains, presumably caused by the larger sizes of Se atoms. Surprisingly, the blend no longer shows superposition from the two homopolymers, and instead, only a weakly structured absorption profile with a λ_{\max} at 607 nm is observed. P3DSV-*co*-P3DTV, on the other hand, shows an even more blue-shifted λ_{\max} at 585 nm and an almost structureless profile. Both the blend and the copolymer have similar absorption onset at ca. 760 nm, corresponding to bandgaps of ca. 1.63 eV. These observations suggest that both the blend and the copolymer are disordered in the solid state.

In order to study the polymer packing structures in detail, powder XRD experiments were performed and the results are shown in Figure 3.6. All three polymers displayed three lamellar (X00) scattering peaks at 2θ values of ca. 5.4° , corresponding to a d -spacing of ca. 16.3 Å that is consistent with previous reports and expected since these polymers all have similar structures and the same n -decyl side-chains.⁶² The peaks of P3DSV and P3DSV-*co*-P3DTV are apparently weaker and broader than those of P3DTV, proving the less crystalline nature of the Se containing polymers. Furthermore, weak scattering peaks are observed at 2θ values of 21.3° for P3DTV and 20.7° for P3DSV and P3DSV-*co*-P3DTV, corresponding to d -spacings of 4.16 Å and 4.29 Å, respectively. Based on previous reports,^{58, 59} we tentatively assign these peaks from π - π stacking of the polymer main-

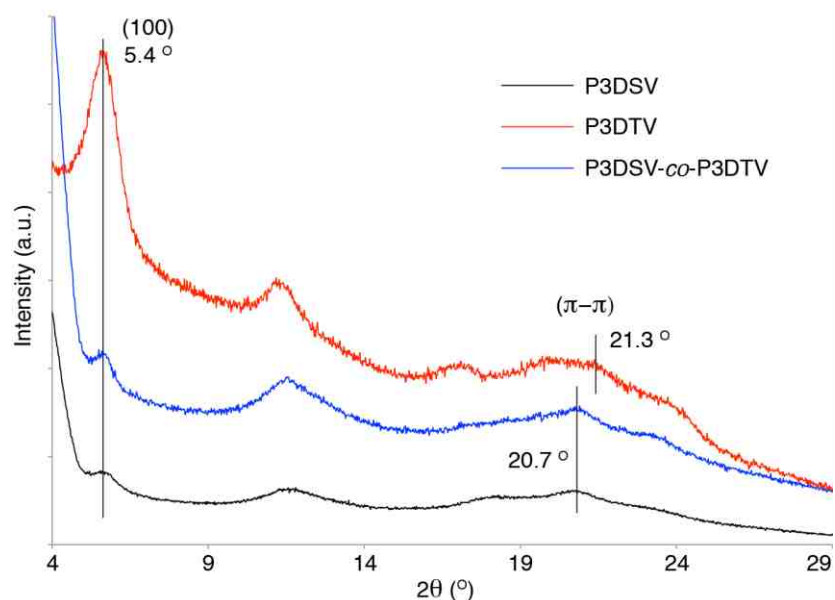


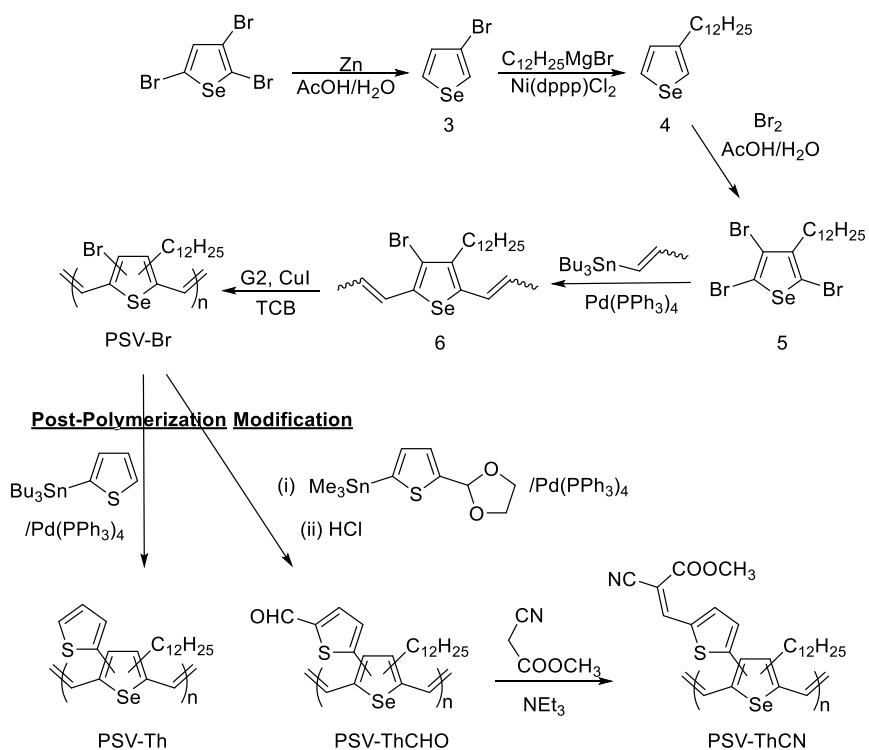
Figure 3.6. Powder X-ray diffraction (XRD) profiles of P3DSV (black), P3DTV (red) and P3DSV-co-P3DTV (blue).

chains. The slightly larger π - π stacking distance observed in Se containing polymers is possibly caused by the larger sizes of Se atoms than those of S atoms, which induces less efficient packing of polymer chains and likely explains the reduced crystallinity in P3DSV and P3DSV-co-P3DTV.

3.3 Synthesis, Characterization and Discussion of Cross-conjugated Poly(selenylene vinylene)s

Synthesis of PSVs, depicted in scheme 3.2, started from 2,3,5-tribromoselenophene, which was prepared according to reported literature.⁶⁸ Debromination of the tribromoselenophene of the 2- and 5-substituted position through reduction reaction with zinc in acetic acid led smoothly to 3-bromoselenophene, followed by Grignard cross-coupling reaction to alkylate the 3 position with dodecyl group, endowing the resulting

PSVs with relatively good solubility. Bromination of 3-dodecylselenophene generated



Scheme 3.2 Synthetic Route of Brominated and Cross-conjugated PSVs.

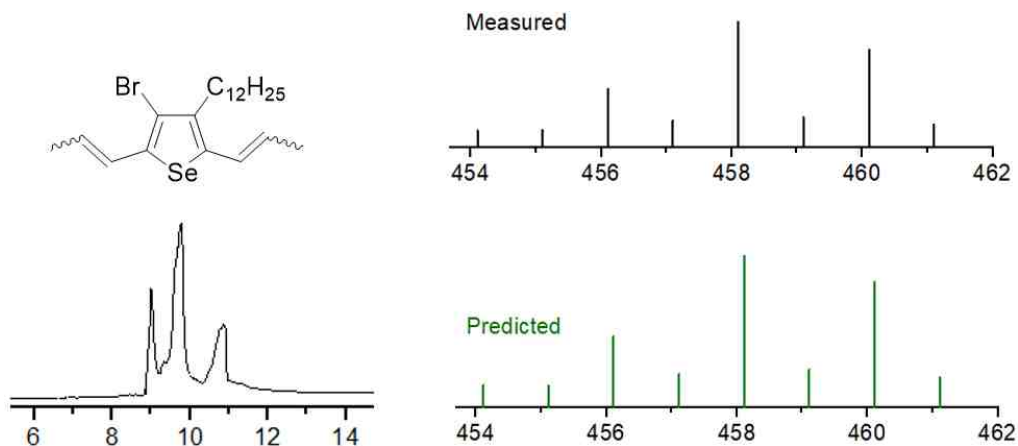


Figure 3.7. Gas chromatograms (GC, left column), measured isotope patterns of mass spectra of molecular ions (MS, black, right column) and predicted isotope patterns (green) of SV-Br.

compound 3, which was subsequently subjected to Stille coupling reaction with exact 2

equivalents tri-*n*-butyl(1-propenyl)tin to install propenyl groups on the 2- and 5- position by taking the advantage of their higher reactivity relative to the 3- position, which has been well-studied in our previous work.⁶⁸ GC-MS analysis of compound 6 resolved the presence of 3 stereoisomers instead of 4 presumably due to reduced stability of the *cis* conformation upon heat converting the all-*cis* isomer to the other 3 when passing through the heated GC column (Figure 3.7). The presence of the stereoisomers of compound 6 is also reflected by the complexity of its ¹H NMR (Figure 3.8) spectrum displaying 4 sets of complicated multiplets ranging from 1.6 ppm to 6.7 ppm, corresponding to protons from the *cis* and *trans* propenyl groups as well as the methylene of the dodecyl group. Since the signals from the β-proton of the *cis* and *trans* propenyl groups, centered at ca. 5.8 ppm, are mixed, not like what we saw in PTV monomers where the signals are well separated, so here it's difficult to estimate the ratio of *cis* and *trans* configurations in compound 6. ADMET polymerization of compound 6 in TCB under dynamic vacuum at 90 °C by using G2 led to formation of the designed poly(3-bromo-4-dodecylselenylene vinylene) (PSV-Br). Detailed synthetic procedure and characterization can be found in experimental section. It's worth noting that addition of 10% CuI into the reaction mixture can greatly facilitate the polymerization rate, which has been studied in detail for poly(3-bromo-4-decylthienylene vinylene) (PTV-Br), and likely from the phosphine sponge effect previously studied by Wagener et al. on olefin metathesis assisted by boron-containing lewis acids.⁶⁹

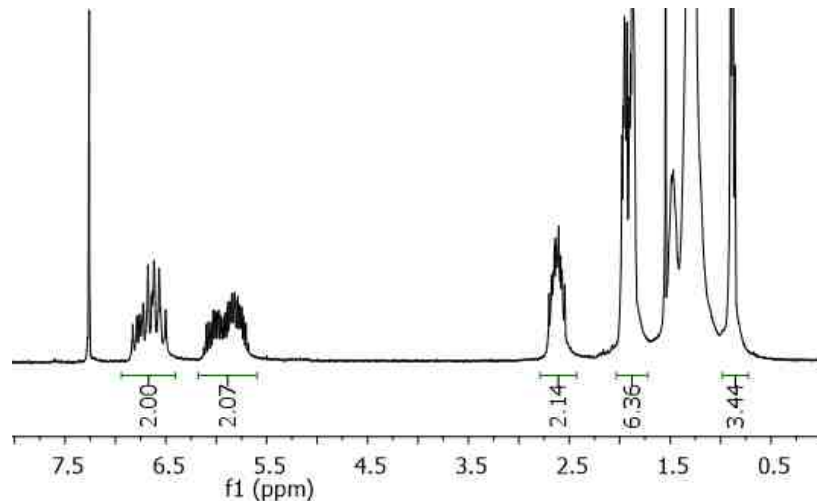


Figure 3.8 ^1H NMR of PSV-Br (Compound 6).

We further attempted to functionalize PSV-Br through post-polymerization modification by replacing the pre-anchored Br atom with various conjugated chromophores. Stille coupling reaction was applied to prepare the cross-conjugated polymers with thienyl groups bearing different substituents on every repeating unit along the polymer backbones. ^1H NMR spectra of these PTVs are overlaid in Figure 3.9. Interestingly, the post-polymerization modified PSVs displayed sharper and more resolved proton signals compared with that from PSV-Br, indicating the more amorphous nature, since peak broadening in polymers can often be ascribed to aggregation, which is reasonable considering that the bulkier thienyl substituents could cause more steric hindrance between polymer main-chain and side-chain. Careful analyses and integrations of these NMR signals suggest quantitative conversion of the post-polymerization modifications with undetectable remaining bromine substituents or debrominated moieties. Degrees of polymerization (DP) of the post-modified PSVs, evaluated through SEC with polystyrene

as the standard (Figure 3.10), close to that of the starting material, PSV-Br, indicating no

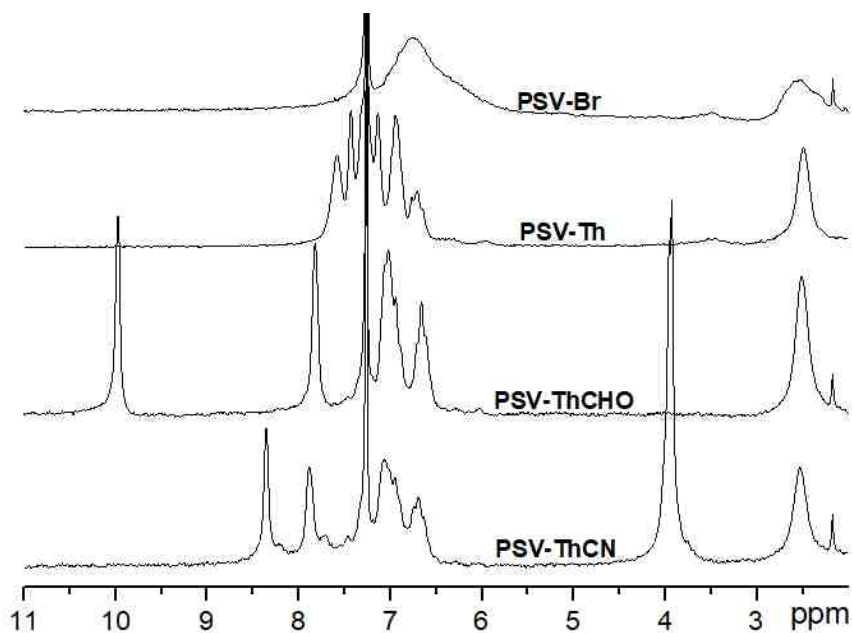


Figure 3.9. ¹H NMR spectra of (top to bottom) PSV-Br, PSV-Th, PSV-ThCHO, and PSV-ThCN in CDCl₃.

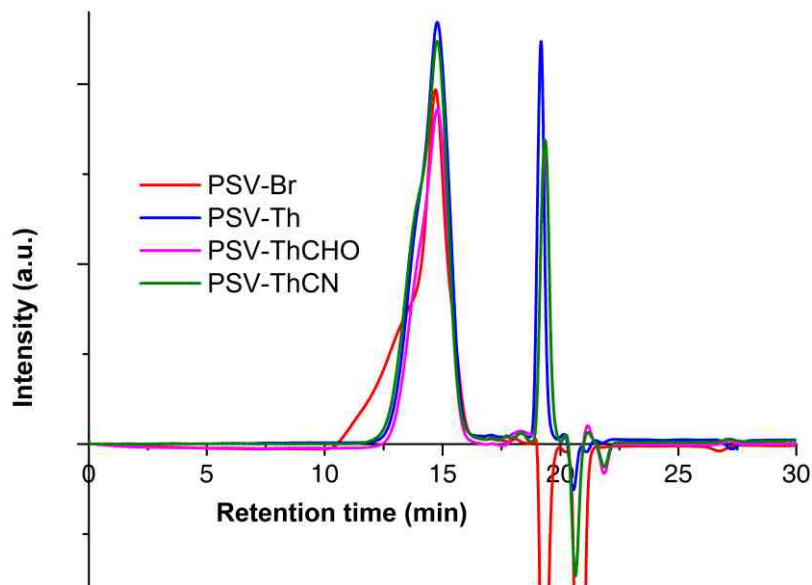


Figure 3.10. Size exclusion chromatograms (SECs) of PSV-Br, PSV-Th, PSV-ThCHO and PSV-ThCN (CHCl₃ w/ 0.5% NEt₃, 1 mL/min, RI detector).

cross-linking or decomposition reactions happened during the post-polymerization

modification process. The slightly differences were likely caused by the different interactions between the functional groups and SEC column materials.

The newly prepared PSVs were first characterized by Raman spectroscopy in chlorobenzene solution (Figure 3.11). All PSVs, including the previously studied

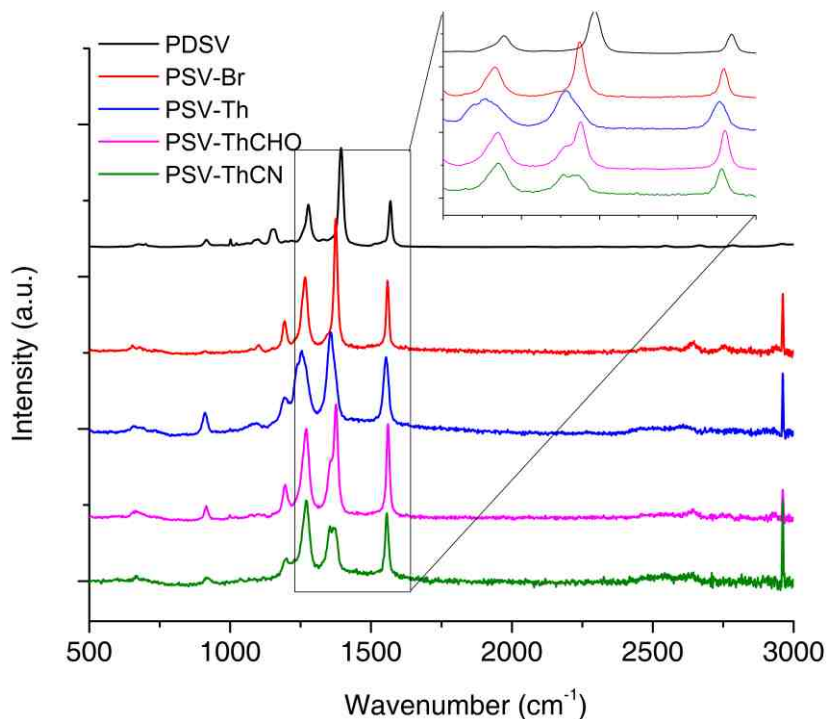


Figure 3.11. Raman spectra of chlorobenzene solutions of PDSV, PSV-Br, PSV -Th, PSV-ThCHO and PSV-ThCN.

poly(3-decylselenylene vinylene) (PDSV)⁶⁸, displayed similar Raman scattering profiles. The three major peaks from 1200 to 1600 cm⁻¹, which have been previously assigned to vinyl C–H bend, ring C=C stretch and vinyl C=C stretch⁵⁹, are slightly red-shifted relative to those from PDSV, indicating weakening of the bond strengths and enhanced conjugated system, caused by the electron withdrawing and conjugation effects from bromine and cross-conjugated side-chains. The optical

properties of the PSVs were further studied in both dilute chlorobenzene solutions and as thin films by performing UV-vis absorption measurement, and the results are summarized in Figure 3.12. We also performed CV measurement on these polymers to assess the frontier energy levels, and the results are summarized in Table 3.2 and Figure 3.13. Compared with PDSV, PSV-Br and post-modified PSVs exhibit slightly red-shifted absorption, resulted from the electron withdrawing effect and the enlarged conjugated system respectively, consistent with Raman scattering

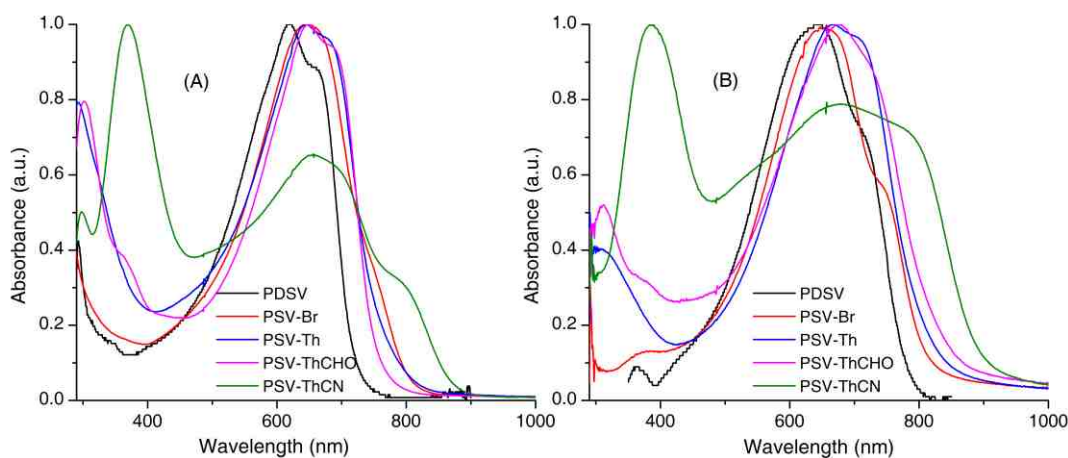


Figure 3.12 UV-vis absorption spectra of PSVs: (A) in chlorobenzene solutions (ca. 10^{-5} M r.p. units) and (B) as thin films spun-cast from chlorobenzene solutions onto glass substrates.

observation, and the new peaks emerged at between 300 and 400 nm from post-modified PSVs were assigned to the absorption of the conjugated side chains, which greatly broadened the overall absorption. In solution, PSV-Br displayed a shoulder absorption at ca. 740 nm, which became greatly enhanced in thin film, and such behaviour has been ascribed to polymer aggregation.¹⁰⁷ However, this shoulder absorption is clearly absent in the post-modified PSVs, indicative of the weaker

aggregation of polymer chains, consistent with ^1H NMR observation in terms of the sharper proton peaks from post-modified PSVs. Intriguingly, a low-energy peak located at ca. 800 nm, resulting in a low bandgap ca.1.4 eV, is observed in PSV-ThCN, which is absent from other PSVs, and we assigned this peak to main-chain to side-chain intramolecular charge transfer (ICT) electronic transition according to

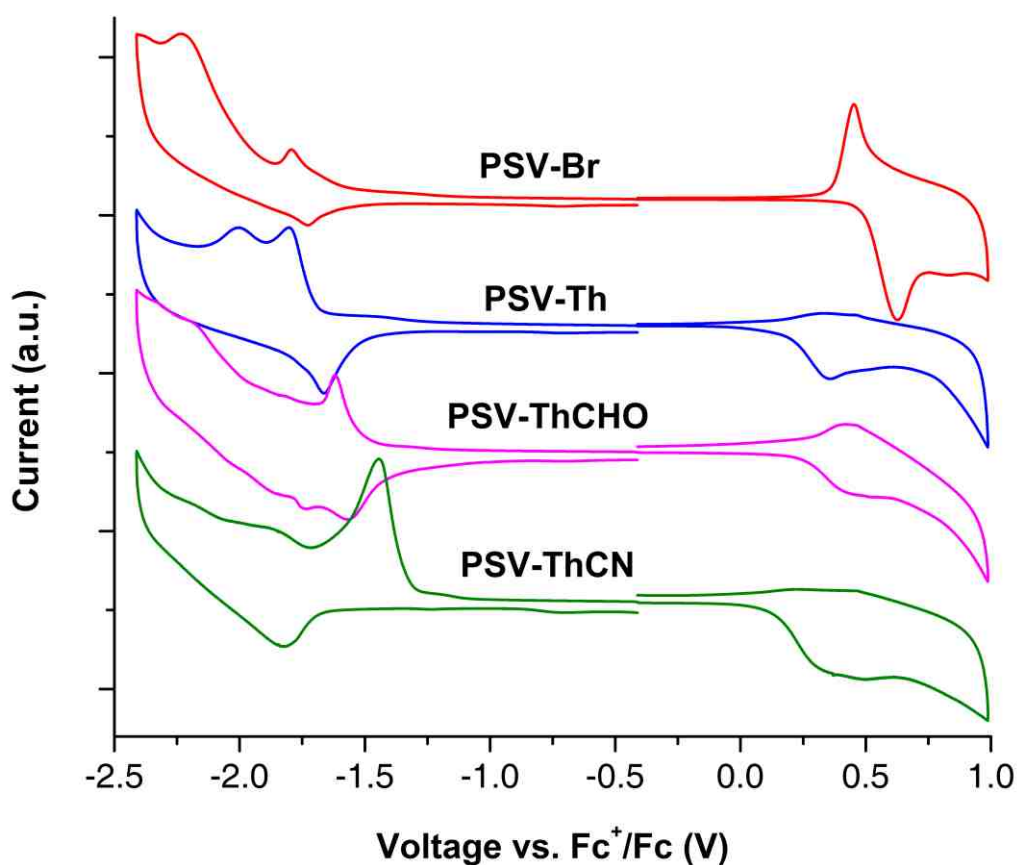


Figure 3.13 Cyclic voltammograms (CV) of thin films of the cross-conjugated of PSV-Br, PSV-Th, PSV-ThCHO and PSV-ThCN deposited onto the glassy carbon working electrodes (supporting electrolytes: 0.1 M Bu_4NPF_6 in acetonitrile, scan rate: 100 mV/s).

Table 3.2. Physical and Optical Properties of the PSV Polymers.

	M_n^a (KDa)	D^b	DP ^c	$\lambda_{\max}^{\text{sol}}$ (nm)	E_g^{opt} ^d (eV)	HOMO ^e (eV)	LUMO ^f (eV)	E_g^{cv} ^g (eV)
PSV	14.4	1.82	49	617	1.72 (1.58)	-4.62	-3.05	1.57
PSV-Br	13.2	3.02	33	646	1.54 (1.52)	-5.07	-3.32	1.75
PSV-Th	11.4	1.67	28	291, 646	1.55 (1.49)	-4.96	-3.16	1.80
PSV- ThCHO	12.1	1.56	28	303, 648	1.64 (1.45)	-5.03	-3.31	1.72
PSV- ThCN	12.8	1.83	25	369, 651	1.43 (1.39)	-4.90	-3.70	1.20

^a Number average molecular weight estimated from size exclusion chromatography (SEC) against polystyrene standards. ^b Dispersity index. ^c Average degree of polymerization estimated from M_n values. ^d Absorption maxima in chlorobenzene solution (ca. 10^{-5} M repeat unit). ^e Absorption maxima of polymer thin films on glass substrates. ^f Electronic bandgap estimated from optical absorption onsets, thin film data in parentheses. ^g Highest occupied molecular orbital energy estimated from cyclic voltammetry. ^h Lowest unoccupied molecular orbital energy estimated from cyclic voltammetry. ⁱ Electronic bandgap estimated from cyclic voltammetry.

the similar phenomenon observed in cross-conjugated PTV¹⁰¹. Once again, introducing electron-deficient moieties into the side chains of conjugated polymers is proved to be an effective means to lower the polymer bandgap and induce new optoelectronic properties. LUMO and HOMO of the brominated and cross-conjugated PSVs are all lowered significantly relative to that of PSV. Surprisingly, PSV-ThCN displayed the deepest LUMO yet the highest HOMO among the brominated and cross-conjugated PSVs despite of the strong electron-withdrawing cyano group on the side chain. This abnormality seems not to be accidental since we observed the same phenomenon in our post-polymerization modified PTV

possessing identical conjugated side chain.¹⁰¹ More sophisticated theoretical calculations will be conducted on these cross-conjugated polymers in the future to understand this interesting observation.

3.4 Solar Cell Performance of PSVs

The newly obtained PSVs were applied in the fabrication of OSCs devices with phenyl-C₇₁-butyric acid methyl ester (PC₇₁BM) as electron acceptors in conventional device geometry, *i.e.*, ITO glass/MoO₃ (10 nm)/actively layer (100 nm)/Al (100 nm). Our previously prepared PDSV together with PC₇₁BM were also tried to be applied in OSCs device, however, smooth and complete active layer film from spun-coating was never obtained due to the wetting issue between polymer solution and the substrate likely caused by the strong interaction tendency among selenium atoms, we thus excluded the performance of PDSV in the following discussion. Spin-coating of the functionalized PSVs all gave smooth film presumably due to the relatively bulky side groups, which disrupted the interactions of polymer chains, leading to better wetting ability with the substrate. The fabrication conditions of the OSCs devices were optimized in terms of PSVs/PC₇₁BM ratio, spin rate, thermal annealing temperature and duration, and solvent annealing time, and the optimal device performances were summarized in table 3.3. Device employing PSV-Br show the best OSCs performance, contributed by relatively large V_{oc} , J_{sc} and FF . V_{oc} has been shown to closely related to the energy offset between HOMO of the donor material and LUMO of the acceptor material,¹⁰⁸

Table 3.3 Optimized OSC Device Performances Employing PSV Polymers.^a

PSVs:PCBM ^b		V_{oc}	J_{sc}	FF	PCE (%)
PSV-Br	1:3	0.73±0 (0.73)	2.94±0.21 (3.30)	0.58±0.014 (0.60)	1.25±0.063 (1.36)
PSV-Th	1:3	0.53±0.005 (0.54)	1.96±0.26 (2.41)	0.42±0.004 (0.43)	0.44±0.06 (0.55)
PSV- ThCHO	1:4	0.66±0.004 (0.66)	1.84±0.25 (2.16)	0.34±0.008 (0.35)	0.41±0.06 (0.48)
PSV- ThCN	1:3	0.64±0 (0.64)	2.11±0.16 (2.32)	0.55±0.012 (0.56)	0.74±0.07 (0.83)

^a Average numbers and standard deviations from at least five devices under optimized conditions are given. Highest parameter numbers are given in parentheses. ^b Weight ratio.

therefore, the deepest HOMO energy level of PSV-Br leads to the largest solar cell V_{oc} among these PSVs as seen in Table 3.2 and 3.3. Although the cross-conjugated PSVs, especially PSV-ThCN, display broader absorption compared to that from PSV-Br, their J_{sc} is smaller likely due to worse active layer morphologies, which are reflected by their lower FF, and this could result from the noneffective polymeric packing caused by the bulkier conjugated side chains relative to Br atom in PSV-Br. The overall OSCs performance of the newly prepared PSVs is still low compared with those from the state-of-the-art devices,^{15, 109} however, to the best of our knowledge, this is the first example to systematically study the OSCs performance of PSV derivatives, and contribution in the near future may be able to make this type of material a better candidate for OSCs. Potential applications of the functionalized PSVs in other fields, like photodetector, are under investigation.

3.5 Conclusion

In summary, we have developed a unique methodology to conveniently prepare PSV and its derivatives by combining ADMET and post-polymerization modification techniques. Through the studies on PSV and PTV-*co*-PSV, we proved that physical and electronic properties of the resulting polymers can be tuned by the extents of replacement of S atoms with Se. Further structure modification was achieved by applying cross-coupling reactions on PSV-Br, leading to the formation of cross-conjugated PSVs, which display broader absorption contributed from both main-chain and side-chain absorptions. Interestingly, charger transfer absorption peak from polymer main-chain to side-chain was observed in PSV-ThCN induced by the strong electron-withdrawing cyano ester group, resulting in low optical band gap ca. 1.4 eV. OSCs performance of the PSVs were systematically investigated, providing better understanding of this class of materials regarding the *structure-property-application* relationships.

3.6 Experimental

Materials and General Methods. All reagents and solvents were used as received from Sigma-Aldrich or Alfa Aesar unless otherwise noted. 2,3,5-Tribromoselenophene and (5-(1,3-Dioxolan-2-yl)thiophen-2-yl)trimethylstannane were synthesized according to literature procedure.^{68, 101} THF was distilled from Na/benzophenone prior to use. The 300.13 MHz ¹H and 75.48 MHz ¹³C NMR spectra were recorded on a Bruker Avance III Solution 300 spectrometer. All solution ¹H and ¹³C NMR spectra were referenced internally

to solvent signals. Size exclusion chromatography (SEC) analyses were performed in chloroform with 0.5% (v/v) triethylamine (1 mL/min) using a Waters Breeze system equipped with a 2707 autosampler, a 1515 isocratic HPLC pump, and a 2414 refractive index detector. Two styragel columns (Polymer Laboratories; 5 μm Mix-C), which were kept in a column heater at 35 $^{\circ}\text{C}$, were used for separation. The columns were calibrated with polystyrene standards (Varian). Ultraviolet–visible (UV–vis) absorption spectra were recorded on a Shimadzu UV-2401 PC spectrometer over a wavelength range of 240–900 nm. Raman spectra were obtained on a DXR SmartRaman spectrometer over a frequency range of 50.5–3350 cm^{-1} . Cyclic voltammetry was performed at 25 $^{\circ}\text{C}$ on a CH Instrument CHI604xD electrochemical analyzer using a glassy carbon working electrode, a platinum wire counter electrode, and a Ag/AgCl reference electrode calibrated using ferrocene redox couple (4.8 eV below vacuum). GC-MS measurements were performed on an Agilent 7820A system.

Solar Cell Fabrication and Testing. PTV/PC₆₁BM or PC₇₁BM blend solutions were prepared by dissolving the polymer and PC₆₁BM at predetermined weight ratios in chlorobenzene at a polymer concentration of 1 wt% and stirred at room temperature for 3-4 hours in a nitrogen glovebox (Innovative Technology, model PL-He-2GB, O₂ < 0.5 ppm, H₂O < 0.5 ppm). Solar cell devices were fabricated according to the following procedure: ITO-coated glass substrates (China Shenzhen Southern Glass Display Ltd.; 8 Ω/\square) were cleaned by ultrasonication sequentially in detergent water, DI water, acetone and isopropyl

alcohol, each for 15 min. These ITO-coated glasses were further treated by UV-ozone (PSD Series, Novascan) for 60 min before being transferred to a nitrogen glovebox (Innovative Technology, model PL-He-2GB, O₂ < 0.1 ppm, H₂O < 0.1 ppm) for MoO₃ deposition. MoO₃ (10 nm) was deposited using an Angstrom Engineering Amod deposition system at a base vacuum level of < 4×10⁻⁷ Torr. The PSVs/fullerene blend solution was first filtered through a 0.45 μm PTFE filter and spin-coated on top of the MoO₃ layer at 800 rpm for 30 s. Al (100 nm) was thermally evaporated through patterned shadow masks as cathodes, the size of the active areas is ca. 7.1 mm². Current-voltage (I-V) characteristics were measured using a Keithley 2400 source-measuring unit under simulated AM 1.5G irradiation (100 mW/cm²) generated by a Xe arc-lamp based Newport 67005 150 W solar simulator equipped with an AM 1.5G filter. The light intensity was calibrated using a Newport thermopile detector (model 818P-010-12) equipped with a Newport 1916-C Optical Power Meter.

2,3,5-Tribromoselenophene (1). A solution of bromine (6.3 mL, 122.1 mmol) in hydrobromic acid (48%, 18.86 mL) was added to a mixture of selenophene (3.5 mL, 38.16 mmol), HBr (48%, 18.86 mL) and Et₂O (5 mL) within 3.5 h with vigorous stirring while the internal temperature was kept below 10 °C. After addition was finished, the mixture was warmed up to room temperature and stirred for 16 h. Then NaHSO₃ solution was added. The mixture was extracted with Et₂O (3x100 mL) and the extract was washed with brine and dried over Na₂SO₄. The product was further purified by distillation to give a pure white

crystal (7g, 50% yield). ^1H NMR (300.13 MHz, CDCl_3): δ (ppm) = 7.10 (s, 1H). ^{13}C NMR (75.48 MHz, CDCl_3): δ (ppm) = 112.83, 114.61, 115.32, 135.04.

3-Bromo-2,5-dipropenylselenophene (2). Compound 1 (500 mg, 1.36 mmol) and tri-*n*-butyl(1-propenyl)tin (900.5 mg, 2.72 mmol) were charged into a pressure vessel. $\text{Pd}(\text{PPh}_3)_4$ (78.6 mg, 0.068 mmol) and DMF (4 mL) were added into the vessel in an argon filled glovebox. The mixture was stirred at 110 °C for 24 h. The reaction mixture was poured into water and extracted with diethyl ether (2×50 mL); the combined organic phase was then dried over anhydrous Na_2SO_4 . After solvent removal under reduced pressure, the residue was further purified by column chromatography over silica gel to give the title compound as a light-yellow liquid (308 mg, 78% yield). ^1H NMR (300.13 MHz, CDCl_3): δ (ppm) = 1.84~1.94 (d, 6H), 5.67~6.10 (m, 2H), 6.37~6.73 (d, 2H), 6.80~7.08 (s, 1H).

3-Decyl-2,5-dipropenylselenophene (3DSV). In a two-neck flask, compound 2 (308 mg, 1.06 mmol), $\text{Ni}(\text{dppp})\text{Cl}_2$ (17.2 mg, 0.0318 mmol) and THF (15 mL) were added. The mixture was kept in ice bath, then fresh decylmagnesium bromide (10 mL, 1.27 mmol) was added. The reaction mixture was stirred at room temperature overnight. The reaction mixture was quenched with water and then extracted with diethyl ether (2×50 mL); the combined organic phase was then dried over anhydrous Na_2SO_4 . After solvent removal under reduced pressure, the residue was further purified by column chromatography over silica gel to give a mixture of different stereoisomers of the product (117 mg, 37.3%) as a colorless liquid. ^1H NMR (300.13 MHz, CDCl_3): δ (ppm) = 0.88 (t, 3H), 1.83~1.96 (d, 6H), δ (ppm) = 2.43~2.58 (t, 2H), 5.60~5.99 (m, 2H), 6.38~6.66 (d, 2H), 6.71~6.98 (s, 1H).

Poly(3-decylselenylene vinylene) (P3DSV). In a two-neck round bottom flask equipped with a condenser and rubber septum were added 3DSV (150 mg, 0.428 mmol) and kept under N₂. Grubbs 2nd generation catalyst (3.6 mg, 0.00428 mmol) in 1.5 mL 1,2,4-trichlorobenzene was then added and the reaction mixture was kept under dynamic vacuum while the condenser was cooled to 5 °C using a circulating chiller. The reaction mixture was gradually heated to 90 °C over 4 h and refluxed for 24 h. The reaction mixture was cooled down to room temperature and 3.6 mg Grubbs 2nd generation catalyst in 0.5 mL 1,2,4-trichlorobenzene was added and the reaction mixture was refluxed at 90 °C under dynamic vacuum for another 24 h. Such process was repeated 3 more times and the mixture was poured into methanol (200 mL) to precipitate the polymer, which was purified by Soxhlet extraction with methanol, acetone, hexanes and THF. The THF portion was precipitated into methanol to give the title compound P3DSV as a dark blue solid (48 mg, 38% yield). ¹H NMR (300.13 MHz, CDCl₃): δ (ppm) = 0.88 (t, 3H), 1.28 (m, 14H), 1.58 (m, 2H), 2.57 (t, 2H), 6.79 (d, 1H), 6.85 (d, 1H), 6.93 (s, 1H). ¹³C NMR (75.48 MHz, CDCl₃): δ (ppm) = 14.10, 22.68, 29.50, 30.75, 31.90, 122.61, 124.83, 133.13, 134.89, 140.25, 144.35. SEC (CHCl₃, 1 mL/min): *M_n* = 14.3 KDa, *M_w* = 26.1 kDa, *PDI* = 1.8.

P3DSV-co-P3DTV. In a two-neck round bottom flask equipped with a condenser and rubber septum were added 3DSV (100 mg, 0.285 mmol) and 3DTV (86.8 mg, 0.285 mmol), and kept under N₂. Grubbs 2nd generation catalyst (4.8 mg, 0.0057 mmol) in 1.5 mL 1,2,4-trichlorobenzene was then added and the reaction mixture was kept under dynamic vacuum while the condenser was cooled to 5 °C using a circulating chiller. The reaction mixture

was gradually heated to 90 °C over 4 h and refluxed for 24 h. The reaction mixture was cooled down to room temperature and 4.8 mg Grubbs 2nd generation catalyst in 0.5 mL 1,2,4-trichlorobenzene was added and the reaction mixture was refluxed at 90 °C under dynamic vacuum for another 24 h. Such process was repeated 3 more times and the mixture was poured into methanol (200 mL) to precipitate the polymer, which was purified by Soxhlet extraction with methanol, acetone, hexanes and THF. The THF portion was precipitated into methanol to give the title compound P3DSV-*co*-P3DTV as a dark blue solid (67 mg, 43.3% yield). ¹H NMR (300.13 MHz, CDCl₃): δ (ppm) = 0.88 (t, 6H), 1.28 (m, 28H), 1.59 (m 4H), 2.58 (t, 4H), 6.78~6.89 (d, 4H), 6.94 (s, 2H). ¹³C NMR (75.48 MHz, CDCl₃): δ (ppm) = 14.12, 22.70, 29.52, 30.75, 31.92, 119.39, 121.14, 122.74, 124.72, 127.39, 129.44, 131.12, 133.11, 135.77, 140.03, 142.15, 144.14. SEC (CHCl₃, 1 mL/min): $M_n = 8.1$ kDa, $M_w = 14.4$ KDa, $PDI = 1.8$.

3-Bromoselenophene (3). CH₃COOH (10 mL), H₂O (26 mL) and Zinc powder (11 g, 168.25 mmol) were charged into a round-bottom flask and heated up to 114 °C to reflux for 10 mins. 2, 3, 5-Tribromoselenophene (10.2 g, 27.74 mmol) was added into the flask after the reaction mixture was cooled down, and then the mixture was put back into the oil bath to reflux for 4 h. The reaction mixture was poured into water and extracted with diethyl ether (2 × 50 mL); the combined organic phase was then dried over anhydrous Na₂SO₄. After solvent removal under reduced pressure, the residue was further purified by distillation to give a colorless liquid (3.82 g, 65.6%). ¹H NMR (300.13 MHz, CDCl₃): δ (ppm) = 7.27 (dd, 1H), 7.87 (dd, 1H), δ (ppm) = 7.92 (dd, 1H).

3-Dodecylselenophene (4). In a two-neck flask, compound 3 (2.60 g, 12.39 mmol), Ni(dppp)Cl₂ (201.5 mg, 0.37 mmol) and THF (10 mL) were added. The mixture was kept in ice bath, then fresh dodecylmagnesium bromide (25 mL, 18.58 mmol) was added. The reaction mixture was stirred at room temperature overnight. The reaction mixture was quenched with water and then extracted with diethyl ether (2×50 mL); the combined organic phase was then dried over anhydrous Na₂SO₄. After solvent removal under reduced pressure, the residue was further purified by column chromatography over silica gel to give a colorless liquid (1.66 g, 44.7 %). ¹H NMR (300.13 MHz, CDCl₃): δ (ppm) = 0.88 (t, 3H), 1.26 (m, 18H), 1.55~1.61 (m, 2H), δ (ppm) = 2.57~2.62 (t, 2H), 7.20~7.26 (dd, 1H), 7.53~7.54 (dd, 1H), 7.90~7.92 (dd, 1H).

2, 3, 5-Tribromo-4-dodecylselenophene (5). To a stirring solution of 3-dodecylselenophene (1.66 g, 5.53 mmol) in AcOH (1.6 mL) and H₂O (4.7 mL) was added Br₂ (2.3 mL, 44.26 mmol) slowly. The reaction mixture was covered with aluminum foil and kept at room temperature for 24 h. The reaction mixture was poured into Na₂SO₃ solution (50 mL) and extracted with diethyl ether (2 × 50 mL); the combined organic phase was then dried over anhydrous Na₂SO₄. After solvent removal under reduced pressure, the residue was further purified by column chromatography over silica gel to give the title compound as a clear liquid (1.65 g, 55.6 % yield). ¹H NMR (300 MHz, CDCl₃): δ (ppm) = 0.86~0.90 (t, 3H), 1.26 (m, 18H), 1.47~1.52 (m, 2H), 2.63~2.68 (t, 2H). ¹³C NMR (75.48 MHz, CDCl₃): δ (ppm) = 14.17, 22.72, 28.41, 29.29, 29.37, 29.66, 31.94, 32.62, 110.59,

111.50, 117.25, 143.15.

3-Bromo-4-dodecyl-2,5-dipropenylselenophene (SV-Br). 2,3,5-Tribromo-4-dodecylselenophene (1.35 g, 2.52 mmol) and tri-n-butyl(1-propenyl) tin (1.67 g, 5.04 mmol) were charged into a pressure vessel. Pd(PPh₃)₄ (145.5 mg, 0.13 mmol) and DMF (3 mL) were added into the vessel in an argon filled glovebox. The mixture was stirred at 110 °C for 24 h. The reaction mixture was poured into water and extracted with diethyl ether (2 × 50 mL); the combined organic phase was then dried over anhydrous Na₂SO₄. After solvent removal under reduced pressure, the residue was further purified by column chromatography over silica gel to give the title compound as a light-yellow liquid (911 mg, 78.9%). ¹H NMR (300 MHz, CDCl₃): δ (ppm) = 0.86~0.90 (t, 3H), 1.26 (m, 18H), 1.47 (m, 2H), 1.84~1.98 (d, 6H), 2.55~2.70 (t, 2H), 5.68~6.10 (m, 2H), 6.50~6.83 (d, 2H).

PSV-Br. In a two-neck round-bottom flask equipped with a condenser and rubber septum were added SV-Br (865 mg, 1.89 mmol) and CuI (35.8 mg, 0.19 mmol). Grubbs second-generation catalyst (16.15 mg, 0.019 mmol) in 5.5 mL of 1,2,4-trichlorobenzene was then added, and the reaction mixture was kept under dynamic vacuum while the condenser was cooled to 5 °C using a circulating chiller. The reaction mixture was gradually heated to 60 °C over 1 h and refluxed for 24 h. The reaction mixture was cooled down to room temperature, 16.15 mg of Grubbs second-generation catalyst in 3 mL of 1,2,4-trichlorobenzene was added, and the reaction mixture was refluxed at 60 °C under dynamic vacuum for another 24 h. Such a process was repeated for a total of five times, and the

mixture was poured into Acetone (200 mL) to precipitate the polymer, which was purified by Soxhlet extraction with acetone, hexanes, and chloroform to give the title compound as a black solid (600 mg, 79.1% yield). ^1H NMR (300 MHz, CDCl_3): δ (ppm) = 0.88 (t, 3H), 1.25 (m, 18H), 1.53 (m, 2H), 2.52 (t, 2H), 6.72 (m, 2H). ^{13}C NMR (125.75 MHz, CDCl_3): δ (ppm) = 14.16, 22.74, 29.75, 31.98, 117.71, 123.86, 138.61, 143.02. SEC (CHCl_3 , 1 mL/min): $M_n = 13.2$ kDa, $M_w = 39.7$ kDa, $D = 3.0$.

PSV-Th. PTV-Br (100 mg, 0.25 mmol) and tri-*n*-butyl(2-thienyl)tin (129.8 mg, 0.35 mmol) were charged into a pressure vessel. $\text{Pd}(\text{PPh}_3)_4$ (57.4 mg, 0.05 mmol), DMF (2.5 mL), and toluene (2.5 mL) were added into the vessel in an argon-filled glovebox. The mixture was stirred at 110 °C for 24 h. PSV-Th was isolated by precipitation into Acetone and drying under high vacuum as a black solid (80 mg, 79.2%). ^1H NMR (300 MHz, CDCl_3): δ (ppm) = 0.87 (t, 3H), 1.23 (m, 20H), 2.49 (t, 2H), 6.95 (d, 2H), 7.14~7.59 (m, 3H). ^{13}C NMR (125.75 MHz, CDCl_3): δ (ppm) = 14.13, 22.70, 29.40, 29.68, 30.97, 31.92, 124.18, 126.32, 126.89, 128.03, 128.52, 129.99, 134.81, 144.74. SEC (CHCl_3 , 1 mL/min): $M_n = 11.4$ kDa, $M_w = 19.2$ kDa, $D = 1.7$.

PSV-ThCHO. PSV-Br (100 mg, 0.25 mmol) and (5-(1,3-Dioxolan-2-yl)thiophen-2-yl)trimethylstannane (111 mg, 0.35 mmol) were charged into a pressure vessel. $\text{Pd}(\text{PPh}_3)_4$ (57.4 mg, 0.05 mmol), DMF (2.5 mL), and toluene (2.5 mL) were added into the vessel in an argon-filled glovebox. The mixture was stirred at 110 °C for 24 h. The reaction mixture was dried under high vacuum to get rid of the solvent, and the residue was used in next

step without further purification. The residual polymer from the previous step, THF (25 mL), H₂O (5 mL), and HCl (0.5 mL) were added into a one-neck flask. The reaction mixture was stirred at room temperature for 24 h. PSV-ThCHO was isolated by precipitation into Acetone and drying under high vacuum as a black solid (64 mg, 59.3% yield). ¹H NMR (300 MHz, CDCl₃): δ (ppm) = 0.86 (t, 3H), 1.22 (m, 18H), 1.37 (m, 2H), 2.51 (t, 2H), 6.66 (d, 1H), 7.02 (d, 2H), 7.82 (d, 1H), 9.98 (s, 1H). ¹³C NMR (125.75 MHz, CDCl₃): δ (ppm) = 14.12, 22.68, 28.77, 29.38, 29.66, 30.94, 31.90, 123.74, 124.86, 129.97, 136.11, 139.63, 140.00, 140.39, 144.36, 145.58, 147.53, 182.74, 182.92. SEC (CHCl₃, 1 mL/min): $M_n = 12.1$ kDa, $M_w = 18.9$ kDa, $D = 1.6$.

PSV-ThCN. PSV-ThCHO (100 mg, 0.23 mmol) and methyl cyanoacetate (45.7 mg, 0.46 mmol) were charged into a pressure vessel. Triethylamine (93.5 mg, 0.92 mmol) and CHCl₃ (3 mL) were added into the vessel in an argon-filled glovebox. The mixture was stirred at room temperature for 24 h. After solvent removal under reduced pressure, the solid was dissolved in chloroform (0.5 mL) and then dropped into Acetone (100 mL) to precipitate the polymer as a black solid after drying under high vacuum (76 mg, 64%). ¹H NMR (300 MHz, CDCl₃): δ (ppm) = 0.85 (t, 3H), 1.21 (m, 20H), 2.53 (t, 2H), 3.93 (s, 3H), 6.70 (d, 1H), 7.09 (d, 2H), 7.88 (d, 1H), 8.36 (s, 1H). ¹³C NMR (125.75 MHz, CDCl₃): δ (ppm) = 14.11, 22.66, 29.37, 29.68, 30.99, 31.90, 53.28, 98.83, 115.76, 123.84, 130.34, 136.68, 137.22, 146.40, 147.90, 163.16. SEC (CHCl₃, 1 mL/min): $M_n = 13.1$ kDa, $M_w = 21.7$ kDa, $D = 1.7$.

Chapter 4. *Acceptor-Donor-Acceptor* Type Pt-containing Conjugated Small Molecule for Photophysical Studies.

4.1 Introduction

OSCs continue to be an attractive research topic both in academia and industry due to our rapidly increasing demand for energy and the nonrenewable nature of fossil fuels. To improve the performance of OSCs, intensive research has been focused on the molecular engineering of donor materials and great success has been seen from the donor-acceptor copolymers, with which PCE of ca. 10% can be reached when combining with PCBM as the active layer in solar cell devices.^{29, 110} However, further PCE improvement requires not only structural optimization of the donor component, but also new design of more efficient acceptor materials. Although the PCBM family has been proved to be a good acceptor candidate with exceptional optoelectronic and physical properties, including high electron affinity,¹¹¹ high electron mobility,¹¹² favorable nanoscale morphology¹¹² and isotropic electron-transport capability,¹¹³ they do suffer from several shortcomings, namely high costs,¹¹⁴ poor absorption in the visible region,¹¹⁵ limited tunability of energy levels and morphology instability, which are believed to be difficult to overcome through chemical modifications. Therefore, in order to push the PCE of OSCs to a higher level and make solar energy more accessible, acceptor material with a better design is prerequisite.

Acceptor materials not based on fullerene derivatives are classified into non-fullerene (NF) acceptors, which usually generate low to moderate PCEs while applying in BHJ solar

cell.^{116, 117} However, this situation has been significantly changed over the past several years with the emerging of the newly designed acceptor-donor-acceptor (*A-D-A*) NF acceptors. Figure 4.1 shows an example of this class of material composing of electron

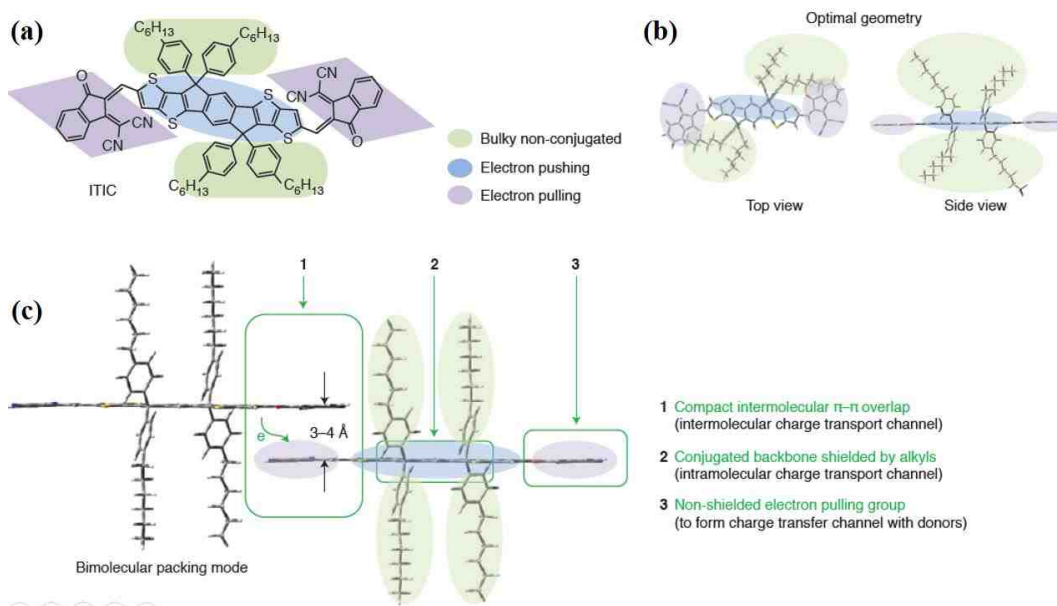


Figure 4.1 (a) The ITIC molecule includes electron-pushing and electron-pulling units, where the electron-pushing units are shield by bulky non-conjugated side chains. (b) Top and side views of the optimal geometry of the ITIC molecule. (c) Bimolecular packing mode. Adapted the copyright of Ref.² Copyright (2018), Springer Nature.

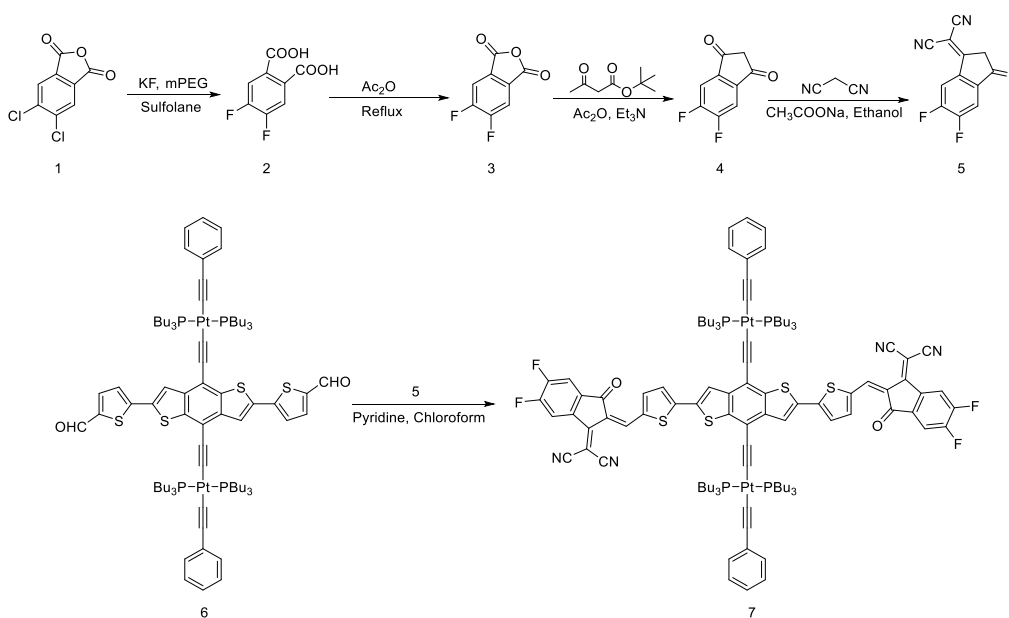
pushing unit as the core and electron pulling units on each terminus. This type of NF acceptor is highly fused, leading to good structural planarity along the backbone and compact intermolecular π - π overlap, which provides the intermolecular charge transport channel. In the solar cell devices employing *A-D-A* acceptors, it is found that efficient exciton dissociation can happen upon even negligible driving force, leading to high photocurrent and low voltage losses at the same time.¹¹⁸⁻¹²³ Nowadays, PCE of 14.1% has been reached in single-BHJ OSCs by applying a chlorinated low-bandgap small-molecule acceptor,¹²⁴ which outperformed the best fullerene-based single-junction OSCs.^{125, 126}

Conjugated materials containing transition metals (TMs) as part of the conjugation system are especially intriguing because of the potential to combine the attractive properties from both organic materials and metals in a constructive manner, as well as to generate emerging new phenomena not observed individually.¹²⁷⁻¹³⁰ Besides, in terms of OSCs, incorporating heavy metals into the organic materials could lead to facile formation of triplet excitons due to the heavy atom effect.¹³¹⁻¹³³ The extended lifetimes and thus longer diffusion lengths of triplet excitons have been suggested to improve the charge separation efficiency,¹³⁴⁻¹⁴⁰ which could potentially benefit solar cell performance. Among the various examples of metal-containing materials applied in OSCs, conjugated small molecules and polymers containing Pt-bisacetylide moieties are the most studied.¹⁴¹⁻¹⁴⁵ We recently reported several Pt-containing conjugated molecules used as the donor materials for OSCs and PCE of 5.9%, the highest among all Pt-containing materials, was achieved after condition optimization.^{141, 142} The excellent performance was ascribed to the outstanding optoelectronic properties and well-ordered intermolecular packing structures. Triplet exciton formation was observed through photoluminescence measurement and transient absorption spectroscopy from our previously prepared Pt-containing OSCs donor materials. Despite of the high device efficiency, there is no evidence showing that the triplet exciton was separated into free charges due to its low energy level, which can't offer enough energy to drive the electron from the triplet exciton to the LUMO of the acceptor material. In order to further study this problem as well as gain a deeper understanding of the generation, transport, or even separation of the triplet excitons for device performance

enhancement, we have proposed to introduce the Pt-bisacetylide moieties into the OSCs acceptor materials. Given the effectiveness of the *A-D-A* structural design of the recently discovered acceptor materials to achieve high OSCs efficiency and the success of our Pt-containing compounds as OSCs donor materials, we have been trying to construct our new Pt-containing OSCs acceptor material by introducing strong electron-deficient units while keeping the electron-rich Pt-containing core.

4.2 Synthesis Characterization and Discussion

Synthetic routes of the non-fullerene OSCs acceptor are summarized in Scheme 4.1 and



Scheme 4.1 Synthetic Route of Pt-containing Non-fullerene OSCs acceptor.

detailed procedures are described in the experimental section. The synthesis starts from 4,5-dichlorophthalic anhydride by replacing the two chlorine atoms with fluorine in aprotic polar solvent under high temperature, followed by substituting the oxygen atom in the anhydride with carbon through reduction, leading to the formation of compound 3. One

thing that is worth to be mentioned here is the fluorination step is water-sensitive, so the solvent and reactants need to be carefully dried. A dicyanovinylene moiety was then introduced to increase the electron-withdrawing strength of the acceptor units. Finally, the *A-D-A* OSCs acceptor was prepared by applying Knoevenagel condensation reaction between our previously prepared Pt-containing electron-pushing unit¹⁴¹ and the strong electron-pulling compound 5. Theoretically, Knoevenagel condensation of compound 5 and 6 will generate several regioisomers due to the *cis/trans* conformations of the formed double bond, however, the possible isomers were not observed from NMR (¹H, ¹³C, ¹⁹F), indicating only one conformation with the lowest energy is adopted.

The obtained compound was first characterized by UV-vis spectroscopy to study it

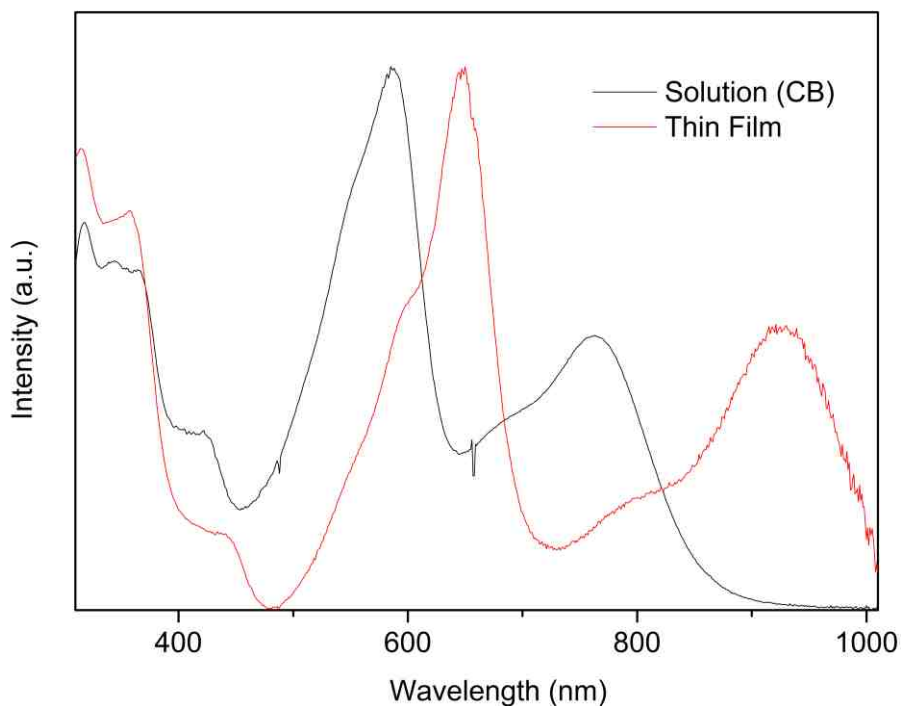


Figure 4.2. UV-vis absorption spectra of the Pt-containing acceptor in chlorobenzene solutions (ca. 10^{-5} M r.p. units) and as thin films spin cast from chlorobenzene solutions onto glass substrates.

optical properties in both dilute solution and spun-cast thin film as shown in figure 4.2. Compared with our previously Pt-containing donor compounds (Pt-SM)¹⁴² with λ_{onset} at ca. 650 nm in solution, the UV-vis absorption of our newly prepared compound is significantly red-shifted with λ_{onset} to ca. 860 nm and estimated bandgap of ca. 1.44 eV, indicating the greatly strengthened intramolecular *push-pull* effect. The incorporation of the much stronger electron-deficient units is also supposed to decrease the HOMO and LUMO

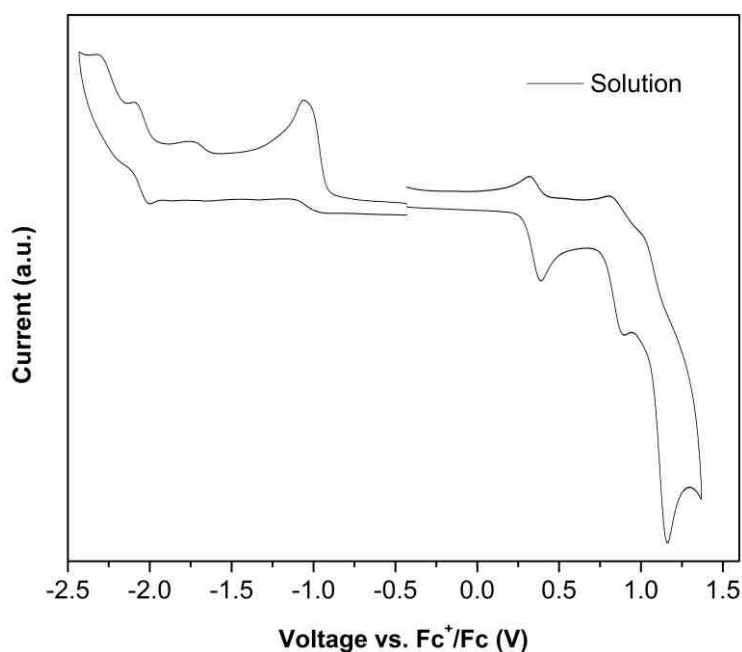


Figure 4.3. Cyclic voltammograms of the Pt-containing acceptor; Bu₄NPF₆ as supporting electrolyte (0.1 M) and referenced against ferrocene/ferrocenium redox couple (scan rate: 100 mV/s).

energy levels and as confirmed through CV measurement (figure 4.3). HOMO and LUMO of the Pt-containing compound were found to be -5.05 eV and -3.88 eV, respectively. As expected, the LUMO is notably lowered compared to Pt-SM with LUMO of ca. -3.2 eV, however, the HOMO is only slightly affected with a negligible decrease ca. 0.05 eV, presumably due to the facts that these two Pt-compounds share the same electron-rich core

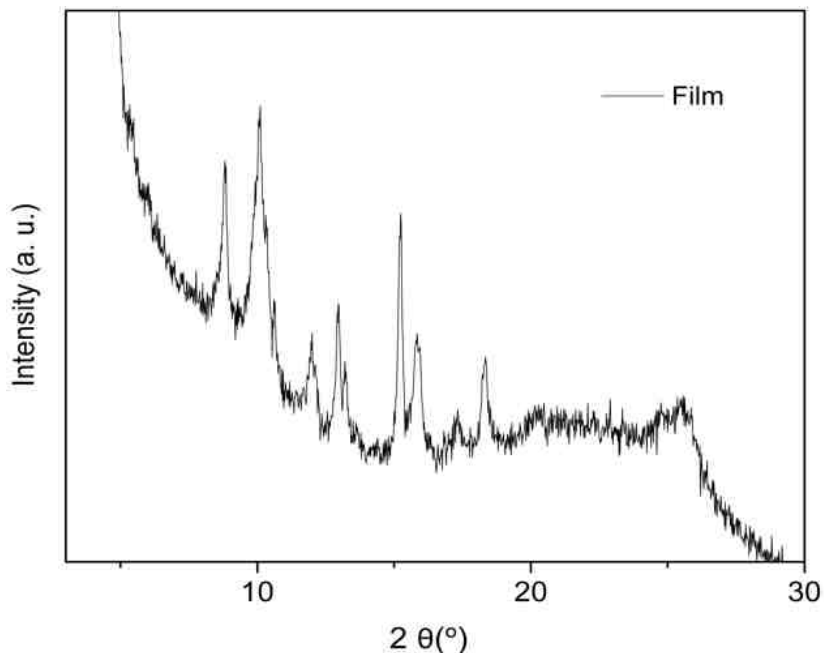


Figure 4.4 X-ray diffraction (XRD) profiles of thin films of the Pt-containing acceptor.

and the LUMO is mostly localized on the electron-deficient units, which can be confirmed by further DFT calculations. It is worth noting that the HOMO of our newly made Pt-containing compound is relatively high than those (ca. -5.4 eV) of the efficient *A-D-A* acceptors,¹²⁰⁻¹²³ which may be responsible for its low device performance.

Upon casting into thin film, the absorption profile of the Pt-containing acceptor experienced further red-shifts of ca. 100 nm, leading to an λ_{onset} of ca. 1000 nm and an estimated solid-state bandgap of ca. 1.24 eV. The large absorption shift from solution to film, which was not further impacted through either solvent or thermal annealing, implies the good packing structure in the solid state as confirmed by the existence of sharp peaks in XRD diffraction spectrum (Figure 4.4). We are currently trying to grow single crystal from this compound and perform single-crystal X-ray diffraction on it, which can help us

to assign these X-ray diffraction peaks in figure 4.4.

4.3 Experimental

Synthesis of 4,5-difluorophthalic anhydride (compound 2). Compound 2 (7.4 g, 33.9 mmol), KF (7.86 g, 135.5 mmol), and poly(ethylene glycol) methyl ether (mPEG) (MW = 2000; 0.68 g) were added to a solution of sulfolane (27 mL), and the mixture was heated to 185 °C for 3 hours under the protection of a nitrogen atmosphere. Then, the title product was distilled ($T_{\text{oil}} = 110\text{ °C}$, $T_{\text{head}} = 59\text{ °C}$, 110 millitorr, 1st fraction) from the reaction along with the solvent, which was subsequently poured into water, followed by extraction with ethyl acetate and distillation ($T_{\text{oil}} = 120\text{ °C}$, $T_{\text{head}} = 63\text{ °C}$, 140 millitorr, desired compound is in the bottom flask as solid) to give the brownish solid compound 2 (3.25g, 47.2%). ¹H NMR (300MHz, CDCl₃): δ (ppm) = 7.75 (t, 2H). ¹⁹F NMR (282.4MHz, CDCl₃): δ (ppm) = -127.69.

Synthesis of 4,5-difluorophthalic anhydride (compound 3). Compound 2 (3.25 g, 16.1 mmol) was added into CH₃COOCH₃ (10 mL). The mixture was refluxed under 140 °C for 6 hours under N₂, followed by distillation ($T_{\text{oil}} = 115\text{ °C}$, $T_{\text{head}} = 60\text{ °C}$, 130 millitorr, 2nd fraction) to give the title compound 3 as a brownish solid (1.5 g, 50.7%). ¹H NMR (300MHz, CDCl₃): δ (ppm) = 7.83 (t, 2H). ¹⁹F NMR (282.4MHz, CDCl₃): δ (ppm) = -119.12.

Synthesis of 5,6-difluoro-1H-indene-1,3(2H)-dione (compound 4). Degassed Ac₂O (5 mL) and dry Et₃N (2.5 mL) were charged into a simulation vial and stirred for 5 mins, followed by the addition of compound 3 (905 mg, 4.9 mmol) and tert-Butyl acetoacetate

(0.83 mL). The reaction mixture was stirred under room temperature overnight in glovebox and then poured into the mixture of ice-water (10 mL) and conc. HCl (4 mL). After one-hour stirring, the mixture was filtrated and washed with water and hexanes to give the title compound as brownish solid (320 mg, 35.8%). ^1H NMR (300MHz, CDCl_3): δ (ppm) = 3.26 (s, 2H), 7.76 (t, 2H). ^{19}F NMR (282.4MHz, CDCl_3): δ (ppm) = -120.18.

Synthesis of 2-(5,6-difluoro-3-oxo-2,3-dihydro-1H-inden-1-ylidene) malononitrile (compound 5). CH_3COONa (128 mg, 1.56 mmol) was added into the dry ethanol solution of compound 4 (240 mg, 1.32 mmol) and malononitrile (174 mg, 2.63 mmol) in glovebox. After stirring for 1 hour, the mixture was heated at 60 °C for 4 hours, followed by the addition of water (3.6 mL) and conc. HCl to acidify the solution to PH of 1-2. The precipitate was filtered out and washed with water and hexanes to give the tittle compound as a green solid (140 mg, 46.2%). ^1H NMR (300MHz, CDCl_3): δ (ppm) = 3.76 (s, 2H), 7.76 (t, 1H), 8.47 (m, 1H). ^{19}F NMR (282.4MHz, CDCl_3): δ (ppm) = -118.26, -117.85.

Synthesis of the Pt-containing A-D-A compound (compound 7). Compound 6 (100 mg, 0.054 mmol) and compound 5 (37.2 mg, 0.161 mmol) were charged into a 50 mL-pressure vessel, followed by additions of the dry CHCl_3 solvent (10 mL) and pyridine (10 drops). The reaction mixture was stirring under 65 °C for 16 hours and then extracted with diethyl ether (2×50 mL); the combined organic phase was dried over anhydrous Na_2SO_4 . After solvent removal under reduced pressure, the residue was further purified by distillation with hexane and dichloromethane to give a black solid (85 mg, 69.2 %). ^1H NMR (300MHz, CDCl_3): δ (ppm) = 0.92 (t, 36H), 1.47 (m, 24H), 1.71 (m, 24H), 2.24 (m,

24H), 7.14 (m, 2H), 7.24 (d, 2H), 7.31 (d, 4H), 7.40 (d, 2H), 7.67 (t, 2H), 7.86 (d, 2H), 8.08 (s, 2H), 8.56 (m, 2H), 8.86 (s, 2H). ^{19}F NMR (282.4MHz, CDCl_3): δ (ppm) = -123.40, -122.43. ^{31}P NMR (121.5MHz, CDCl_3): δ (ppm) = 4.01.

Conclusion

In conclusion, we have developed a versatile methodology for the synthesis of structurally diverse poly(thienylene vinylene) and poly(selenylene vinylene) derivatives by the combination of acyclic diene metathesis polymerization and post-polymerization modification technique. After introducing halogen atoms and thiophene-based conjugated side chains, we have shown that both the LUMO and HOMO energy levels of PTV can be effectively lowered and the crystallinity of the polymer was gradually decreased, resulting from the electron-withdrawing effects, increased conjugated system and larger sizes of the introduced functional groups. The post-polymerization modified PTVs were found to possess much broader absorption due to the contribution from both mainchain and conjugated side chains. Interestingly, intramolecular charge transfer from electron-rich polymer mainchain to electron-deficient sidechain was observed from the UV-vis absorption of PTV-ThCN, which significantly reduced the polymeric bandgap to ca. 1.5 eV. Besides, PTV-ThCN shows relatively strong photoluminescence, which has been rarely observed in this type of material, indicating that the incorporation of strong electron-deficient group indeed changed the electronic structures of PTV. Replacement of the sulfur atoms in PTV with selenium atoms and subsequently halogenation and post-polymerization modification generated PSV derivatives possessing similar properties with that from their PTV analogues. However, the bandgaps of PSVs were decreased compared with those of PTVs, ascribed to the stabilization of LUMO upon introducing selenium

atoms into the polymer. Compared to PTVs, PSVs were found to possess better crystallinity as confirmed by the appearance of diffraction peaks from the films of cross-conjugated PSVs, which were absent in post-polymerization modified PTVs, presumably due to the stronger Se-Se interactions in solid state. After optimizing both molecular properties and device fabrication conditions, solar cell efficiency of ca. 1.6%, 3-fold higher than that of pristine PTV, was achieved from PTV-ThCN-based device. The overall performance of PSVs was lower than that of PTVs, likely due to the lower LUMO decreasing the driving force to separate excitons and stronger intermolecular interactions impeding an intimate mixing between PSVs and PCBM acceptors while fabricating into devices, given the similar excited state-lifetime of PDTV and PDSV.¹⁴⁶ Our studies on PTVs and PSVs proved the effectiveness of structural modifications on manipulating the molecular properties and significantly enhanced our understanding on the “*structure-property*” relationship of this class of material.

Reference

1. B. C. Thompson and J. M. Fréchet, *Angewandte chemie international edition*, 2008, **47**, 58-77.
2. J. Hou, O. Inganäs, R. H. Friend and F. Gao, *Nature materials*, 2018, **17**, 119.
3. Y.-J. Cheng, S.-H. Yang and C.-S. Hsu, *Chemical reviews*, 2009, **109**, 5868-5923.
4. A. J. Musser, M. Al-Hashimi, M. Maiuri, D. Brida, M. Heeney, G. Cerullo, R. H. Friend and J. Clark, *Journal of the American Chemical Society*, 2013, **135**, 12747-12754.
5. E. I. Administration and G. P. Office, *International Energy Outlook 2016: With Projections to 2040*, Government Printing Office, 2016.
6. M. A. Green, K. Emery, Y. Hishikawa and W. Warta, *Progress in photovoltaics: research and applications*, 2011, **19**, 84-92.
7. A. Goetzberger, C. Hebling and H.-W. Schock, *Materials Science and Engineering: R: Reports*, 2003, **40**, 1-46.
8. C. A. Wolden, J. Kurtin, J. B. Baxter, I. Repins, S. E. Shaheen, J. T. Torvik, A. A. Rockett, V. M. Fthenakis and E. S. Aydil, *Journal of Vacuum Science & Technology A: Vacuum, Surfaces, and Films*, 2011, **29**, 030801.
9. E. Bundgaard, O. Hagemann, M. Manceau, M. Jørgensen and F. C. Krebs, *Macromolecules*, 2010, **43**, 8115-8120.
10. G. Li, R. Zhu and Y. Yang, *Nature photonics*, 2012, **6**, 153.
11. J.-L. Brédas, D. Beljonne, V. Coropceanu and J. Cornil, *Chemical reviews*, 2004, **104**, 4971-5004.

12. O. V. Mikhnenko, H. Azimi, M. Scharber, M. Morana, P. W. Blom and M. A. Loi, *Energy & Environmental Science*, 2012, **5**, 6960-6965.
13. G. Chamberlain, *Solar cells*, 1983, **8**, 47-83.
14. A. J. Heeger, N. S. Sariciftci and E. B. Namdas, *Semiconducting and metallic polymers*, Oxford University Press, 2010.
15. B. Kan, H. Feng, X. Wan, F. Liu, X. Ke, Y. Wang, Y. Wang, H. Zhang, C. Li and J. Hou, *Journal of the American Chemical Society*, 2017, **139**, 4929-4934.
16. H. Yao, L. Ye, J. Hou, B. Jang, G. Han, Y. Cui, G. M. Su, C. Wang, B. Gao and R. Yu, *Advanced Materials*, 2017, **29**, 1700254.
17. W. Zhao, S. Li, H. Yao, S. Zhang, Y. Zhang, B. Yang and J. Hou, *Journal of the American Chemical Society*, 2017, **139**, 7148-7151.
18. C. W. Tang, *Applied Physics Letters*, 1986, **48**, 183-185.
19. G. Yu, J. Gao, J. C. Hummelen, F. Wudl and A. J. Heeger, *Science*, 1995, **270**, 1789-1791.
20. H. Hoppe and N. S. Sariciftci, *Journal of materials research*, 2004, **19**, 1924-1945.
21. S. Yanagida, Y. Yu and K. Manseki, *Accounts of chemical research*, 2009, **42**, 1827-1838.
22. J. Burroughes, D. Bradley, A. Brown, R. Marks, K. Mackay, R. Friend, P. Burns and A. Holmes, *nature*, 1990, **347**, 539.
23. M. M. Wienk, J. M. Kroon, W. J. Verhees, J. Knol, J. C. Hummelen, P. A. van Hal and R. A. Janssen, *Angewandte Chemie International Edition*, 2003, **42**, 3371-3375.
24. J. Y. Kim, S. H. Kim, H. H. Lee, K. Lee, W. Ma, X. Gong and A. J. Heeger, *Advanced materials*, 2006, **18**, 572-576.

25. F. Li, K. G. Yager, N. M. Dawson, Y.-B. Jiang, K. J. Malloy and Y. Qin, *Polymer Chemistry*, 2015, **6**, 721-731.
26. B. W. Watson, L. Meng, C. Fetrow and Y. Qin, *Polymers*, 2016, **8**, 408.
27. Q. T. Zhang and J. M. Tour, *Journal of the American Chemical Society*, 1998, **120**, 5355-5362.
28. G. Dennler, M. C. Scharber and C. J. Brabec, *Advanced materials*, 2009, **21**, 1323-1338.
29. Z. He, C. Zhong, S. Su, M. Xu, H. Wu and Y. Cao, *Nature photonics*, 2012, **6**, 591.
30. S. H. Liao, H. J. Jhuo, Y. S. Cheng and S. A. Chen, *Advanced materials*, 2013, **25**, 4766-4771.
31. Z. He, B. Xiao, F. Liu, H. Wu, Y. Yang, S. Xiao, C. Wang, T. P. Russell and Y. Cao, *Nature Photonics*, 2015, **9**, 174.
32. H. E. A. Huitema, G. H. Gelinck, J. B. P. van der Putten, K. E. Kuijk, C. Hart, E. Cantatore and D. M. de Leeuw, *Advanced Materials*, 2002, **14**, 1201-1204.
33. A. P. Smith, R. R. Smith, B. E. Taylor and M. F. Durstock, *Chemistry of materials*, 2004, **16**, 4687-4692.
34. I. W. Hwang, Q. H. Xu, C. Soci, B. Chen, A. Y. Jen, D. Moses and A. J. Heeger, *Advanced Functional Materials*, 2007, **17**, 563-568.
35. E. Lafalce, X. Jiang and C. Zhang, *The Journal of Physical Chemistry B*, 2011, **115**, 13139-13148.
36. E. Lafalce, P. Togliola, C. Zhang and X. Jiang, *Applied Physics Letters*, 2012, **100**, 119.
37. E. Olejnik, B. Pandit, T. Basel, E. Lafalce, C.-X. Sheng, C. Zhang, X. Jiang and Z. Vardeny, *Physical Review B*, 2012, **85**, 235201.

38. Y. Jiang, Q. Peng, X. Gao, Z. Shuai, Y. Niu and S. H. Lin, *Journal of Materials Chemistry*, 2012, **22**, 4491-4501.
39. L. Huo, T. L. Chen, Y. Zhou, J. Hou, H.-Y. Chen, Y. Yang and Y. Li, *Macromolecules*, 2009, **42**, 4377-4380.
40. Z. Fei, P. Boufflet, S. Wood, J. Wade, J. Moriarty, E. Gann, E. L. Ratcliff, C. R. McNeill, H. Siringhaus and J.-S. Kim, *Journal of the American Chemical Society*, 2015, **137**, 6866-6879.
41. Y.-Q. Zheng, Z. Wang, J.-H. Dou, S.-D. Zhang, X.-Y. Luo, Z.-F. Yao, J.-Y. Wang and J. Pei, *Macromolecules*, 2015, **48**, 5570-5577.
42. J. Hou, Z. a. Tan, Y. He, C. Yang and Y. Li, *Macromolecules*, 2006, **39**, 4657-4662.
43. S. S. Zade, N. Zamoshchik and M. Bendikov, *Chemistry—A European Journal*, 2009, **15**, 8613-8624.
44. A. Patra and M. Bendikov, *Journal of Materials Chemistry*, 2010, **20**, 422-433.
45. J. Hollinger, D. Gao and D. S. Seferos, *Israel Journal of Chemistry*, 2014, **54**, 440-453.
46. M. Heeney, W. Zhang, D. J. Crouch, M. L. Chabinye, S. Gordeyev, R. Hamilton, S. J. Higgins, I. McCulloch, P. J. Skabara and D. Sparrowe, *Chemical Communications*, 2007, 5061-5063.
47. M. Al-Hashimi, Y. Han, J. Smith, H. S. Bazzi, S. Y. A. Alqaradawi, S. E. Watkins, T. D. Anthopoulos and M. Heeney, *Chemical science*, 2016, **7**, 1093-1099.
48. F.-Y. Cao, C.-C. Tseng, F.-Y. Lin, Y. Chen, H. Yan and Y.-J. Cheng, *Chemistry of Materials*, 2017, **29**, 10045-10052.
49. Z. Xu, Q. Fan, X. Meng, X. Guo, W. Su, W. Ma, M. Zhang and Y. Li, *Chemistry of Materials*, 2017, **29**, 4811-4818.

50. N. B. Kolhe, H. Lee, D. Kuzuhara, N. Yoshimoto, T. Koganezawa and S. A. Jenekhe, *Chemistry of Materials*, 2018, **30**, 6540-6548.
51. S. GILLISSEN, A. HENCKENS, L. LUTSEN, D. VANDERZANDE and J. GELAN, 2003.
52. K.-Y. Jen, M. Maxifield, L. W. Shacklette and R. L. Elsenbaumer, *Journal of the Chemical Society, Chemical Communications*, 1987, 309-311.
53. S. Yamada, S. Tokito, T. Tsutsui and S. Saito, *Journal of the Chemical Society, Chemical Communications*, 1987, 1448-1449.
54. R. S. Loewe and R. D. McCullough, *Chemistry of materials*, 2000, **12**, 3214-3221.
55. Y. Qin and M. A. Hillmyer, *Macromolecules*, 2009, **42**, 6429-6432.
56. M. Hanna and A. Nozik, *Journal of Applied Physics*, 2006, **100**, 074510.
57. W. Shockley and H. J. Queisser, *Journal of applied physics*, 1961, **32**, 510-519.
58. J. Y. Kim, Y. Qin, D. M. Stevens, O. Ugurlu, V. Kalihari, M. A. Hillmyer and C. D. Frisbie, *The Journal of Physical Chemistry C*, 2009, **113**, 10790-10797.
59. J. Gao, A. K. Thomas, J. Yang, C. Aldaz, G. Yang, Y. Qin and J. K. Grey, *The Journal of Physical Chemistry C*, 2015, **119**, 8980-8990.
60. J. C. Speros, B. D. Paulsen, B. S. Slowinski, C. D. Frisbie and M. A. Hillmyer, *ACS Macro Letters*, 2012, **1**, 986-990.
61. J. C. Speros, B. D. Paulsen, S. P. White, Y. Wu, E. A. Jackson, B. S. Slowinski, C. D. Frisbie and M. A. Hillmyer, *Macromolecules*, 2012, **45**, 2190-2199.
62. G. Yang, K. Hu and Y. Qin, *J. Polym. Sci. Part A Polym. Chem.*, 2014, **52**, 591-595.

63. R. H. Grubbs and A. G. Wenzel, *Handbook of Metathesis, Volume 1: Catalyst Development and Mechanism*, John Wiley & Sons, 2015.
64. Y. Imamogamalu, *Metathesis polymerization of olefins and polymerization of alkynes*, Springer Science & Business Media, 2012.
65. K. L. Opper and K. B. Wagener, *J. Polym. Sci. Part A Polym. Chem.*, 2011, **49**, 821-831.
66. P. A. Delgado, D. Y. Liu, Z. Kean and K. B. Wagener, *Macromolecules*, 2011, **44**, 9529-9532.
67. J. C. Speros, H. Martinez, B. D. Paulsen, S. P. White, A. D. Bonifas, P. C. Goff, C. D. Frisbie and M. A. Hillmyer, *Macromolecules*, 2013, **46**, 5184-5194.
68. Z. Zhang and Y. Qin, *ACS Macro Letters*, 2015, **4**, 679-683.
69. C. Simocko and K. B. Wagener, *Organometallics*, 2013, **32**, 2513-2516.
70. Y. Li and Y. Zou, *Advanced Materials*, 2008, **20**, 2952-2958.
71. J. C. Earles, K. C. Gordon, D. L. Officer and P. Wagner, *The Journal of Physical Chemistry A*, 2007, **111**, 7171-7180.
72. S. S. Zade, N. Zamoshchik and M. Bendikov, *Accounts of Chemical Research*, 2010, **44**, 14-24.
73. R. Berger, G. Resnati, P. Metrangolo, E. Weber and J. Hulliger, *Chemical Society Reviews*, 2011, **40**, 3496-3508.
74. B. D. Cullity and S. R. Stock, *Elements of X-ray Diffraction*, Pearson Education, 2014.
75. J. Rivnay, S. C. Mannsfeld, C. E. Miller, A. Salleo and M. F. Toney, *Chemical reviews*, 2012, **112**, 5488-5519.

76. G. Lanzani, *Photophysics of molecular materials: from single molecules to single crystals*, John Wiley & Sons, 2006.
77. K. Hu, H. Yang, W. Zhang and Y. Qin, *Chemical Science*, 2013, **4**, 3649-3653.
78. A. V. Gavrilenko, T. D. Matos, C. E. Bonner, S.-S. Sun, C. Zhang and V. Gavrilenko, *The Journal of Physical Chemistry C*, 2008, **112**, 7908-7912.
79. F. C. Spano, *Accounts of chemical research*, 2009, **43**, 429-439.
80. F. C. Spano and C. Silva, *Annual review of physical chemistry*, 2014, **65**, 477-500.
81. K. L. Opper and K. B. Wagener, *J. Polym. Sci. A. Polym. Chem.*, 2011, **49**, 821-831.
82. P. A. Delgado, D. Y. Liu, Z. Kean and K. B. Wagener, *Macromolecules*, 2011, **44**, 9529-9532.
83. Z. Zhang and Y. Qin, *ACS Macro Lett.*, 2015, **4**, 679-683.
84. L. C. da Silva, G. Rojas, M. D. Schulz and K. B. Wagener, *Prog. Polym. Sci.*, 2017, **69**, 79-107.
85. Z. Zhang and Y. Qin, *Macromolecules*, 2016, **49**, 3318-3327.
86. C. J. Brabec, *Sol. Energy Mater. Sol. Cells*, 2004, **83**, 273-292.
87. M. Jørgensen, J. E. Carlé, R. R. Søndergaard, M. Lauritzen, N. A. Dagnæs-Hansen, S. L. Byskov, T. R. Andersen, T. T. Larsen-Olsen, A. P. L. Böttiger, B. Andreasen, L. Fu, L. Zuo, Y. Liu, E. Bundgaard, X. Zhan, H. Chen and F. C. Krebs, *Sol. Energy Mater. Sol. Cells*, 2013, **119**, 84-93.
88. A. P. Smith, R. R. Smith, B. E. Taylor and M. F. Durstock, *Chem. Mater.*, 2004, **16**, 4687-4692.

89. D. M. Stevens, Y. Qin, M. A. Hillmyer and C. D. Frisbie, *J. Phys. Chem. C*, 2009, **113**, 11408-11415.
90. B. Qi and J. Wang, *J. Mater. Chem.*, 2012, **22**, 24315-24325.
91. S. S. Zade, N. Zamoshchik and M. Bendikov, *Chem. Eur. J.*, 2009, **15**, 8613-8624.
92. A. Patra and M. Bendikov, *J. Mater. Chem.*, 2010, **20**, 422-433.
93. J. Hollinger, D. Gao and D. S. Seferos, *Isr. J. Chem.*, 2014, **54**, 440-453.
94. M. Heeney, W. Zhang, D. J. Crouch, M. L. Chabinye, S. Gorddeyev, R. Hamilton, S. J. Higgins, I. McCulloch, P. J. Skabara, D. Sparrowe and S. Tierney, *Chem. Commun.*, 2007, 5061-5063.
95. A. M. Ballantyne, L. Chen, J. Nelson, D. D. C. Bradley, Y. Astuti, A. Maurano, C. G. Shuttle, J. R. Durrant, M. Heeney, W. Duffy and I. McCulloch, *Adv. Mater.*, 2007, **19**, 4544-4547.
96. M. Al-Hashimi, M. A. Baklar, F. Colleaus, S. E. Watkins, T. D. Anthopoulos, N. Stingelin and M. Heeney, *Macromolecules*, 2011, **44**, 5194-5199.
97. A. Bedi, S. S. P., K. S. Narayan and S. S. Zade, *Macromolecules*, 2013, **46**, 5943-5950.
98. C. W. Lehmann and K. B. Wagener, in *Handbook of Metathesis*, ed. R. B. Grubbs, Wiley-VCH Verlag GmbH&Co, Weinheim, 2003, vol. 3.
99. H. Mutlu, L. M. de Espinosa and M. A. R. Meier, *Chem. Soc. Rev.*, 2011, **40**, 1404-1445.
100. J. Hollinger, A. A. Jahnke, N. Coombs and D. S. Seferos, *J. Am. Chem. Soc.*, 2010, **132**, 8546-8547.
101. Z. Zhang and Y. Qin, *Macromolecules*, 2016, **49**, 3318-3327.

102. P. Maity, D. Kundu, R. Roy and B. C. Ranu, *Org. Lett.*, 2014, **16**, 4122-4125.
103. C. Zhang, T. Matos, R. Li, S.-S. Sun, J. E. Lewis, J. Zhang and X. Jiang, *Polymer Chemistry*, 2010, **1**, 663-669.
104. M. Al-Hashimi, M. A. Baklar, F. Colleaux, S. E. Watkins, T. D. Anthopoulos, N. Stingelin and M. Heeney, *Macromolecules*, 2011, **44**, 5194-5199.
105. H. Gerding, G. Milazzo and H. Rossmark, *Recueil des Travaux Chimiques des Pays-Bas*, 1953, **72**, 957-962.
106. A. Poletti, R. Cataliotti and G. Paliani, *Chemical Physics*, 1974, **5**, 291-297.
107. A. Gavrilenko, T. Matos, C. Bonner, S.-S. Sun, C. Zhang and V. Gavrilenko, *The Journal of Physical Chemistry C*, 2008, **112**, 7908-7912.
108. B. Qi and J. Wang, *Journal of Materials Chemistry*, 2012, **22**, 24315-24325.
109. S. Li, L. Ye, W. Zhao, S. Zhang, S. Mukherjee, H. Ade and J. Hou, *Advanced Materials*, 2016, **28**, 9423-9429.
110. J. You, C. C. Chen, Z. Hong, K. Yoshimura, K. Ohya, R. Xu, S. Ye, J. Gao, G. Li and Y. Yang, *Advanced Materials*, 2013, **25**, 3973-3978.
111. N. S. Sariciftci, L. Smilowitz, A. J. Heeger and F. Wudl, *Science*, 1992, **258**, 1474-1476.
112. V. D. Mihailetschi, H. Xie, B. de Boer, L. A. Koster and P. W. Blom, *Advanced Functional Materials*, 2006, **16**, 699-708.
113. B. A. Gregg, *The Journal of Physical Chemistry Letters*, 2011, **2**, 3013-3015.
114. R. B. Ross, C. M. Cardona, D. M. Guldi, S. G. Sankaranarayanan, M. O. Reese, N. Kopidakis, J. Peet, B. Walker, G. C. Bazan and E. Van Keuren, *Nature materials*, 2009, **8**, 208.

115. M. C. Scharber, D. Mühlbacher, M. Koppe, P. Denk, C. Waldauf, A. J. Heeger and C. J. Brabec, *Advanced materials*, 2006, **18**, 789-794.
116. J. J. M. Halls, C. A. Walsh, N. C. Greenham, E. A. Marseglia, R. H. Friend, S. C. Moratti and A. B. Holmes, *Nature*, 1995, **376**, 498.
117. L. Schmidt-Mende, A. Fechtenkötter, K. Müllen, E. Moons, R. H. Friend and J. D. MacKenzie, *Science*, 2001, **293**, 1119-1122.
118. D. Baran, T. Kirchartz, S. Wheeler, S. Dimitrov, M. Abdelsamie, J. Gorman, R. S. Ashraf, S. Holliday, A. Wadsworth and N. Gasparini, *Energy & environmental science*, 2016, **9**, 3783-3793.
119. H. Bin, L. Gao, Z.-G. Zhang, Y. Yang, Y. Zhang, C. Zhang, S. Chen, L. Xue, C. Yang and M. Xiao, *Nature communications*, 2016, **7**, 13651.
120. Y. Li, X. Liu, F.-P. Wu, Y. Zhou, Z.-Q. Jiang, B. Song, Y. Xia, Z.-G. Zhang, F. Gao and O. Inganäs, *Journal of Materials Chemistry A*, 2016, **4**, 5890-5897.
121. J. Liu, S. Chen, D. Qian, B. Gautam, G. Yang, J. Zhao, J. Bergqvist, F. Zhang, W. Ma and H. Ade, *Nature Energy*, 2016, **1**, 16089.
122. S. Chen, Y. Liu, L. Zhang, P. C. Chow, Z. Wang, G. Zhang, W. Ma and H. Yan, *Journal of the American Chemical Society*, 2017, **139**, 6298-6301.
123. P. Cheng, M. Zhang, T. K. Lau, Y. Wu, B. Jia, J. Wang, C. Yan, M. Qin, X. Lu and X. Zhan, *Advanced Materials*, 2017, **29**, 1605216.
124. B. Kan, H. Feng, H. Yao, M. Chang, X. Wan, C. Li, J. Hou and Y. Chen, *Science China Chemistry*, 2018, 1-7.
125. S. Zhang, L. Ye and J. Hou, *Advanced Energy Materials*, 2016, **6**, 1502529.
126. J. Zhao, Y. Li, G. Yang, K. Jiang, H. Lin, H. Ade, W. Ma and H. Yan, *Nature Energy*, 2016, **1**, 15027.

127. B. Jiang, S. W. Yang, S. L. Bailey, L. G. Hermans, R. A. Niver, M. A. Bolcar and W. E. Jones Jr, *Coordination chemistry reviews*, 1998, **171**, 365-386.
128. T. Hirao, *Coordination chemistry reviews*, 2002, **226**, 81-91.
129. C. Moorlag, B. C. Sih, T. L. Stott and M. O. Wolf, *Journal of Materials Chemistry*, 2005, **15**, 2433-2436.
130. W. C. Choy, W. K. Chan and Y. Yuan, *Advanced Materials*, 2014, **26**, 5368-5399.
131. A. Harriman, *Journal of the Chemical Society, Faraday Transactions 2: Molecular and Chemical Physics*, 1981, **77**, 1281-1291.
132. G. G. Giachino and D. R. Kearns, *The Journal of Chemical Physics*, 1970, **52**, 2964-2974.
133. S. McGlynn, T. Azumi and M. Kasha, *The Journal of Chemical Physics*, 1964, **40**, 507-515.
134. Y. Shao and Y. Yang, *Advanced Materials*, 2005, **17**, 2841-2844.
135. L. S. Devi, M. K. Al-Suti, C. Dosche, M. S. Khan, R. H. Friend and A. Köhler, *Physical Review B*, 2008, **78**, 045210.
136. I. I. Fishchuk, A. Kadashchuk, L. S. Devi, P. Heremans, H. Bässler and A. Köhler, *Physical Review B*, 2008, **78**, 045211.
137. S. T. Hoffmann, E. Scheler, J.-M. Koenen, M. Forster, U. Scherf, P. Strohriegl, H. Bässler and A. Köhler, *Physical Review B*, 2010, **81**, 165208.
138. A. Köhler and H. Bässler, *Journal of Materials Chemistry*, 2011, **21**, 4003-4011.
139. Z. Chen, H.-Y. Hsu, M. Arca and K. S. Schanze, *The Journal of Physical Chemistry B*, 2014, **119**, 7198-7209.

140. M. Qian, R. Zhang, J. Hao, W. Zhang, Q. Zhang, J. Wang, Y. Tao, S. Chen, J. Fang and W. Huang, *Advanced Materials*, 2015, **27**, 3546-3552.
141. W. He, M. Y. Livshits, D. A. Dickie, Z. Zhang, L. E. Mejiaortega, J. J. Rack, Q. Wu and Y. Qin, *Journal of the American Chemical Society*, 2017, **139**, 14109-14119.
142. W. He, M. Y. Livshits, D. A. Dickie, J. Yang, R. Quinnett, J. J. Rack, Q. Wu and Y. Qin, *Chemical Science*, 2016, **7**, 5798-5804.
143. W.-Y. Wong and C.-L. Ho, *Accounts of chemical research*, 2010, **43**, 1246-1256.
144. W. Y. Wong, *Macromolecular Chemistry and Physics*, 2008, **209**, 14-24.
145. K. Glusac, M. E. Köse, H. Jiang and K. S. Schanze, *The Journal of Physical Chemistry B*, 2007, **111**, 929-940.
146. B. D. Datko, M. Y. Livshits, Z. Zhang, D. Portlock, Y. Qin, J. J. Rack and J. K. Grey, *Physical Chemistry Chemical Physics*, 2018, **20**, 22159-22167.